DESIGN AND SYNTHESIS OF CHROMONE DERIVATIVES AS TOPOISOMERASE I INHIBITORS

CHIRATTIKAN MAICHEEN

A THESIS SUBMITTED IN PARTIAL FULFILLMENT
OF THE REQUIREMENTS FOR
THE DEGREE OF MASTER OF SCIENCE IN PHARMACY
(PHARMACEUTICAL CHEMISTRY)
FACULTY OF GRADUATE STUDIES
MAHIDOL UNIVERSITY
2011

Thesis
entitled

DESIGN AND SYNTHESIS OF CHROMONE DERIVATIVES AS TOPOISOMERASE I INHIBITORS

Chirattikan Maicheen

Miss Chirattikan Maicheen
Candidate

Jiraporn Ungwittayatorn

Assoc.Prof. Jiraporn Ungwittayatorn,
Ph.D. (Medicinal Chemistry)
Major advisor

Jiraphun Jittikoon

Lect. Jiraphun Jittikoon,
Ph.D. (Biochemistry)
Co-advisor

B. Mahaisavariya

Prof. Banchong Mahaisavariya,
M.D., Dip Thai Board of Orthopedics
Dean
Faculty of Graduate Studies
Mahidol University

Leena S.

Prof. Leena Suntornsuk,
Ph.D. (Pharmaceutical Chemistry)
Program Director
Master of Science in Pharmacy
(Pharmaceutical Chemistry)
Faculty of Pharmacy, Mahidol University

Thesis
entitled

DESIGN AND SYNTHESIS OF CHROMONE DERIVATIVES AS TOPOISOMERASE I INHIBITORS

was submitted to the Faculty of Graduate Studies, Mahidol University
for the Master of Science in Pharmacy
(Pharmaceutical chemistry)
on
September 19, 2011

Chirattikan Maicheen

Miss Chirattikan Maicheen
Candidate

Assoc.Prof. Weerasak Samee,
Ph.D. (Pharmaceutical Chemistry and Phytochemistry)
Chair

Jiraporn Ungwitayatorn

Assoc.Prof. Jiraporn Ungwittayatorn,
Ph.D. (Medicinal Chemistry)
Member

Jiraphun Jittikoon

Lect. Jiraphun Jittikoon,
Ph.D. (Biochemistry)
Member

B. Mahai

Prof. Banchong Mahaisavariya,
M.D., Dip Thai Board of Orthopedics
Dean
Faculty of Graduate Studies
Mahidol University

C. Suthisisang

Assoc. Prof. Chuthamanee Suthisisang,
Ph.D. (Pharmacology)
Dean
Faculty of Pharmacy
Mahidol University

ACKNOWLEDGEMENTS

I am sincerely indebted to my thesis advisor, Associate Professor Dr. Jiraporn Ungwitayatorn, for her kindness, helpful suggestion, guidance and constructive criticism during my entire study.

My sincere and grateful appreciation is also expressed to Dr. Jiraphun Jittikoon, my co-advisor, for her kindness and suggestion in bioassay section.

I am also thankful to all graduate students at Mahidol University for their helpful, friendship and encouragement.

A special acknowledgement is extended to

- High Performance Computer Center (HPCC), National Electronics and Computer Technology Center (NECTEC) of Thailand for providing SYBYL version 8.0 facility.

- Department of Pharmaceutical Chemistry, Faculty of Pharmacy, Mahidol University, for providing research facilities and supporting the important information.

- Department of Biochemistry, Faculty of Pharmacy, Mahidol University, for providing research facilities.

The most important, my gratitude must be extended to my parents and my brother for their love, inspiration, encouragement and cheerfulness throughout my study.

Chirattikan Maicheen

DESIGN AND SYNTHESIS OF CHROMONE DERIVATIVES AS TOPOISOMERASE I INHIBITORS

CHIRATTIKAN MAICHEEN 5136807 PYPE/ M

M.SC. in Pharm. (MASTER OF SCIENCE IN PHARMACY (PHARMACEUTICAL CHEMISTRY))

THESIS ADVISORY COMMITTEE: JIRAPORN UNGWITAYATORN, Ph.D., JIRAPHUN JITTIKOON, Ph.D.

ABSTRACT

The new chromone derivatives were designed and synthesized as potential topoisomerase I (TOP I) inhibitors. The structures were designed based on the docking simulation study using the AutoDock program. Compound **11c** was the best docked ligand for DNA TOP I with a binding energy of -11.39 kcal/mole. The 2-substituted phenyl and 3-substituted benzoyl chromones were used as starting structures. The steric substituent was added at the 7-OH of the chromone nucleus. Sixteen designed compounds were synthesized using one-pot cyclization with 1,8-diazabicyclo[5.4.0]-undec-7-ene (DBU) as the catalyst. The steric group was added by esterification or etherification reactions at 7-OH. The synthesized compounds were tested for their inhibitory activity against TOP I by gel electrophoresis using a eukaryotic TOP I drug screening kit. The synthesized chromone compounds showed 33.41-66.03 % inhibition. Structure-activity relationships revealed that R_1 and R_2 preferred no substituent at benzoyl or phenyl rings respectively, but electron withdrawing substituent such as NO_2 was allowed at *para*- position while substituent at R_3 could be varied. The IC_{50} values were determined from the calibration curve plotted between inhibition percentage and log concentration (logC). The most potent inhibitor, compound **11b** (IC_{50} = 1.46 μM) showed greater inhibitory activity than the known TOP I inhibitors, camptothecin, fisetin and morin.

KEY WORDS: TOPOISOMERASE I INHIBITORS / CHROMONE DERIVATIVES DOCKING / AUTODOCK / SYNTHESIS /

124 pages

การออกแบบและสังเคราะห์อนุพันธ์ของโครโมนเพื่อใช้ในการยับยั้งเอนไซม์โทโพไอโซเมอเรส I
DESIGN AND SYNTHESIS OF CHROMONE DERIVATIVES AS TOPOISOMERASE I INHIBITORS

จิรัฐติกาล ไม้จีน 5136807 PYPE/ M

ภ.ม. (เภสัชเคมี)

คณะกรรมการที่ปรึกษาวิทยานิพนธ์: จิรภรณ์ อังวิทยาธร, Ph.D., จิระพรรณ จิตติคุณ, Ph.D.

บทคัดย่อ

ในงานวิจัยนี้ได้ทำการออกแบบและสังเคราะห์อนุพันธ์ของโครโมนชนิดใหม่เพื่อใช้ยับยั้งเอนไซม์โทโพไอโซเมอเรส 1 การออกแบบโครงสร้างของสารทำโดยการศึกษา docking simulation โดยใช้โปรแกรม AutoDock พบว่าสารที่สามารถจับกับเอนไซม์ได้ดีที่สุดคือ สาร **11c** มีค่า binding energy เท่ากับ -11.39 kcal/mole ทำการสังเคราะห์โดยใช้โครงสร้าง 2-substituted phenyl and 3-substituted benzoyl chromones เป็นโครงสร้างตั้งต้นและเติมหมู่แทนที่ที่มี steric ที่ตำแหน่ง 7-OH ของโครโมน สังเคราะห์สารทั้งสิ้น 18 อนุพันธ์ด้วยวิธี one-pot cyclization โดยใช้ DBU เป็นเบส จากนั้นจึงทำการเติมหมู่แทนที่ที่ตำแหน่ง 7-OH ด้วยปฏิกิริยา esterification หรือ etherification ทำการทดสอบหาความสามารถในยับยั้งเอนไซม์โทโพไอโซเมอเรส 1 ด้วยวิธีเจลอิเลคโตรโฟเรซิสโดยใช้ชุดทดสอบ eukaryotic TOP I drug screening kit พบว่าสารสังเคราะห์ทั้งหมดยับยั้งเอนไซม์อยู่ในช่วงร้อยละ 33.41-66.03 ความสัมพันธ์ระหว่างโครงสร้างของสารกับการออกฤทธิ์พบว่า R_1 และ R_2 ไม่ควรมีหมู่แทนที่ที่ benzoyl ring และ phenyl ring ตามลำดับ ยกเว้นหมู่แทนที่ที่มีคุณสมบัติดึงอิเล็คตรอน เช่น NO_2 แต่ต้องอยู่ที่ตำแหน่ง para เท่านั้น สำหรับในกรณีของตำแหน่ง R_3 อาจเป็นหมู่แทนที่ชนิดต่างๆได้ การหาค่า IC_{50} ทำได้โดยสร้างกราฟระหว่างร้อยละของการยับยั้งกับค่า log ของความเข้มข้นของสาร พบว่าสาร **11b** ยับยั้งเอนไซม์ได้ดีที่สุด (IC_{50} = 1.46 ไมโครโมลาร์) และดีกว่าสารที่มีการศึกษามาแล้วว่ามีฤทธิ์ยับยั้งเอนไซม์โทโพไอโซเมอเรส 1 ได้แก่ camptothecin, fisetin และ morin

124 หน้า

CONTENTS

CONTENTS (cont.)

CONTENTS (cont.)

LIST OF TABLES

LIST OF FIGURES

LIST OF FIGURES (cont.)

LIST OF ABBREVIATIONS

Å	angstrom
ADCC	antitumor-dependent cellular cytotoxic
AML	myelogenous leukemia
AO	antisense oligonucleotides
AR	amphiregulin
Arg	arginine
Asn	asparagine
Asp	aspartic acid
ATR	attenuated total reflectance
bp	base pair
Bcl-2	B-cell lymphoma 2
CCD	charge-coupled device
Cdc7	cell division cycle 7
Cdks	cyclin dependent kinase
cm^{-1}	per centimeter
CPT	camptothecin
ºC	degree Celsius
d	doublet
δ	chemical shift
DBU	1,8-diazabicyclo [5,4,0] undec-7-ene
Dd	doublet of doublet
DMSO	dimethyl sulfoxide
DNA	deoxyribonucleic acid
dsRNA	double strand ribonucleic acid
EGF	epidermal growth factor
EGFR	epidermal growth factor receptor
EI	electron impact

LIST OF ABBREVIATIONS (cont.)

FTIR	Fourier transform infared spectroscopy
g	gram
Gln	glutamine
HB-EGF	heparin-binding epidermal growth factor
HERs	human epidermal growth factor receptors
His	histidine
^{1}H NMR	proton nuclear magnetic resonance
HTS	high through put screening
IAP	inhibitor of apoptosis
IC_{50}	50 % inhibitory concentration
IgG1	immunoglobulin G1
IL-3	interleukin
J	coupling constant
Kcal	kilo calorie
kDa	kilo Dalton
KRAS	Kristen rat sarcoma
Lys	lysine
m	multiplet
MAPK	mitogen-activated protein kinases
Met	methionine
mg	milligram
MHz	megahertz
mL	milliliter
mmol	millimole
mRNA	messenger ribonucleic acid
m.p.	melting point
MW	molecular weight

LIST OF ABBREVIATIONS (cont.)

PDB	protein data bank
Phe	phenylalanine
RNA	ribonucleic acid
RNAi	ribonucleic acid interference
RNase H	ribonuclease H
SAR	structure activity relationship
S.E.	standard error
siRNA	small interfering ribonucleic acid
st.	stretching
t	triplet
TGF-α	transforming growth factor-alpha
Thr	threonine
TKIs	tyrosine kinase inhibitors
TLC	thin layer chromatography
TMS	tetramethylsilane
TOP	topoisomerase
Tyr	tyrosine
nM	nanomolar
NSCLC	non-small cell lung cancer
PI3K	phosphatidylinositol 3-kinases
µL	microlitre
µM	micromolar

CHAPTER I
INTRODUCTION

Combination chemoradiations, alone or as an adjuvant to surgery, has been shown to improve treatment outcomes in a number of human malignancies, but may be limited by normal tissue toxicities. A primary challenge in radiation oncology is the development of drugs that can selectively enhance the cytotoxicity of ionizing radiation against tumor cells. Mamalian DNA topoisomerase I (DNA TOP I) is the major target of a number of newly developed anticancer drugs that have shown efficacy against solid tumors, including colon, ovarian, lung, head and neck, and pediatric cancers (1).

TOP-DNA complexes have been implicated as the primary target of several clinically important antitumor agents. These agents have been shown to increase the number of TOP-associated DNA strand breaks in cells, apparently by stabilizing the covalent enzyme-DNA complex and thereby diminishing the resealing of the DNA phosphodiester linkages. Inhibition of TOP function in this manner results in cytotoxicity to proliferating cells (2). The inhibitor-trapped TOP I-cleavable complex triggers replication fork arrest and breakage to generate a DNA break that is responsible for the G2/M arrest and activation of DNA damage signals (3). Camptothecin (CPT), a cytotoxic alkaloid, was found to inhibit TOP I by reversibly stabilizing an enzyme-DNA complex (2).

From the previous docking simulation study using AutoDock 3.0 (4), a flavonoid compound, myricetin showed good binding interaction with DNA TOP I with binding and docking energy values were -11.70 and -12.00 kcal/mole, respectively. The docking result supported the agarose gel assays which showed that myricetin was the most potent TOP I and II inhibitors (IC_{50} 11.9 µg/ml against both enzymes) among several studied flavonoids (5).

In this study the new chromone derivatives were designed and synthesized as potential TOP I inhibitors. The structures were designed based on the docking

simulation study using AutoDock program (6). The docking study revealed that the 2-substituted phenyl-3-substituted benzoyl chromones showed better binding energy than 2-substituted phenyl chromones, therefore the 2-substituted phenyl-3-substituted benzoyl chromones were used as starting structures and the steric substituent was added at the 7-OH of the chromone nucleus.

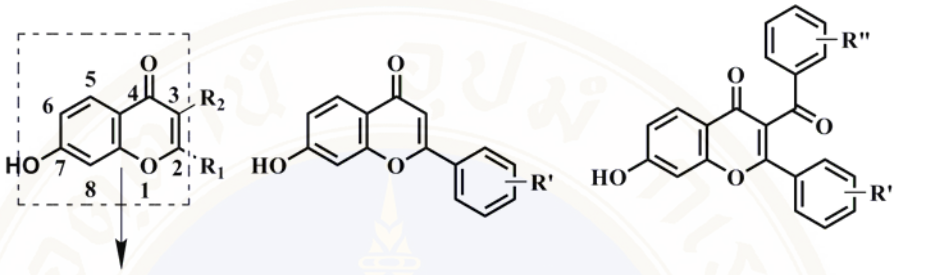

The designed structures were synthesized using 2 main steps. First, the chromone structure was prepared by one-pot cyclization using 1,8-diazabicyclo[5.4.0]undec-7-ene (DBU) as catalyst (7). Second, the steric group was added by esterification or etherification reactions (8-11). The synthesized compounds were tested for their inhibitory activity against TOP I by gel electrophoresis using eukaryotic TOP I drug screening kit.

CHAPTER II
LITERATURE REVIEW

A. Cancer

Cancer is a group of diseases characterized by uncontrolled growth and spread of abnormal cells. Cancer is caused by both external factors (tobacco, infectious organisms, chemicals and radiation) and internal factors (inherited mutations, hormones, immune conditions and mutations that occur from metabolism). These causal factors may act together or in sequence to initiate or promote carcinogenesis. In 2008, there were more than 156,000 cancer deaths in the UK, and one in four (27%) of all deaths in the UK were due to cancer. Deaths from cancers of the lung, bowel, breast and prostate together account for almost a half (47%) of all cancer deaths. More than 1 in 5 (22%) of all cancer deaths are from lung cancer, largely due to smoking. Colorectal cancer was the second most common cause of cancer death (10% and despite being extremely rare in men, breast cancer was the third most common cause of cancer death (8%).

1. Tumor cell properties

The basic differences between cancer cells and normal cells are uncontrolled cell proliferation, decreased cellular differentiation, ability to invade surrounding tissue and ability to establish new growth at ectopic sites (metastasis). Development and homeostasis in multicellular organisms are controlled by processes of cell division, differentiation and death. In the adult, the steady-state number of differentiated cells is maintained by balance between cell proliferation and cell death. Cell death is a complex and actively regulated process known as apoptosis. Apoptosis is a defined process of cell shrinkage, membrane blebbing and nuclear condensation. Cancer can be considered a failure of cells to undergo apoptosis. In normal cells, sensors to cell abnormalities lead to withdrawal of survival signals, resulting in cell

death. In contrast, cancer cells circumvent the need for survival signals by increasing their abundance of anti-apoptotic proteins (12).

2. Treatment of cancer

There are three traditional approaches for the treatment of cancer, i.e., surgery radiotherapy and chemotherapy. Chemotherapy is usually used alongside surgery and radiotherapy. Moreover, it is often the case that combination therapy (the simultaneous use of various anticancer drugs with different mechanism of action) is more effective than using a single drug. The advantages include increased efficacy of action, decreased toxicity and evasion of drug resistance.

Most traditional anticancer drugs work by disrupting the function of DNA and are classed as cytotoxic. Some act on DNA directly; others (antimetabolites) act indirectly by inhibiting the enzymes involved in DNA synthesis. Cancer chemotherapy is now entering a new era which can be described as molecular targeted therapeutics highly selective agents which act through specific molecular targets that are abnormal or over expressed in the cancer cell. Knowledge of the cell cycle is important in chemotherapy. Some drugs are more effective during one part of the cell cycle than another. For example, drug which affect microtubules are effective when cells are actively dividing (the M-phase), whereas drug acting on DNA are more effective if the cells are in the S-phase. Some drugs are effective regardless of the phase; for example, alkylating agents such as cisplatin. For this reason, anticancer drugs are most effective against cancers which are rapidly proliferating, since they are more likely to become susceptible when they reach the relevant part of the cycle. Conversely, slower growing cancers are less effectively treated.

Finally, one of the best ways of reducing cancers is to reduce the risk. Public education campaigns are important in highlighting the dangers of smoking, excessive drinking and hazardous solvents, as well as promoting healthy diets and lifestyles. The benefits of eating high-fiber foods, fruit and vegetables are clear. Indeed, there have been various research projects animal at identifying the specific chemicals in these foods which are responsible for this protective property. For example, dithiolthiones are a group of chemicals in broccoli, cauliflower and cabbage which appear to have protective properties, one of which involves the activation of

enzymes in the liver to detoxify carcinogens. Genistein is a protective compound found in soy products used commonly in Asian diets. It is notable that Asian populations have a low incidence of breast, prostate and colon cancers. Epigallocatechin gallate, an antioxidant present in green tea, is another potential protective agent. Synthetic drugs are also being investigated as possible cancer preventives (e.g., finasteride, aspirin, ibuprofen and difluoromethylornithine) (13).

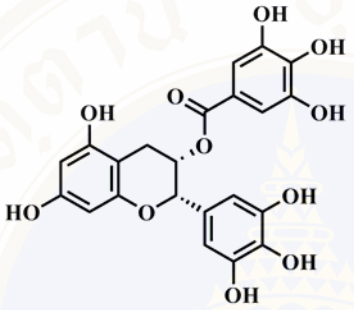

epigallocatechin gallate

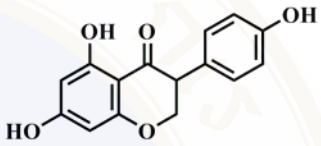

genistein

Current clinical used anticancer agents, their mechanism of actions and indications are summarized in Table 2.1.

Table 2.1. Current clinical used anticancer agents, their mechanism of actions and indications.

Drugs	Mechanism of action	Indications
1. Cyclophosphamide	DNA alkylating agent: involve cross-linking of tumor cell DNA (14)	- Neuroblastoma - Hodgkin's disease - Retinoblastoma (14-15)
2. Paclitaxel	Anti-microtubule agent: placlitaxel promotes the assembly of microtubules from tubulin dimers and stabilizes microtubules by preventing depolymerization (16-17)	- ovarian cancer - breast cancer - Kaposi's sarcoma (15, 18)
3. Vinblastine	Mitosis inhibitor: vinblastine inhibit microtubule formation in the mitotic spindle, resulting in an arrest of dividing cells at the metaphase stage (19)	- lymphocytic lymphoma - advanced testicular carcinoma - Kaposi's sarcoma (15)

Table 2.1. Current clinical used anticancer agents, their mechanism of actions and indications (cont.).

Drugs	Mechanism of action	Indications
4. Methotrexate	Anitimetabolite: inhibits dihydrofolic acid reductase in DNA synthesis, repair and replication (20)	- breast cancer - lung cancer - gestational choriocarcinoma - non-Hodgkin's lymphoma
5. Tamoxifen	Potent antiestrogen: binds the estrogen receptors (21)	- breast cancer (21)
6. Doxorubicin	Intercalating agent: inhibits nucleotide replication and action of DNA and RNA polymerases, interaction with TOP II to form DNA-cleavable complexes appears to be an important mechanism of doxorubicin cytocidal activity (22-23)	- acute lymphoblastic leukemia - acute myeloblastic leukemia - Wilms' tumor - neuroblastoma - breast carcinoma - ovarian carcinoma - thyroid carcinoma - gastric carcinoma - Hodgkin's disease
7. Rituximab	Anticancer monoclonal antibody: decrease expression of CD20 and enhance expression of anti-apoptotic molecules (24)	- non-Hodgkin's lymphoma - chronic lymphocytic leukemia (24-25)

3. New targets for anticancer treatment

3.1 The epidermal growth factor (EGF) family and their receptors, human epidermal growth factor receptors (HERs)

EGF family and their receptors, HERs, are expressed in various tissues of epithelial, mesenchymal and neuronal origin, as well as in human cancers (26-28). The EGF family of growth factors and HER members are involved in a range of cancer cell behaviors, including excess growth, invasion and blood vessel formation. Accordingly, the functions of these ligands and receptors functions have been widely investigated, and a number of therapeutic strategies targeting EGFR or HER2 are now being developed and used in clinical practice (29). Inhibition of the EGFR pathways in cancer cells reportedly blocks cell cycle progression, apoptosis and angiogenesis. Numerous EGFR blockers have been investigated, and some of these are now being used clinically, including anti-EGFR monoclonal antibodies, tyrosine kinase inhibitors (TKIs), ligand conjugates, immunoconjugates and antisense oligonucleotides. Monoclonal antibodies bind to the extracellular domain of the EGFR, competing with EGFR ligands, including EGF, transforming growth factor-α (TGF-α), amphiregulin (AR) and heparin-binding EGF-like growth factor (HB-EGF). Another important mechanism is antibody-receptor internalization, in which the antibody/EGFR complex is internalized from the cell surface to cytoplasm. This prevents ligand induced autophosphorylation of EGFR. Monoclonal antibodies may also stimulate immunologically mediated mechanisms, including antitumor-dependent cellular cytotoxicity (ADCC) and complement-mediated cytotoxicity. On the other hand, TKIs bind to the EGFR catalytic domain in the cytoplasm to block signaling molecules (30).

Cetuximab is the most commonly used anti-EGFR therapeutic agent for the treatment of colorectal cancer and squamous cell carcinoma of the head and neck. Cetuximab is a chimeric immunoglobulin G1 (IgG1) antibody that induces EGFR internalization and activates the complement pathway and ADCC (31-33).

Panitumumab is a human IgG2 monoclonal antibody against EGFR that blocks ligand-binding to EGFR and causes receptor internalization, but is unable to induce degradation of EGFR and ADCC (34).

The human homolog of the Kirsten rat sarcoma-2 (KRAS) virus oncogene, encodes a small G-protein that functions downstream of EGFR-induced signaling. Mutations in the KRAS oncogene are frequently found in human cancers, particularly colorectal, pancreatic and lung tumors. Recently, the presence of KRAS mutations in metastatic colorectal cancer patients has been reported to correlate with a lack of response to EGFR inhibitor therapies, such as panitumumab and cetuximab (34).

Trastuzumab is an anti-HER-2 receptor humanized IgG1 monoclonal antibody that has shown significant clinical benefits in the treatment of HER-2/neu(+ve) metastatic breast cancer. Trastumab can also help fight breast cancer by alerting the immune system to destroy cancer cells onto which it is attached. Erlotinib, gefitinib and lapatinib are the small molecule TKIs.

Erlotinib and gefitinib inhibit tyrosine kinase activity of EGFR, and lapatinib inhibits the tyrosine kinase activity of both EGFR and HER2. Gefitinib has shown effectiveness in patients with refractory non-small cell lung cancer (NSCLC), but only a fraction of patients respond to it. Gefitinib sensitivity has been associated with never-smokers, women, Asian ethnicity, and adenocarcinoma histology; however, high EGFR protein levels are not associated with EGFR TKI sensitivity. A correlation between EGFR mutations and EGFR TKI sensitivity has also been reported in several clinical trials (35).

Lapatinib is a member of the orally active small molecules that reversibly inhibit both EGFR and HER2 tyrosine kinases, which consequently leads to the downregulation of both the mitogen-activated protein kinases (MAPK) and phosphatidylinositol 3-kinases (PI3K) signaling cascades. As a dual kinase inhibitor, lapatinib has shown activity in a number of different metastatic and advanced tumors. Recent studies have demonstrated that it may be advantageous to inhibit EGFR and HER2 simultaneously in patients overexpressing the ErbB2/HER-2/neu gene in primary breast cancer (36).

3.2 The cell division cycle 7 (Cdc7)

All major transitions through the cell cycle are tightly controlled by the cyclin-dependent kinases (Cdks) that signal at the cell cycle checkpoints. DNA damaging events modulate checkpoint signalling to facilitate DNA

repair or programmed cell death depending on the damage incurred by the cells. Many cancers with proliferative mutations often have abnormal checkpoint responses allowing tumor cells to remain viable and for a survival advantage to be passed on when the genome is duplicated. Mutations in checkpoint regulators cause a variety of human tumors (37-38). Potential targets for anticancer therapy have emerged as a result of improved understanding of these mechanisms and of checkpoint signaling events. One of these targets, the highly conserved Cdc7, is critical for normal cell cycle progression and has several structure/function relationships with the Cdks, making it an important target for pharmacological inhibition. Mechanistically, the role of Cdc7 in tumorigenesis is not fully understood. In fact, there may be none and Cdc7 may simply be expressed and regulated as a function of the mechanisms responsible for the transformed character of the cells. Because of its pivotal role in S phase progression, increased levels may serve to drive the proliferative capacity of the tumors, however, this does not appear to be the case when proliferation indices are correlated with Cdc7 expression levels. *In vitro*, downregulation of Cdc7 expression using small interfering RNA (siRNA) knockdown models produces an abortive S phase progression and cell death in HeLa cell lines independent of p53 (39). In tumor cells, therefore, inhibitory signals preventing further cell cycle progression are not generated. However, in normal fibroblasts, a p53-dependent system prevents progression through a lethal S phase and protects the cell from the effects of reduced Cdc7 (39).

Using high through put screening (HTS), Vanotti *et al* (40)., developed a first class group of Cdc7 kinase inhibitors, the 2-heteroaryl-pyrrolopyridones. The screening of 100 Cdk inhibitors produced a 65 % successful hit rate. Of these, the pyrrolopyridinones had the most favorable characteristics by having low molecular weights, good solubility and low plasma protein binding. From these data, the lead compound PHA-767491 emerged as the first nanomolar. Following optimization of the PHA-767491 scaffold, the important effects of Cdc7 depletion were reproduced in pre-clinical models. *In vitro* and cell-based assays PHA-767491 of target effects on Cdk9 and RNA polymerase II phosphorylation were observed. Depletion of Cdk9, however, does not impact significantly on cell viability in yeast models and Drosophila melanogaster embryos are capable of prolonged survival

without Cdk9 expression (41-42). Importantly, depletion of Cdk9 in human cells did not alter growth rates or rates of cellular transcription (43). Inhibition of Cdk9 may in fact augment the effects of Cdc7 depletion through downregulation of the anti-apoptotic protein Mcl-1 and Xiap (44-45), both of which are critical for the survival of many tumor types. Activity of PHA-767491 has been shown in several cell lines and its dual inhibition of both Cdc7 and Cdk9 may be important for this to occur (46). Antitumor activity of PHA-767491 has been confirmed in acute myelogenous leukemia (AML), colon and breast xenograft models as well as in rodents with induced mammary tumors (46-48). Selectivity for tumor cells was confirmed by showing preserved cell viability in drug-treated normal human dermal fibroblasts. PHA-767491 efficacy was confirmed in a wide variety of pre-clinical tumor models irrespective of p53 in addition to activity in treatment resistant model.

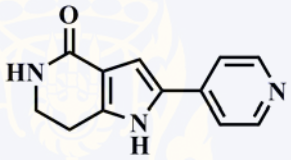

PHA-767491

3.3 Survivin

Survivin, a member of the inhibitor of apoptosis (IAP) family of proteins, regulates two essential cellular processes, i.e., it inhibits apoptosis and promotes cell proliferation. Although expressed at high levels during fetal development, surviving is rarely expressed in normal healthy adult tissues. It is however, upregulated in the majority of cancers. Because of this upregulation in malignancy, and its functional involvement in apoptosis as well as proliferation, surviving is currently attracting considerable interest both as a potential cancer biomarker and as new target for cancer treatment (49). Multiple *in vitro* and *in vivo* studies have shown that surviving inhibits cell death, especially apoptosis. *In vitro*, surviving was found to counteract both intrinsic and extrinsic mediators of apoptosis, including interleukin-3 (IL-3) withdrawal, FAS stimulation, TRAIL, overexpression of BAX, p53, caspase-3, -7 and -8, methotrexate, taxol and TNFα/cyclophosphamide. In certain cell types however, the level of inhibition was less potent than that achieved with B-cell lymphoma 2 (BCl-2) or other IAP members. Similarly, survivin has been shown to block apoptosis *in vivo* (50-51). The ability of survivin to counteract

apoptotic stimuli enhances cell survival, which in turn facilitates cell proliferation, including the proliferation of mutant cells. This proliferation may ultimately give rise to malignancy. The failure to execute apoptosis also renders malignant cells resistant to various forms of therapy including chemotherapy and radiotherapy (52). As survivin is not a cell surface protein and does not have an intrinsic enzymatic activity, targeting of survivin for therapeutic purposes might be expected to be difficult. In addition, crystallographic data has revealed few potential drugable sites on surviving protein (53). Despite these problems, a multiplicity of strategies have been employed to target the expression/function of survivin, either by binding to the survivin promoter, by inhibiting protein translation (e.g. antisense oligonucleotides and siRNA), or by interfering with survivin function (e.g. dominant-negative mutants).

Antisence oligonucleotides (AO) are short sequences of single stranded DNA or RNA complimentary to an RNA strand. These sequences are designed to hybridize by base-pairing to mRNA transcripts and thereby prevent the expression of a particular gene and subsequently its protein product. Following binding of an AO to its mRNA target, recruitment of endogenous ribonuclease H (RNase H) occurs. RNase H recognizes the mRNA-AO complex and cleaves the RNA strand. Other mechanisms of inhibition may occur as a result of modulation of splicing and inhibition of protein translation. The specificity of AO is based on the fact that any nucleotide sequence of approximately 13 bases in RNA and 17 bases in DNA is thought to be found only once in the human genome. While this may theoretically be true, in practice non-specific off-target effects can be found with AOs (54). Early studies using several different types of cancer cell lines showed that the addition of AO against survivin resulted in decreased expression of survivin mRNA and protein, inhibition of proliferation and induction of apoptosis (55). Furthermore, treatment with survivin AO enhanced anticancer activity against established and potential novel therapies. Thus, AO-mediated downregulation of survivin in cancer cells enhanced sensitivity to TRAIL, cisplatin, imatinib, taxol and etoposide. Increased sensitivity to radiation treatment has also been reported following AO-mediated downregulation of surviving (56-57).

In murine models, administration of survivin AO resulted in inhibition of tumor growth. Kanwar et al (58)., reported that intra-tumor injection

with a plasmid containing AO against survivin inhibited the growth of thymic lymphoma cells. This growth inhibition was further enhanced by immunotherapy with B7-1A, a lymphocyte co-stimulatory cell adhesion protein that has been shown to stimulate anti-tumor immunity (58). Treatment with AO against surviving has also been shown to block growth of gastric cancers in xenograft models (59). In this situation, the inhibition of tumor growth was mediated not only by induction of tumor cell apoptosis but also by inhibition of tumor angiogenesis.

A second approach for inactivation of specific mRNAs involves the use of ribozymes. Ribozymes are small RNA molecules with specific endonucleolytic activity. They catalyze the hydrolysis of phosphodiester bonds and thus the cleavage of RNA targets (60). The hammerhead domain, which is approximately 30 nucleotides long, is the smallest endonucleolytic *cis*-acting ribozyme structure found in natural circular RNAs of certain plant viroids. Hammerhead ribozymes became potential therapeutic agents following the production of *trans*-acting ribozymes directed against specific RNA sequences. Compared with AO, ribozymes have been less investigated for knock-down of specific mRNAs. Pennati et al., transfected melanoma cells with a plasmid vector containing hammerhead ribozymes targeting the 30-end of the CUA_{110} and the GUC_{294} triplets of survivin mRNA (61). The treatment resulted in decreased expression of survivin protein and an increased caspase-9-dependent apoptotic response to radiation, *cis*-platinum and topotecan. The increased response to topotecan was also found in ribozyme-expressing cells grown as xenografts in athymic mice (62).

RNA interference (RNAi) is a natural regulatory mechanism that uses small double stranded RNA (dsRNA) molecules to inhibit gene expression. The dsRNA molecules are typically 21–22 bp in length and have a 2 nucleotide 30 overhang that allows sequence specific post-transcriptional gene silencing. RNAi is generally more effective than conventional antisense strategies, presumably because it relies on natural site-directed cleavage machinery. This is an important factor when considering clinical utility, as the increased effectiveness of the knockdown should allow the molecules to function at a low concentration, and thus result in fewer side effects or adverse events (63).

RNAi-mediated decreased expression of survivin was first demonstrated in HeLa cells (64). The effect was delayed mitosis, misaligned chromosomes and accumulation in prometaphase. Subsequently, several preclinical studies showed that chemically synthesized siRNAs or plasmid/viral vectors encoding short hairpin RNAs targeting survivin, inhibited expression of the IAP, decreased cell proliferation, induced spontaneous apoptosis and inhibited tumor growth. In a recent study, siRNA-mediated suppression of survivin induced apoptosis in a caspase-independent manner (65). As with antisense oligonucleotides and ribozymes, RNAi-mediated downregulation of survivin augmented the sensitivity of cancer cell lines to a variety of treatments, including vincristine, doxorubicin, 17-allylamino-17-demethoxygeldanamycin, TNF-alpha, APO2L/TRAIL, and radiation (66-68).

B. Topoisomerase enzymes

Topoisomerases (TOPs) are enzymes which relieve the torsional stress in the DNA helix that is generated as a result of replication, transcription, and other nuclear processes (69). TOPs are classified as type I and II on the basis of two different sequences and functions. All TOPs act through an active-site tyrosine residue to cleave the phosphodiester backbone and form a covalent phosphotyrosine intermediate with the DNA. Type I TOP is a 100 kDa monomeric enzyme, which acts by introducing transient single-stranded breaks, whereas type II TOP is a 106-108 kDa dimeric enzyme which introduces transient double-stranded breaks and requires ATP as a cofactor (70).

Human TOP I is comprised of 765 amino acids with four major domains. The N-terminal domain (24 kDa) is between Met1 and Lys197. Residues Glu198 to Ile651 form the core domain (54 kDa), followed by a short 3 kDa linker domain. This linker has been found to be highly positive charged and may bind directly to DNA. It has also been proven that this region is essential for enhancing the sensitivity of some inhibitors. The C-terminal domain comprised between Gln697 and Phe795, and contains the active site Tyr723 (71). Reconstituted human TOP I structure is shown in Figure 2.1. Subdomain I consists of residues 215 to 232 and 320 to 433 and is made up of two α helices and nine β strands. Subdomain II, residues 233 to 319, is

composed of five α helices and two β strands. Subdomain III, residues 434 to 635 is a complex arrangement of ten α helices and three β strands. This subdomain contains all the active-site residues, with the exception of the catalytic Tyr723. The compact C-terminal domain runs from residues 713 to 765, is composed of five short α helices (72). TOP I plays a crucial role in the normal replication of DNA. In its physiological state in the chromosome, the DNA helix is supercoiled and tightly packed into chromatin. Replication requires transient relaxation and unwinding of the parent DNA to allow the replication fork to proceed down the DNA strand and serve as a template for synthesis of new strands of DNA (73). As a consequence of the involvement of TOP I essential cell processes such as replication and transcription, inhibitors of the topoisomerases can be cytotoxic. In fact, several classes of compounds that inhibit eukaryotic TOP I or II have antitumor activity (70, 74).

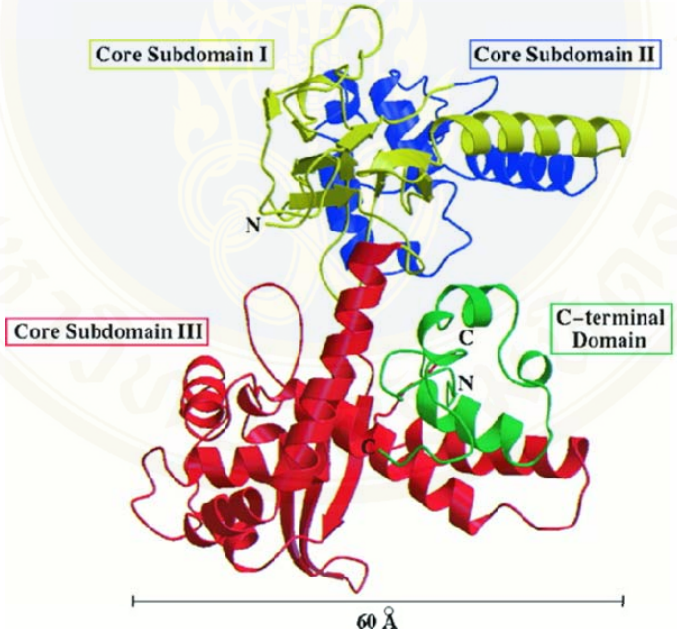

Figure 2.1. The structure of reconstituted human TOP I. Core subdomains I, II and III are shown in yellow, blue and red, respectively, and the C-terminal domain is shown in green (72).

Topoisomerase I function

TOP I produces a single strand break in DNA, allowing relaxation of DNA during its replication. The enzymatic cycle can be divided into four steps: binding of the enzyme to DNA, DNA cleavage, strand passage and DNA religation. 1) The protein and the nucleic acid are bound to each other. 2) The phenolic OH of a tyrosine residue (Tyr723 in human TOP I) in the catalytic pocket reacts with a DNA phosphodiester bond by a transesterification process, producing a covalent enzyme-DNA intermediate linked through a phosphotyrosine bond (cleavage complex), while the DNA strand is cleaved. 3) The strand passing process, which involves a conformational rearrangement of the enzyme to allow one strand of DNA to pass through the gap generated by the cleavage step. 4) The religation process corresponds to the attack of the free 5'- or 3'-hydroxyl terminus of the cleaved bond onto the phosphotyrosine linkage to reseal the original phosphodiester bond and then enzyme is released (75).

Relaxation of DNA supercoiling is a key function of TOP I enzyme. Cellular DNA must therefore be highly compacted, which creates many curved DNA domains (loops) and points of contact between these DNA domains. Moreover, DNA metabolism requires the two strands of the duplex to be separated for them to serve as templates for transcription, replication, recombination and repair. Because of the size and mass of the replication and transcription complexes it is possible that such complexes do not rotate freely around the DNA helix. In addition, because of the limited free rotation of the DNA domain flanking a given replication or transcription complex, DNA supercoiling is generated by DNA metabolism (Figure 2.2a). Therefore, DNA tends to be overwound (positively supercoiled) upstream of replication or transcription forks and underwound (negatively supercoiled) downstream of these forks. Furthermore, nucleosome formation constrains negative supercoiling by wrapping the DNA around the histone octamer, which tends to generate positive supercoiling in the flank of the nucleosome. Such supercoiling tightens the DNA duplex and needs to be relaxed by topoisomerases (Figure 2.2b). TOP I relaxed DNA supercoiling in the absence of an energy cofactor by nicking the DNA and enabling the broken strand to rotate around the TOP I-bound DNA strand (Figure 2.2c; curved arrow). The crystal structures of TOP I show the enzyme

encircling the DNA tightly like a clamp, which accounts for the fact that TOP I controls the processive relaxation of supercoiled DNA. Once the DNA is relaxed, TOP I religates the breaks by reversing its covalent binding. Religation requires the 5'-hydroxyl-group at the DNA end to be aligned with the tyrosine-DNA phosphodiester bond (Figure 2.2c). Under normal conditions, the cleavage intermediates are transient and religation is favored over cleavage (76-77).

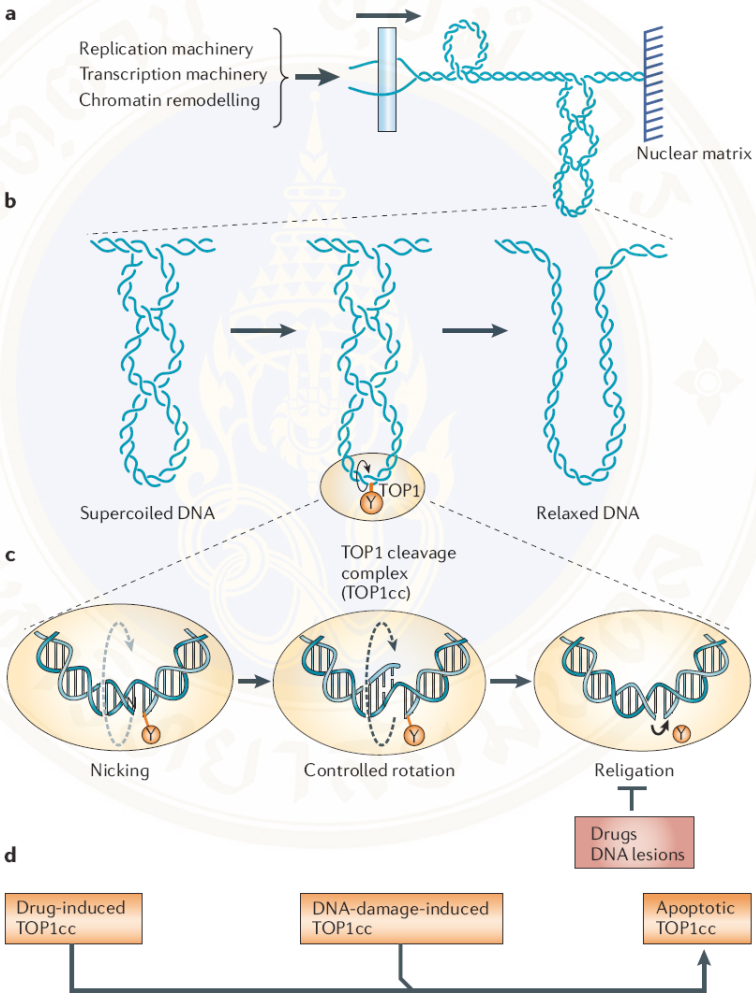

Figure 2.2. Relaxation of DNA supercoiling by TOP I-mediated DNA cleavage complexes, and the trapping of TOP I cleavage complexes by drugs, DNA modifications and during apoptosis (76).

DNA topoisomerases are particularly vulnerable to TOP I inhibitors during their cleavage intermediate step. Despite their frequency throughout the genome, TOP

I cleavage complexes are normally so transient that they are not detectable, but it is these complexes that are specifically and reversibly trapped by CPT and its pharmaceutical derivatives. It is also important to note that high levels of cellular TOP I cleavage complexes can accumulate owing to DNA modifications or apoptosis (Figure 2.2d). Because of religation of TOP I cleavage complexes requires nucleophilic attack of the tyrosyl-DNA-phosphodiester bond by the free DNA end (Figure 2.2c), it is crucial for the 5'-hydroxyl-DNA end to be perfectly aligned with the scissile tyrosyl-phosphodiester bond. Any misalignment prohibits religation and leads to an accumulation of TOP I cleavage complex. Therefore, TOP I cleavage complexes accumulate at sites of base mismatches, base oxidation, abasic sites, carcinogenic adducts and pre-existing DNA breaks because of the misalignment of the 5'-hydroxyl end of the DNA caused by such lesions. Apoptotic TOP I cleavage complexes are among the early biochemical changes that are observed during apoptosis. They results at least in part, from oxidative DNA modifications generated by reactive oxygen species that are produced during apoptosis. The attack of the phosphodiester bond by the 5'-OH DNA (reverse) or tyrosine (forward) nucleophile is greatly activated by specific contacts between the non bridging scissile phosphodiester oxygens and the side chains of Arg488, Arg590, Lys532 and His632 residues (Figure 2.3). These interactions would facilitate the formation of a pentacoordinate phosphorane transition state. The His632 residue would serve to stabilize this pentavalent transition state through hydrogen bonding to one of the nonbridging oxygens (76).

In the forward reaction, the nucleophilic attack of the scissile phosphate group in DNA leads to the phosphotyrosine adduct (the cleavable complex) produced concomitantly to the 5'-hydroxy polynucleotide strand. In the reverse reaction, the attack of the phosphotyrosine linkage by the 5'-OH DNA expels the active site tyrosine residue of enzyme. Tyr723 refers to the active site tyrosine residue involved in the transesterification reaction with DNA. Arg488, Arg590, Arg532 and His652 refer to the key amino acids implicated in the enzyme-DNA bonding and cleaving processes. The bases flanking the cleavage site are designed +1 and -1 for the 5' and 3' termini, respectively.

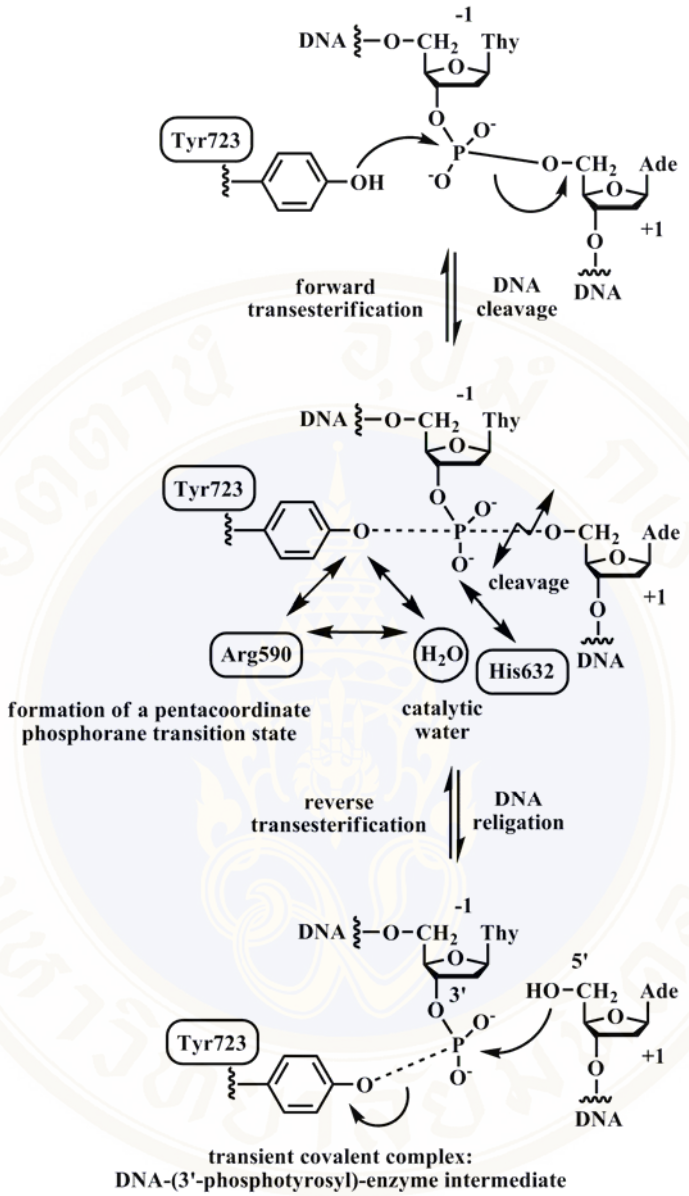

Figure 2.3. The transesterification reaction catalyzed by TOP I.

Redibo *et al*. have solved the structure of a human TOP I protein fragment bound to two 22 base pair duplexes in which the central sequence is

−5				−1		+1				+5
G	A	C	T	[C/T]	↓	A	G	A	A	A
C	T	G	A	[G/A]		T	C	T	T	T

In both C^{-1} and T^{-1} structures, the O-2 position of the pyrimidine is hydrogen bonded to the ε-amino of the conserved Lys532 residue which is also at a

hydrogen bonding distance of one of the nonbridging phosphate oxygens. The interaction between the -1 pyrimidine and Lys532 residue of TOP I plays a critical role in the association of the enzyme to DNA. In the C^{-1} structure, the localization of a water molecule adjacent to the scissile phosphate and the active site residues leads to propose a putative catalytic mechanism whereby this ordered solvent molecule would serve as a specific base to activate the catalytic Tyr723 residue. This catalytic water lies at hydrogen-bonding distance from the Arg590 residue and the tyrosyl hydroxyl residue. The water molecule is supposed to play a direct role in the deprotonation process of the active site Tyr723 residue, as recently suggested by a computational study. Molecular dynamics simulation of the TOP I-DNA complex served to identify several water-mediated hydrogen bonds playing a crucial role in mediating affinity and specificity. The formation of the deprotonated, phenolate form, of the catalytic tyrosine at physiological pH would be facilitated by the neighboring guanidinium group of Arg590. One of the nonbridging oxygen is contacted by guanidinium of Arg488 and by either the Arg590 residue in the T^{-1} structure of the Lys532 residue in the C^{-1} structures. The other nonbridging oxygens make a close contact to the imidazole of His632 residue which assists in the stabilization of the pentacovalently coordinated phosphorane intermediate. This positively charged imidazole ring could also play a direct role in the catalytic mechanism by promoting the protonation of the leaving 5'-oxygen to generate the free 5'-OH (78).

The rate of DNA religation by TOP I is normally much faster than the rate of cleavage and this ensures that the steady-state concentration of the covalent 3'-phosphotyrosine TOP I-DNA complex remain low. This is important to maintain the integrity of the genome; however, TOP I-DNA adducts can accumulate in the presence of naturally occurring DNA damage, such as nicks, modified bases, modified sugars, or as a result of exposure to a variety of anticancer compounds.

C. Topoisomerase I inhibitors

Some TOP I-targeted drugs were reported to stabilize the covalent TOP-DNA complex, thereby preventing religation, for example, the natural product CPT (Figure 2.4). TOP I inhibitors that bind to the covalent complex are termed poisons,

since they convert an essential enzyme into a DNA-damaging agent. The cytotoxic effects of TOP poisons are S-phase specific, and are roughly proportional to their capacity to stabilize the covalent enzyme-DNA complex.

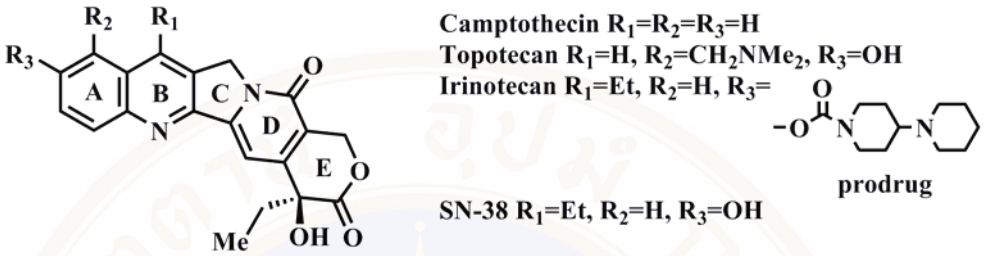

Figure 2.4. Structures of camptothecins.

1. Camptothecin (CPT) and related compounds

CPT is a naturally occurring cytotoxic alkaloid extracted from a Chinese bush (*Camptotheca acuminate*) in 1966. CPT binds reversibly to the covalent intermediate DNA-enzyme (Figure 2.5), stabilizing the cleavable complex and reducing the rate of religation (79). This leads to DNA cleavage and cell death if DNA synthesis is in progress, but it has been observed that these agents are also toxic to cancer cells which are not synthesizing new DNA. As shown in Figure 2.4, the transient covalent binary complex formed between TOP I and DNA involves attachment of the enzyme via an oligonucleotide 3'-phosphate, with the release of a free DNA strand containing a 5'-OH group (74, 80). It is believed that TOP I first binds non-covalently to its DNA substrate and then mediates cleavage of one strand by the use of an active tyrosine hydroxyl group, which becomes covalently attached to the enzyme.

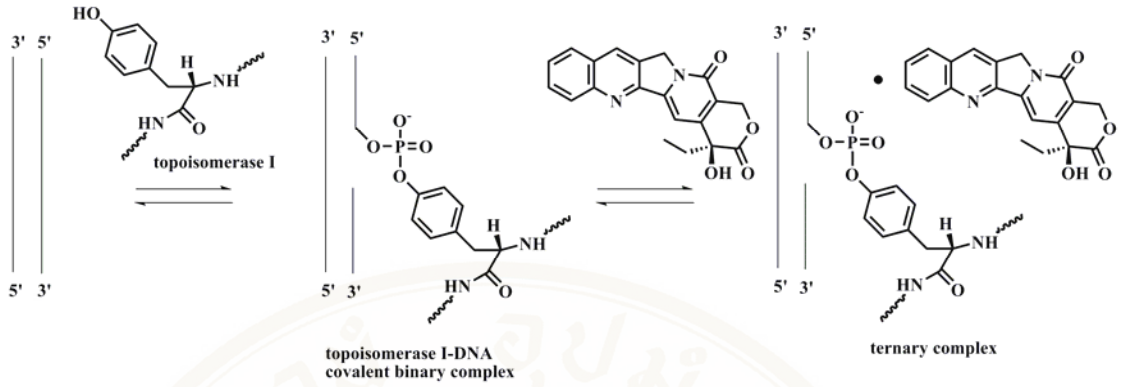

Figure 2.5. Putative mechanism of DNA nicking via a TOP I-DNA covalent binary complex, and of covalent complex stabilization by binding to CPT.

CPT has been shown to target TOP I by binding to the covalent TOP I-DNA complex with Arg364, Asp533 and Asn722 using hydrogen bonding interactions (Figure 2.6) (81). The lactone group is important for activity, but at blood pH it is in equilibrium with the less active ring-opened carboxylate structure. Introducing substituents into the A and B rings can alter the relative binding affinities of these structures to serum albumin such that the level of the lactone present is altered favorably. Unfortunately, CPT itself shows poor aqueous solubility and has unacceptable toxic side effects. CPT is a highly phase specific cytotoxic drug; S-phase cells are selectively killed. This cytotoxic is thought to be caused by the cessation of DNA synthesis followed by a double-strand breakage when the replication fork encounters the CPT-trapped TOP I-DNA complex (termed as "ternary complex").

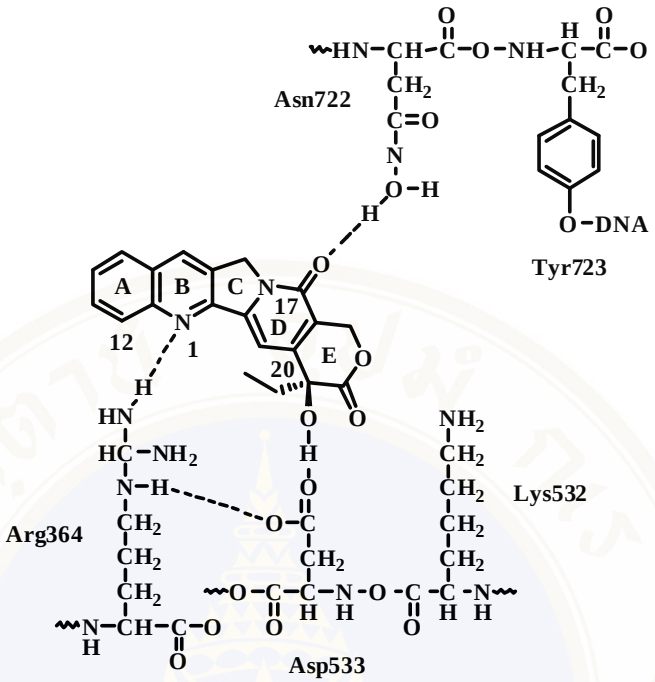

Figure 2.6. The interactions between TOP I-DNA complex and CPT. Hydrogen bonds are shown as dotted lines.

The camptothecins show selectivity for cancer cells over normal cells. TOP I can also be more active in certain cancer cells which may also account for the antitumour selectivity observed. All camptothecins have a basic heterocyclic five ring structure with a lactone moiety and an α-hydroxyl moiety on the E ring. For those agents under clinical development, substitutions on the A ring tend to increase the aqueous solubility while retaining cytotoxicity (topotecan and irinotecan). Irinotecan and topotecan are clinically useful, semi-synthetic analogs of CPT. They retain the important lactone group and were designed to have aqueous solubility by adding suitable polar functional groups such as alcohols and amines. Irinotecan is a urethane prodrug that is converted to the active phenol (SN-38) by carboxylesterases, predominantly in the liver.

2. Flavonoids

Flavonoids are among the active components in vegetables and fruits that prevent or inhibit cancer development. These compounds possess a common phenylbenzopyrone structure (C6-C3-C6), and they are categorized according to the

saturation level and opening of the central pyran ring, mainly into flavones, flavanols, isoflavones, flavonols, flavanones and flavanonols (Figure 2.7). Flavonoids have shown anticancer effects *in vitro* and in animal models of carcinogenesis, and some entered clinical trials for the prevention or treatment of specific cancers. Evidence suggests that DNA topoisomerases may play a role in the anticancer and carcinogenic effects shown by some flavonoids (82-84).

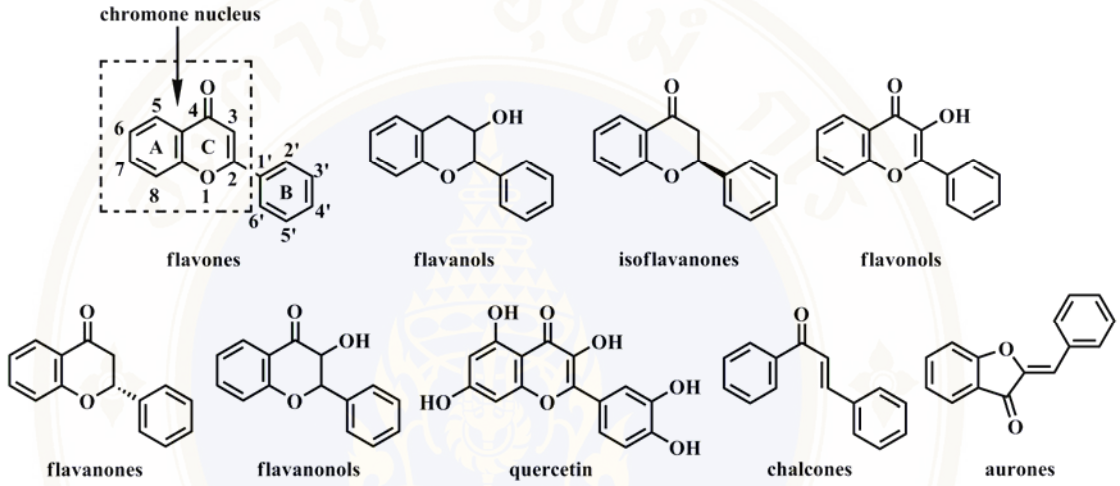

Figure 2.7. Structures of flavones, flavanols, isoflavanones, flavonols, flavanones, flavanonols, quercetin, chalcones and aurones**.**

Among naturally occurring flavonoids, quercetin (3,3',4',5,7-pentahydroxy flavone), is most widely studied *in vitro* and *in vivo*. It is known to interfere with several pathways of intermediary metabolism and various components of signal transduction cascades, especially those stimulated by the tumor promoter 12-*O*-tetradecanoylphorbol-13-acetate (82). Quercetin and related flavonoids are known to inhibit the growth of tumor cells and to potentiate the cytotoxicity of DNA-damaging anti-cancer drugs such as *cis*-platinum. Genistein is also known to inhibit TOP I *in vitro.* Thus, TOP-mediated DNA damage seems to be a candidate mechanism, by which some flavonoids may exert their cytotoxic potential. Only certain flavones are potent and selective inhibitors of TOP I-catalyzed DNA religation. Their ability to stabilize the covalent TOP I-DNA complex *in vitro* and in living cells is similar to that of the known TOP I inhibitor CPT, although the mechanism of interaction appears to be different. Moreover, molecular substitutions of the flavone structure (such as

quercetin, morin and fisetin) generate a new class of TOP I-targeted compounds that inhibit selectively the DNA binding of the enzyme. Thus, flavones seem to be an ideal model for the study of structural requirements for selective interaction with DNA cleavage and religation reactions catalyzed by TOP I that may serve for the development of new anti-cancer drugs.

Inhibition of TOP I is restricted to the group of the flavones, whereas chalcones, aurones, flavanones and isoflavanones are inactive. The ability of these compounds to form a planar, conjugated A-C-ring system appears to be essential for inhibition. Flavones can either stabilize the catalytic TOP I-DNA intermediate or inhibit the DNA binding of the free enzyme. These two effects, which are selective with respect to the catalytic step and antagonistic to each other, can be related to certain substitutions of the flavones structure.

The potency of quercetin and related compounds for stabilizing the covalent TOP I-DNA intermediate requires hydroxyl substitutions in positions 5 and 7 and a hydroxy or methoxy substituent in the 4' position. Flavones lacking OH in the 4', 5, or 7 positions are inactive. However, OH in the 5 position is not essential, because fisetin is inhibitory. Hydroxylation in the 2' position or substituents in the 3 position reduce the inhibitory potency. Thus, a planar A-C benzopyron structure seems to be important in forming ternary complexes with enzyme and DNA. The 3',4'-ortho-dihydroxy substitution pattern in the B-ring of quercetin could also indicate a catechol-type mechanism of inhibition known from inhibition of other enzymes. A similar ortho-dihydroxy-substituted phenolic ring is also essential for inhibition of topoisomerase I by certain tyrphostins. However, flavones with methoxy substituents preventing catechol-like reactions are also effective inhibitors (82).

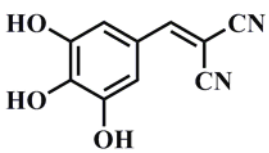

tyrphostin

D. Topoisomerase I inhibitory activity assay

The ability of specific agents to interfere with the catalytic cycle of DNA TOP I and stabilize the covalent complex may be biochemically addressed in plasmid DNA nicking assays or in linear DNA cleavage assays (85). Mechanistic and specificity studies often require that one experimentally interrupt the nicking-closing cycle of the TOP-catalyzed reaction to trap the covalent intermediate. For *Escherichia coli* TOP I and single-stranded substrate, the addition of denaturant, such as alkali or SDS, results in strand breakage and formation of the covalent complex. These same denaturants are trap the covalent complex on double-stranded circular DNA provided one starts with negatively superhelical substrate. Similarly, covalent complexes can be trapped for the eukaryotic TOP I using either double-stranded or single-stranded DNAs by stopping the reactions with SDS, alkali or low pH. If prior to treatment with a strong protein denaturant, the reaction is diluted, challenged with excess second DNA, or adjusted to 0.5 M NaCl, DNA cleave is greatly reduced (70, 86).

A convenient procedure for detecting the enzyme-DNA covalent complex is to start with a supercoiled or relaxed closed-circular duplex DNA (form I) and analyze the products of the cleavage reaction by electrophoresis through an agarose gel. Although the protein-DNA complexes can be visualized directly owing to their slower mobilities relative to the substrate DNA, the protein-DNA complexes bands are quite diffuse and difficult to quantitate, owing in part to the fact that more than one protein molecule can become attached to each DNA. A more sensitive and quantitative approach is to treat the enzyme-DNA complexes with proteinase K to remove all bound protein and resulting nicked DNA plasmid (form II). Nicked DNA plasmid (form II) are separated from supercoiled (form I) and covalently closed circular relaxed (form I^r) DNA in the present of ethidium bromide. The relative amount of form II DNA can be determined by a variety of methods. By digitizing the image using a charge-coupled device (CCD) camera or scanner, quantitation can easily be accomplished using readily available software. Alternatively, a photographic negative can be scanned using a densitometer. If radioactively labeled DNA is available, the DNA bands can be excised from the gel and quantitated with a scintillation counter (87-88). The process of TOP I inhibition test is illustrated below (89).

E. Docking

Docking is an automated computer algorithm that determines how a compound will bind in the active site of protein. This includes determining the orientation of the compound, its conformational geometry, and the scoring. The scoring may be a binding energy, free energy or a qualitative numerical measure. In some way, every docking algorithms automatically tries to put the compound in many different orientations and conformations in the active site, and then computes a score for each. Some programs store the data for all of the tested orientations, but most only keep a number of those with the best scores. Docking is probably the most heavily used tool in computational drug design. It is also the most accurate method for predicting whether a particular compound will be a good inhibitor of a particular protein. For this reason, pharmaceutical companies analyze very large numbers of compounds with docking. Those compounds that have the best docking results will be synthesized if necessary, and analyzed in the laboratory. The last lists of compounds that are analyzed computationally may be of compounds designed in the computer, compounds that are available for purchase, or compounds in the company compound library. By using the knowledge gained from the docking study, fewer compounds need be synthesized and assayed and a higher percentage of compounds assayed are found to be active.

Because docking calculations simulate the interaction between a compound and a protein's active site, the results are comparable to those of biochemical assays. Most scoring functions compute some sort of energy. Most biochemical assays compute an inhibition rate constant K_I. Thus, the binding energy from the docking calculation should be proportional to ln K_I from biochemical assay (a simple Arrhenius equation relationship). Docking results do not show a high degree of correlation to cell culture assays, efficacy in animals, or other tests. Like biochemical assays, the trends shown by docking results may be qualitatively similar to the trends in these other experiments. However, docking does not take into account bioavailability, toxicity and other factors present in the body (90).

1. Searching the entire space

There are two key components of a docking program: the search algorithm and the scoring algorithm. The search algorithm positions molecules in various locations, orientations and conformation within the active site. Some of the earliest docking programs positioned a molecule in the active site, holding it rigid with respect to conformational changes, but all modern docking algorithm determines how thoroughly the program checks possible molecule positions, and how long it takes to run. Note that the search algorithm does not determine whether the docking program gives accurate results. The scoring function is responsible for determining if the orientations chosen by the search algorithm are the most energetically favorable, and is responsible for computing the binding energy. Thus, a search algorithm that does not sample the space thoroughly will give inaccurate results if the correct orientation is not sampled. However, most search function will sample the space adequately if they are given the correct input parameters, thus making the accuracy of the results primarily dependent upon the accuracy of the scoring function.

A Monte Carlo search is built around a random number generator. In the simplest implementation, position, orientation and conformation are all chosen at random. Some Monte Carlo searches only change conformations of the rotatable bonds (single bond not in rings), whereas others will reposition ring atom. Monte Carlo algorithm, such as a tabu algorithm or a simulated annealing algorithm, often give the same accuracy of results with fewer iterations and thus a faster run time.

Genetic algorithms follow a different strategy. They are modeled after the process by which optimal genetic traits are obtained in a population through inheritance, mutation, elitism, etc. Thus the calculation may start by generating a population (each member of which is a particular ligand position) at random. Then successive generations of molecules are generated by keeping mostly the best (survival of the fittest) and combining traits from parents and random mutations. After several generations, the most fit (best scoring energy) should be well optimized. Genetic algorithms can sample a space thoroughly, if the parameters are chosen wisely, and can run very quickly. Genetic algorithms can require more memory than the other docking algorithm, as the entire population is often held in memory.

Most of the time, the implementation of these algorithms includes a bump check. This is a check that determines if two atoms are too close together. If this check fails, the orientation is discarded without going on to compute a score. Many of these algorithms also include at least a few steps of downhill minimization from each sampled position in order to obtain more accurate optimized positions. Some hold rings rigid, while others allow for ring inversions. Most prevent inversions of stereocenters. Upon starting a large docking project, the researcher should run some validation tests to make sure that the parameters being used give acceptable results. This might mean setting the number of iterations, size of area to be searched, grid size or any other adjustable parameter. One reason that docking simulations can give incorrect results is insufficient tortional sampling. In many programs, this can be fixed by increasing the number of iterations in the search. The necessary number of iterations will be larger for larger molecules, more flexible molecules or larger active sites (91).

A variety of docking programs use Monte Carlo algorithms for docking, including AutoDock, MCDOCK, Prodock and PRO-LEADS. A disadvantage of this approach is that the quality of results often depends on how the initial structure is placed in the binding site. Some research groups have used a combination of programs to address this problem. For example, DOCK can be used to identify binding modes for a specific ligand conformation based on a rigid fit and steric complementarity. Each of the binding modes identified can then be used as the starting structure for a Monte Carlo based docking program which generates different conformations and orientations in that area of the binding site. Programs using evolutionary and genetic algorithms have also been used in docking studies. Mutations and cross-over procedures not only change the conformation, they reorientate the molecule through translation and/or rotation of the whole molecule. Selection of the best dockingmodes is based on how well each molecule interacts with the binding site. Examples of programs that use genetic algorithms include AutoDock, GOLD and later version of DOCK (92).

2. Energy expressions and consensus scoring

The scoring method is the single most important aspect of a docking program, as it is used for compound selection. In general, docking programs that have accurate scoring functions tend to give ligand positions that accurately reproduce results from crystallographic analysis. There are a number of different types of scoring functions, which were developed for various reasons. Some of the simplest scoring functions are simply a quantification of how well the ligand fits in the active site. These shape-based functions generally execute quickly, but are among the least accurate scoring functions.

Most scoring functions are based on the molecular mechanics energy equation. Some are formulated as binding enthalpies or Gibbs free energies, or from a potential of mean force equation. The most accurate include entropy and solvation terms. Consensus scoring utilizes the results of several scoring functions. The compounds that rank the best are those that were chosen by multiple scoring functions. This is an empirical attempt to improve accuracy by combining multiple scoring functions in the hope that the strengths of one will negate the weaknesses of another. At present, some of the most accurate results come from consensus scoring (93).

3. Binding free energies

In an ideal world, docking scores would be free energies of binding. In the past, most scoring functions have been energies that do not include and entropy term. Entropy may make only a small contribution to the free energy relative to the enthalpy but it becomes important when comparing more and less flexible ligands. Entropy corrections using a potential of mean force or free energy perturbation formulation are possible, but are very time-consuming. Most recently, several docking programs such as MOE and AutoDock have included a conformational entropy correction based on the torsions of the rotatable bonds in the molecule. Many scoring functions are parameterized from sources such as experimental binding energies. Thus, the parameterization has effectively added in an entropy contribution in the energy of the single bond functions, even though the terms in the scoring equation may look like enthalpy term only.

There are docking programs, such as the Liaison module from Schrödinger Inc., that can compute an entropy correction. This can be done as a post-docking calculation that incorporates additional optimization and utilizes a free energy perturbation (FEB) technique. Also, the London dG scoring function included in the MOE program from Chemical Computing Group has an entropy correction, as does version 4 of AutoDock.

4. The docking process

The process of docking is illustrated in Figure 2.8.

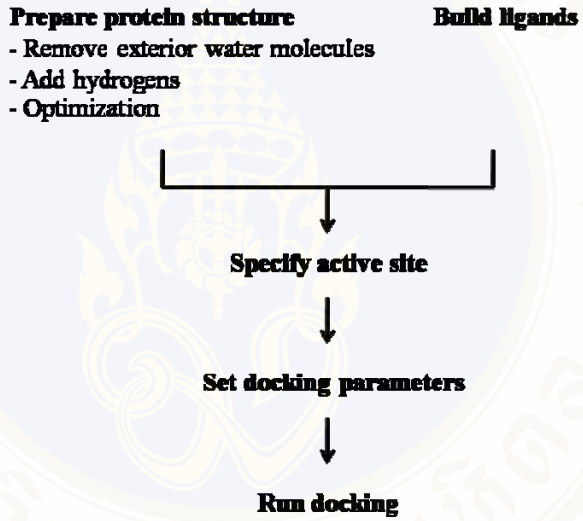

Figure 2.8. Illustration of the docking process.

4.1 Protein preparation: The accuracy of docking results is directly related to the quality of the crystallographic structure for the protein's active site. If the enzyme requires a cofactor, then the crystallographic structure of the haloenzyme (with the cofactor attached) should be used. Since even the best crystallographic structures often have a resolution of the order of 1 Å or more, most researchers will start with the crystallographic structure with an inhibitor in the active site and then add hydrogens that cannot usually be seen by protein crystallography. Water molecules are removed, sometimes with the exception of structural waters in the interior of the protein. Finally, a sample minimization is performed to find the nearest minimized structure, as predicted by the force field being used. This

minimized structure is often the best structure to utilize for docking studies, particularly if the crystallographic resolution was marginal.

4.2 Building the ligand: Docking programs offer several options for creating ligands and placing them in the active site. At the most automated end of the spectrum, some docking programs can take a database of ligands, place each one in the active site and do the docking run. This completely automated approach allows thousands of compounds to be analyzed without manual intervention from the user. Some docking programs are slightly less automated in that they automatically dock a list of ligands from a database, but each ligand must be stored in the database with its position, orientation and conformation set within the coordinate system to put the initial placement in the protein's active site.

4.3 Setting the bounding box: The entire protein is read into the computer in order to obtain a correct geometry for the structure. However, docking calculations can take a significant amount of time and anything that speeds them up without loss of accuracy is utilized. Protein residues far from the active site do not generally have any measurable effect on the scoring results. In order to speed the calculation, a cutoff distance is set and no interactions are computed for residues beyond that distance from the ligand. For ease of coding, this cutoff is usually a rectangular box, called a bounding box. In the case of grid potentials, the grid is only computed for points within the cutoff distance. Many docking packages default to setting the bounding box far enough out from the ligand or active site that there is no need to alter it. However (at least when starting on a set of docking runs), the user should verify that the bounding box extends a reasonable distance beyond the active site in all directions.

4.4 Docking options: When setting up the inputs to a docking calculation, there will be options for flexible active sites, scoring method, search method, solvation, handling encapsulated active sites, etc. Some packages many have an option to do a fast initial check and then continue only if the first check criterion is satisfied. Nearly always, the docking results will be more accurate with the calculation running more slowly, if an optimization (or at least a few optimization steps) is performed for each pose.

4.5 Running the docking calculation: Once the inputs have been set, the docking calculation can be run. Most docking programs allow individual docking runs to be started from the graphical interface. A few docking programs can run many docking calculations in a batch mode. These calculations are sometimes run on the same computer where the graphical interface is used and sometimes can be sent off to a different server.

4.6 Analysis of results: The most important result from a docking calculation is the binding energy of the ligand to the active site. This is the value that is compared between different compounds to determine which will be the best inhibitor. The pose of the ligand in the active site associated with a few of the best binding energies is examined visually to ensure that it looks reasonable. Sometimes, the pose generated by one docking calculation gives the researcher an idea for how to alter the compound on the next round of calculations. The fit to the active site should be examined. Functional groups that hang out of the active site may be extraneous and suggest that having a salvation term in the scoring function might be particularly important for this target. Areas where the molecule does not fill the active site indicate spots where a functional group could be added to give stronger binding. Too tight a fit into the active site, particularly of a pathogen protein, may indicate that resistance to the drug could be built up easily by a minor modification of one of the active site residues (94).

CHAPTER III
MOLECULAR MODELING EXPERIMENTAL

A. Materials

1. Computers

Internet network, silicon graphics SGI Iris R800

Silicon graphics SGI O2 Webforce R5000 SC

Personal computer (PC) Intel core 2 duo

2. Softwares

AutoDock 4.0 for Windows

SYBYL software version 8.0

B. Methods

1. Docking studies of chromone derivatives with topoisomerase I

The docking calculations were performed using AutoDock program version 4.0 (Scripps Research Institute, USA). The docking study was carried out using the Lamarckian genetic algorithm, applying a standard protocol, with an initial population of 150 randomly placed individuals, a mutation rate of 0.02, and a crossover rate of 0.80. One hundred independent docking runs were carried out for each ligand. Results differing by less than 2.0 Å in positional root mean-square deviation (RMSD) were clustered together and represented by the result with the most favorable free energy of binding.

1.1 Ligand preparation: The molecular structures of all compounds were modeled with SYBYL 8.0 molecular modeling program (Tripos Associates, Saint Louis, MO) on an Indigo Elan workstation (Silicon Graphics Inc., Mountain View, CA) using the sketch approach. Each structure was energy minimized using the standard Tripos force field (Powell method and 0.05 kcal/mol.Å energy

gradient convergence criteria) and electrostatic charge was assigned by the Gasteiger-Hückel method. These conformations were used as starting conformations to perform docking.

1.2 Receptor preparation: The crystal structures of TOP I complexed with inhibitor were obtained from the Brookhaven Protein Database (PDB). The inhibitor structures and all heteroatoms were removed from the complex structures, and added polar hydrogen parameters. Gasteiger charges were assigned.

1.3 Docking method validation: To ensure that the ligand orientations and positions obtained from the docking studies were likely to represent valid and reasonable potential binding modes of the inhibitors, the docking methods and parameters used were validated by redocking and cross-docking experiments. First, each ligand was docked into the native protein to determine the ability of AutoDock program to reproduce the orientation and position of the ligand observed in the crystal structure. Second, cross-docking of every ligand into each nonnative protein was undertaken. The cross-docking experiment was performed for DNA TOP I using crystal complexes that possess superimpossible atom coordinates. The crystal structures 1T8I and 1K4T were used in this study (Table 3.1).

Table 3.1. The structures of TOP I inhibitor complexed in the crystal structures**.**

PDB code	Inhibitor	Structure
1T8I	Camptothecin	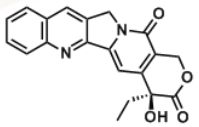
1K4T	Topotecan	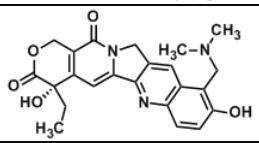

The RMSD values were obtained from the best cluster conformation of cross-docking validation of DNA TOP I (Table 3.2). 1T8I, the crystal structure with the lowest RMSD value was selected for further study.

Table 3.2. Matrix of RMSD obtained by cross-docking two different crystal complexes of DNA TOP I.

Target macromolecule	RMSD	
	1T8I	1K4T
1T8I	0.53	0.93
1K4T	0.66	0.72

1.4 Grid setup: The grid maps representing the protein in the actual docking process were calculated with AutoGrid. The grids (one for each atom type in the ligand, plus one for electrostatic interactions) were chosen to be sufficiently large to include not only the active site but also significant portions of the surrounding surface. The parameters used for autogrid are shown in Table 3.3.

Table 3.3. Autogrid parameters.

Parameters	
PDB code	1T8I
Resolution	3.00
Num. Grid point in x, y, z	40, 40, 40
Spacing (Å)	0.375
Grid center	center on ligand
Smooth	0.5

CHAPTER IV
CHEMICAL EXPERIMENTAL

A. Equipment and chemicals

1. Equipment

Analytical balance model 2842	Sartorius , Germany
Elemental analyzer (PE2400 series II)	Perkin Elmer, Germany
FTIR (FTIR 6700)	Nicolet, USA
^{1}HNMR (Avance 300)	Bruker, Switzerland
Magnetic stirrer (MR 3001K)	Heidolph, Germany
Mass spectrometer (Polaris Q)	Finnigan, Germany
Melting point apparatus (Model 9100)	Electrothermal, UK
Rotary evaporator	Eyela, Japan

2. Chemicals

Acetone	J.T Baker, USA
Benzoyl chloride	Aldrich, USA
Benzyl chloride	Fluka, Switzerland
Chloroform	J.T Baker, USA
DBU (1,8-diazabicyclo[5,4,0]undec-7-ene)	Fluka, Switzerland
2,4-Dihydroxyacetophenone	Aldrich, USA
3,5-Dinitrobenzoyl chloride	Aldrich, USA
Dimethyl sulfoxide	Sigma, USA
Ethyl acetate	J.T Baker, USA
Hexane	J.T Baker, USA
Hydrochloric acid	E. Merck, Germany
Methanol	J.T Baker, USA
3-Methoxybenzoyl chloride	Aldrich, USA
4-Methoxybenzoyl chloride	Aldrich, USA

3-Methoxybenzyl chloride	Aldrich, USA
4-Methoxybenzyl chloride	Aldrich, USA
3-Nitrobenzoyl chloride	Aldrich, USA
4-Nitrobenzoyl chloride	Aldrich, USA
Pyridine	Labscan, Thailand
Sea sand	Fluka, Switzerland
Silica gel F_{254} (0.2 mm.)	E. Merck, Germany
Silica gel 60 No. 1.07734	E. Merck, Germany
Sodium hydroxide	Fluka, Switzerland
Sodium sulfate anhydrous	Fischer sciencetific, UK

B. Methods

Melting point of all compounds was determined on an Electrothermal model 9100 capillary melting point apparatus. Infrared (IR) spectra were run on FTIR Nicolet 6700, using the attenuated total reflectance (ATR) technique. Proton nuclear magnetic resonance (^{1}HNMR) spectra were obtained on an Advance 300 MHz NMR Spectroscopy (Bruker Switzerland). Chemical shifts were reported in ppm related to the internal standard, tetramethylsilane (TMS). The NMR solvents used were deuterated dimethylsulfoxide (DMSO, δ = 2.49 ppm) and deuterated chloroform ($CDCl_3$, δ = 7.25 ppm). Mass spectra were determined on a Polaris Q Mass Spectrometry using EI method. Percentage of carbon, hydrogen and nitrogen were obtained from an elemental analyzer (Perkin Elmer PE2400 series II). Silica gel, E. Merck (70-230 mesh), was used for column chromatography. Thin layer chromatography (TLC) was carried out on silica gel GF_{254} coated aluminum sheets 20x20 cm (E. Merck) with spots visualized by UV light (254 nm). All solvents were reagent grade and when necessary, were purified and dried by standard methods.

1. 7-Hydroxy-2-phenyl-3-benzoyl chromone 7.

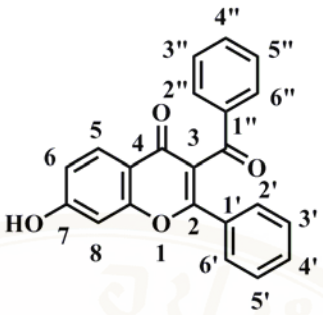

To a stirred solution of 2,4-dihydroxyacetophenone (0.5 g, 3.29 mmol) in pyridine (20 mL) was slowly added benzoyl chloride (1.0 mL, 8.61 mmol) and then DBU (1.4 mL, 9.37 mmol). The reaction mixture was refluxed at 120-140 ºC for 24 hours and pyridine was evaporated in vacuo. The mixture was poured into 5 mL of concentrated HCl in 100 mL water and extracted with ethyl acetate (2 x 50 mL). The combined organic layers were washed with water (2 x 50 mL), dried over anhydrous sodium sulfate, and filtered. After evaporation, the crude product was hydrolyzed by the mixture of dioxane (2 mL), methanol (4 mL), water (1 mL) and 10 % NaOH (2 mL), the mixture was stirred at room temperature for 3-4 hours. The reaction mixture was acidified with 4N HCl and poured into 50 mL water, and then extracted with ethyl acetate (2 x 50 mL). The combined organic layers were washed with water (2 x 50 mL), dried over anhydrous sodium sulfate, and filtered. After evaporation, the crude product was purified by column chromatography (ethyl acetate/hexane [1:1] to provide the white solid (280.5 mg, 24.83 %); m.p. 270-271 ºC; ^{1}H NMR 300 MHz (DMSO): δ 6.94-7.03 (m, 2H, H6, H8), 7.34-7.50 (m, 5H, H4', H5', H3", H4", H5"), 7.53-7.64 (m, 3H, H3', H2", H6"), 7.83-7.93 (m, 3H, H5, H2', H6'); FTIR (ATR) (cm^{-1}): 3187 (O-H st.), 3061 (aromatic C-H st.), 1671, 1618 (C=O st.), 1577, 1506, 1450 (C=C st.), 1377 (bending C-H), 1241, 1112 (C-O st.); TLC (silica gel GF 254, ethyl acetate/hexane [1:1]). R_f of 2,4-dihydroxyacetophenone = 0.63, compound **7** = 0.53.

2. 7-Hydroxy-2-(3'-methoxy)phenyl-3-(3"-methoxy)benzoyl-chromone 8.

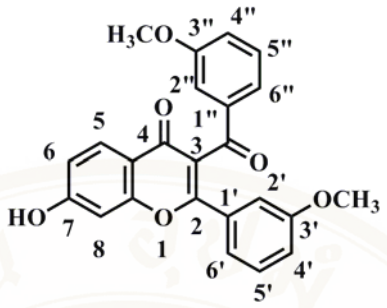

Compound **8** was synthesized using the same procedure as described for compound **7** from 2,4-dihydroxyacetophenone (0.5 g, 3.29 mmol), 3-methoxybenzoyl chloride (1.0 mL, 7.12 mmol) and DBU (1.0 mL, 6.69 mmol). After hydrolysis and purification by column chromatography (ethyl acetate/hexane [1:1]), the desired compound **8** was obtained as a yellow solid (513.4 mg, 38.62 %); m.p. 253-254 °C; ^{1}H NMR 300 MHz (DMSO): δ 3.65 (s, 3H, OCH_3), 3.75 (s, 3H, OCH_3), 6.97 (dd, *J* = 8.04, 2.29 Hz, 1H, H6), 6.99 (d, *J* = 2.29 Hz, 1H, H8), 7.04 (dd, *J* = 8.91, 1.98 Hz, 1H, H4"), 7.12-7.22 (m, 3H, H4', H2", H5"), 7.32-7.41 (m, 3H, H2', H5', H6"), 7.45-7.50 (m, 1H, H6'), 7.89 (d, *J* = 8.04 Hz, 1H, H5); FTIR (ATR)(cm^{-1}): 3046 (O-H st.), 2887, 2840 (aliphatic C-H st.), 1680, 1627 (C=O st.), 1609, 1583, 1489 (C=C st.), 1459 (bending C-H), 1233, 1168, 1047 (C-O st.); TLC (silica gel GF 254, ethyl acetate/ hexane [1:1]). R_f of 2,4-dihydroxyacetophenone = 0.63, compound **8** = 0.48.

3. 7-Hydroxy-2-(4'-methoxy)phenyl-3-(4"-methoxy)benzoyl-chromone 9.

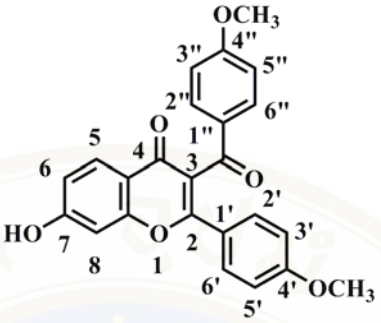

Compound **9** was synthesized using the same procedure as described for compound **7** from 2,4-dihydroxyacetophenone (0.5 g, 3.29 mmol), 4-methoxybenzoyl chloride (1.0 mL, 7.12 mmol) and DBU (1.0 mL, 6.69 mmol). After hydrolysis and purification by column chromatography (ethyl acetate/hexane [1:1]), the desired compound **9** was obtained as a yellow solid (372.4 mg, 27.97 %); m.p. 300-301 °C; ^{1}H NMR 300 MHz (DMSO): δ 3.75 (s, 3H, OCH_3), 3.79 (s, 3H, OCH_3), 6.90-7.02 (m, 6H, H6, H8, H3', H5', H3", H5"), 7.57 (d, *J* = 8.98 Hz, 2H, H2", H6"), 7.83 (d, *J* = 8.86 Hz, 2H, H2', H6'), 7.87 (d, *J* = 8.50 Hz, 1H, H5); FTIR (ATR)(cm^{-1}): 3108 (O-H st.), 3075 (aromatic C-H st.), 2957, 2834 (aliphatic C-H st.), 1662, 1606 (C=O st.), 1571, 1506 (C=C st.), 1456 (bending C-H), 1262, 1185, 1029 (C-O st.); TLC (silica gel GF 254, ethyl acetate/hexane [1:1]). R_f of 2,4-dihydroxyacetophenone = 0.63, compound **9** = 0.41.

4. 7-Hydroxy-2-(4'-nitro)phenyl-3-(4"-nitro)benzoyl chromone 11.

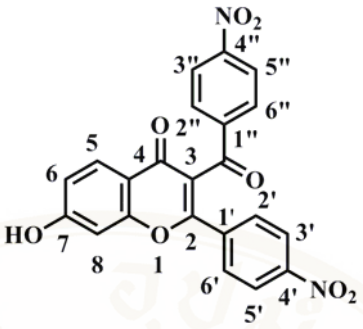

Compound **11** was synthesized using the same procedure as described for compound **7** from 2,4-dihydroxyacetophenone (0.5 g, 3.29 mmol), 4-nitrobenzoyl chloride (1.0 mL, 5.39 mmol) and DBU (1.0 mL, 6.69 mmol). After hydrolysis and purification by column chromatography (ethyl acetate/hexane [1:1]), the desired compound **11** was obtained as a yellow solid (74.7 mg, 5.24 %); m.p. 290-291 °C; ^{1}H NMR 300 MHz (DMSO): δ 6.97-7.06 (m, 2H, H6, H8), 7.84 (d, *J* = 8.56 Hz, 2H, H2", H6"), 7.90 (d, *J* = 9.34 Hz, 1H, H5), 8.13-8.24 (m, 2H, H3", H5"), 8.24-8.36 (m, 4H, H2', H3', H5', H6'); FTIR (ATR)(cm^{-1}): 3225 (O-H st.), 3108 (aromatic C-H st.), 1680, 1621 (C=O st.), 1600, 1524 (C=C st.), 1453 (bending C-H), 1347 (C-N st.), 1238, 1109 (C-O st.); TLC (silica gel GF 254, ethyl acetate/hexane [1:1]). R_f of 2,4-dihydroxyacetophenone = 0.63, compound **11** = 0.54.

5. 7-Benzyloxy-2-phenyl-3-benzoyl chromone 7a.

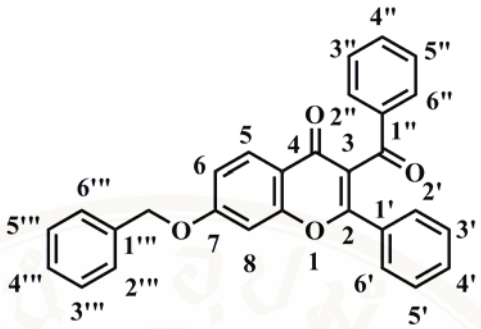

A solution of 10 % sodium hydroxide in water (1 mL) was added to a stirring solution of compound **7** (0.34 g, 1 mmol) in ethanol (10 mL). After stirring for 10 minutes, benzyl chloride (0.44 mL, 4 mmol) was added into the reaction mixture. The reaction mixture was allowed to reflux at 120 ºC for 7 hours and then ethanol was evaporated under vacuo. The mixture was extracted with ethyl acetate (3 x 50 mL). The combined organic layers were washed with saturated sodium bicarbonate (3 x 50 mL), dried over anhydrous sodium sulfate, and filtered. After evaporation, the crude product was purified by column chromatography (ethyl acetate/hexane [1:2]M to provide the yellow solid (48.3 mg, 11.13 %); m.p. 129-130 ºC; ^{1}H NMR 300 MHz ($CDCl_3$): δ 5.25 (s, 2H, CH_2), 7.08 (d, *J* = 2.26 Hz 1H, H8), 7.14 (dd, *J* = 8.86, 2.26 Hz, 1H, H6), 7.31-7.61 (m, 11H, H3', H4', H5', H3", H4", H5", H2"', H3"', H4"', H5"', H6"'), 7.65 (d, *J* = 7.02 Hz, 2H, H2", H6"), 7.94 (d, *J* = 7.76 Hz, 2H, H2', H6'), 8.18 (d, *J* = 8.86 Hz, 1H, H5); FTIR (ATR) (cm^{-1}): 3061 (aromatic C-H st.), 2928, 2869 (aliphatic C-H st.), 1671, 1618 (C=O st.), 1563, 1503, 1442 (C=C st.), 1374 (bending C-H), 1245, 1103 (C-O st.); EIMS: m/z (relative intensity) M^+ 432.02(28.31), 403.20(36.41), 355.17 (3.85), 341.17(7.36), 313.28(11.57), 105.22(16.63), 91.20(100.00), 77.25 (18.75). TLC (silica gel GF 254, ethyl acetate/hexane [1:2]). R_f of compound **7** = 0.36, compound **7a** = 0.52.

6. 7-(3"'-Methoxy)benzoate-2-phenyl-3-benzoyl chromone 7d.

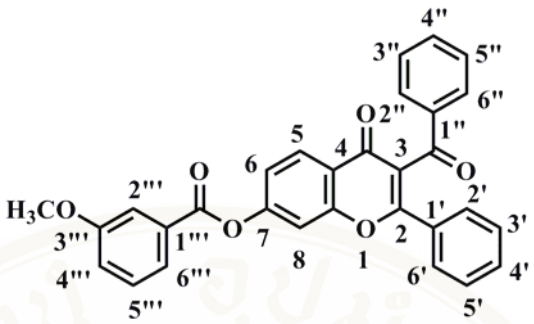

3-Methoxybenzoyl chloride (0.28 mL, 2 mmol) was added to a stirring solution of compound **7** (0.34 g, 1 mmol) in pyridine (10 mL). The reaction mixture was allowed to reflux at 120 ºC for 5 hours and then pyridine was evaporated under vacuo. The mixture was extracted with ethyl acetate (3 x 50 mL). The combined organic layers were washed with water (3 x 50 mL), dried over anhydrous sodium sulfate, and filtered. After evaporation, the crude product was purified by column chromatography (ethyl acetate/hexane [1:2] to provide the white solid (351.7 mg, 73.76 %); m.p. 145-146 ºC; ^{1}H NMR 300 MHz ($CDCl_3$): δ 3.95 (s, 3H, OCH_3), 7.22-7.28 (m, 1H, H4"'), 7.33-7.52 (m, 7H, H6, H4', H5', H3", H4", H5", H5"'), 7.55 (dd, *J* = 8.39, 1.61 Hz, 1H, H3'), 7.59 (d, *J* = 2.11 Hz, 1H, H8), 7.68 (dd, *J* = 7.68, 1.53 Hz, 2H, H2", H6"), 7.73-7.78 (m, 1H, H2"'), 7.86 (dd, *J* = 7.68, 1.11 Hz, 1H, H6"'), 7.96 (dd, *J* = 8.39, 1.39 Hz, 2H, H2', H6'), 8.34 (d, *J* = 8.71 Hz, 1H, H5); FTIR (ATR) (cm $^{-1}$): 3061 (aromatic C-H st.), 2963, 2837 (aliphatic C-H st.), 1739, 1671, 1639 (C=O st.), 1565, 1489, 1436 (C=C st.), 1368 (bending C-H), 1238, 1150, 1038 (C-O st.); EIMS: m/z (relative intensity) M^+ 476.00(28.75), 447.10(9.83), 399.21(1.28), 341.13(2.44), 313.18(6.22), 135.11(100.00), 107.19(33.65), 77.14(42.86). Anal. Calcd. for $C_{30}H_{20}O_6.H_2O$ (494.50): C, 72.87; H, 4.08. Found: C, 73.01; H, 4.13. TLC (silica gel GF 254, ethyl acetate/hexane [1:2]). R_f of compound **7** = 0.36, compound **7d** = 0.56.

7. 7-(4"'-Methoxy)benzoate-2-phenyl-3-benzoyl chromone 7e.

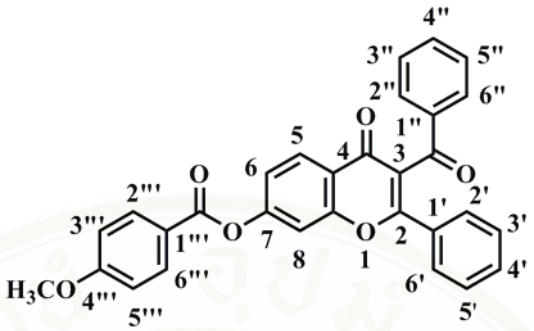

Compound **7e** was synthesized using the same procedure as described for compound **7d** from 4-methoxybenzoyl chloride (0.28 mL, 2 mmol) and compound **7** (0.34 g, 1 mmol). After purification by column chromatography (ethyl acetate/hexane [1:2]), the desired compound **7e** was obtained as a white solid (293.5 mg, 61.60 %); m.p. 144-145 ºC; ^{1}H NMR 300 MHz ($CDCl_3$): δ 3.95 (s, 3H, OCH_3), 7.05 (dd, *J* = 7.49, 2.02 Hz, 2H, H3"', H5"'), 7.31-7.49 (m, 6H, H6, H4', H5', H3", H4", H5"), 7.51-7.61 (m, 2H, H8, H3'), 7.67 (dd, *J* = 8.26, 1.42 Hz, 2H, H2", H6"), 7.95 (dd, *J* = 7.78, 1.41 Hz, 2H, H2', H6'), 8.21 (dd, *J* = 7.49, 2.02 Hz, 2H, H2"', H6"'), 8.33 (d, *J* = 8.69 Hz, 1H, H5); FTIR (ATR) (cm^{-1}): 3061 (aromatic C-H st.), 2963, 2837 (aliphatic C-H st.), 1730, 1674, 1639 (C=O st.), 1600, 1580, 1512, 1439 (C=C st.), 1371 (bending C-H), 1256, 1147, 1050 (C-O st.); EIMS: m/z (relative intensity) M^+ 476.05(19.20), 446.96(4.26), 341.01(9.49), 313.20(25.12), 135.15(100.00), 107.05(34.21), 77.04 (46.40). Anal. Calcd. for $C_{30}H_{20}O_6$ (476.48): C, 75.62; H, 4.23. Found: C, 75.99; H, 3.87. TLC (silica gel GF 254, ethyl acetate/hexane [1:2]). R_f of compound **7** = 0.36, compound **7e** = 0.49.

8. 7-(3"'-Nitro)benzoate-2-phenyl-3-benzoyl chromone 7f.

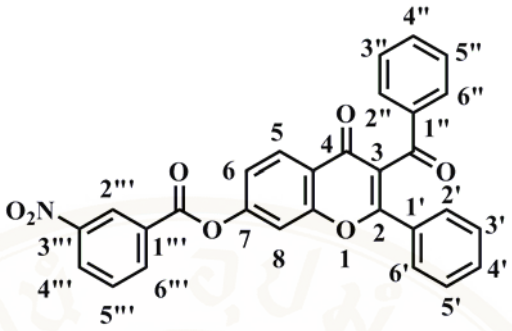

Compound **7f** was synthesized using the same procedure as described for compound **7d** from 3-nitrobenzoyl chloride (0.37 mL, 2 mmol) and compound **7** (0.34 g, 1 mmol). After purification by column chromatography (ethyl acetate/hexane [1:2]), the desired compound **7f** was obtained as a white solid (83.5 mg, 18.07 %); m.p. 174-175 ºC; ^{1}H NMR 300 MHz ($CDCl_3$): δ 7.34-7.50 (m, 6H, H6, H4', H5', H3", H4", H5",), 7.56 (t, *J* = 7.31 Hz, 1H, H3'), 7.63 (d, *J* = 2.14 Hz, 1H, H8), 7.68 (d, *J* = 7.76 Hz, 2H, H2", H6"), 7.82 (t, *J* = 8.01 Hz, 1H, H5"'), 7.95 (d, *J* = 7.31 Hz, 2H, H2', H6'), 8.36 (d, *J* = 8.70 Hz, H5), 8.54-8.62 (m, 2H, H4"', H6"'), 9.10 (s, 1H, H2"'); FTIR (ATR) (cm^{-1}): 3081 (aromatic C-H st.), 1748, 1674, 1633 (C=O st.), 1615, 1565, 1533, 1436 (C=C st.), 1371 (bending C-H), 1347 (C-N, st.), 1250, 1112, 1053 (C-O st.); EIMS: m/z (relative intensity) M^+ 491.07(51.56), 462.05(100.00), 444.18(2.15), 414.10(9.55), 388.23(8.03), 341.10(8.10), 313.21(18.78), 205.17(2.24), 150.07(43.88), 104.07(26.66), 77.03(18.27). Anal. Calcd. for $C_{29}H_{17}NO_7$ (491.45): C, 70.87; H, 3.49; N, 2.85. Found: C, 71.18; H, 2.79; N, 3.30. TLC (silica gel GF 254, ethyl acetate /hexane [1:2]). R_f of compound **7** = 0.36, compound **7f** = 0.44.

9. 7-(4"'-Nitro)benzoate-2-phenyl-3-benzoyl chromone 7g.

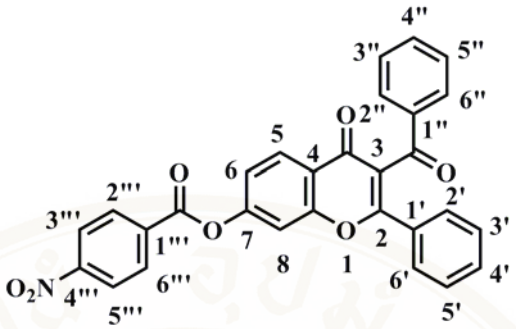

Compound **7g** was synthesized using the same procedure as described for compound **7d** from 4-nitrobenzoyl chloride (0.37 g, 2 mmol) and compound **7** (0.34 g, 1 mmol). After purification by column chromatography (ethyl acetate/hexane [1:2]), the desired compound **7g** was obtained as a white solid (175.8 mg, 35.75 %); m.p. 220-221 ºC; ^{1}H NMR 300 MHz ($CDCl_3$): δ 7.34-7.50 (m, 6H, H6, H4', H5', H3", H4", H5"), 7.57 (t, *J* = 7.30 Hz, 1H, H3'), 7.63(d, *J* = 2.09 Hz, 1H, H8), 7.68 (d, *J* = 6.99 Hz, 2H, H2", H6"), 7.95 (d, *J* = 7.30 Hz, 2H, H2', H6'), 8.36 (d, *J* = 8.71 Hz, 1H, H5), 8.40-8.48 (m, 4H, H2"', H3"', H5"', H6"'); FTIR (ATR) (cm^{-1}): 3063 (aromatic C-H st.), 1745, 1674, 1636 (C=O st.), 1618, 1562, 1521, 1439 (C=C st.), 1368 (bending C-H), 1344 (C-N st.), 1259, 1109, 1065 (C-O st.); EIMS: m/z (relative intensity) M^+ 491.11(54.96), 462.06(100.00), 444.16(2.35), 416.18(8.77), 388.23(10.99), 341.09 (7.58), 313.19(17.40), 239.25(2.40), 205.21(2.29), 150.07(30.26), 104.13(14.17), 77.04(17.66). TLC (silica gel GF 254, ethyl acetate/hexane [1:2]). R_f of compound **7** = 0.36, compound **7g** = 0.58.

10. 7-Benzyloxy-2-(3'-methoxy)phenyl-3-(3''-methoxy)benzoyl-chromone 8a.

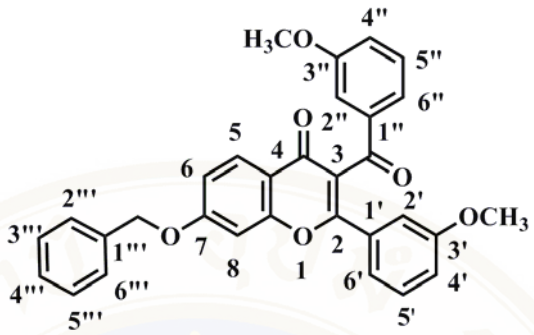

Compound **8a** was synthesized using the same procedure as described for compound **7a** from benzyl chloride (0.44 mL, 4 mmol) and compound **8** (0.40 g, 1 mmol). After purification by column chromatography (ethyl acetate/hexane [1:2]), the desired compound **8a** was obtained as a white solid (94.50 mg, 19.17 %); m.p. 163-164 ºC; ^{1}H NMR 300 MHz ($CDCl_3$): δ 3.70 (s, 3H, OCH_3), 3.80 (s, 3H, OCH_3), 5.20 (s, 2H, CH_2), 6.95 (d, *J* = 7.90 Hz 1H, H4''), 7.03-7.36 (m, 7H, H6, H8, H4', H2'', H3''', H4''', H5'''), 7.36-7.57 (m, 7H, H2', H5', H6', H5'', H6'', H2''', H6'''), 8.16 (d, *J* = 8.90 Hz, 1H, H5); FTIR (ATR) (cm^{-1}): 3066 (aromatic C-H st.), 2934, 2831 (aliphatic C-H st.), 1674 , 1624 (C=O st.), 1604, 1560, 1486 (C=C st.), 1445, 1377 (bending C-H), 1243, 1166, 1048 (C-O st.); EIMS: m/z (relative intensity) M^{+} 492.14(34.15), 463.09(42.70), 401.08(19.48), 385.20(10.48), 373.22(20.70), 294.08(8.73), 265.15 (4.21), 238.21(2.16), 159.14(17.43), 135.09(20.49), 107.11(7.00), 91.06(100.00), 77.09(16.74). TLC (silica gel GF 254, ethyl acetate/hexane [1:2]). R_f of compound **8** = 0.17, compound **8a** = 0.41.

11. 7-(3"'-Methoxy)benzyloxy-2-(3'-methoxy)phenyl-3-(3"-methoxy)-benzoyl chromone 8b.

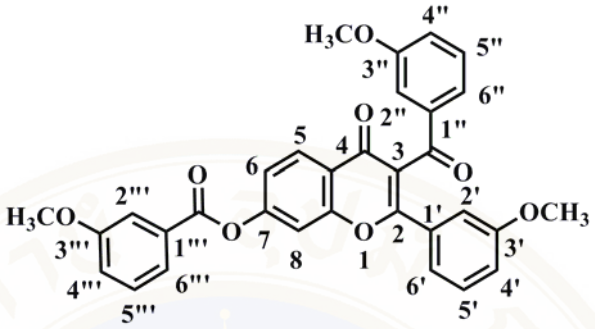

Compound **8b** was synthesized using the same procedure as described for compound **7a** from 3-methoxybenzyl chloride (0.56 mL, 4 mmol) and compound **8** (0.40 g, 1 mmol). After purification by column chromatography (ethyl acetate/hexane [1:2]), the desired compound **8b** was obtained as a white solid (53.1 mg, 10.16 %); m.p. 128-129 ºC; ^{1}H NMR 300 MHz ($CDCl_3$): δ 3.75 (s, 3H, OCH_3), 3.85 (s, 3H, OCH_3), 3.90 (s, 3H, OCH_3), 5.25 (s, 2H, CH_2), 6.93 (dd, *J* = 7.93, 2.18 Hz, 1H, H4'''), 6.95-7.00 (m, 1H, H4"), 7.04 (dd, *J* = 7.93, 2.18 Hz, 1H, H6'''), 7.00-7.20 (m, 2H, H8, H2'''), 7.10 (dd, *J* = 8.05, 2.49 Hz, 1H, H4'), 7.13 (dd, *J* = 8.83, 2.38 Hz, 1H, H6), 7.17 (d, *J* = 2.18 Hz, 1H, H2"), 7.20-7.40 (m, 2H, H5", H6"), 7.34 (t, *J* = 8.05 Hz, 1H, H5'), 7.36 (t, *J* = 7.93 Hz, 1H, H5'''), 7.49 (d, *J* = 8.05 Hz, 1H, H6'), 7.53 (d, *J* = 2.49 Hz, 1H, H2'), 8.17 (d, *J* = 8.83 Hz, 1H, H5); FTIR (ATR) (cm^{-1}): 3069 (aromatic C-H st.), 2940, 2834 (aliphatic C-H st.), 1674, 1624 (C=O st.), 1600, 1497 (C=C st.), 1439, 1377 (bending C-H), 1268, 1168, 1044 (C-O st.); EIMS: m/z (relative intensity) M^{+} 522.15(28.03), 493.29(17.20), 415.19(14.49), 401.20(16.38), 373.18(16.43), 295.18 (5.72), 266.17(3.44), 238.29(3.50), 159.08(17.66), 135.17(21.03), 121.09(100.00), 107.08(13.03), 91.09(55.47), 77.04(38.33). TLC (silica gel GF 254, ethyl acetate/ hexane [1:2]). R_f of compound **8** = 0.17, compound **8b** = 0.31.

12. 7-Benzoate-2-(3'-methoxy)phenyl-3-(3"-methoxy)benzoyl-chromone 8d.

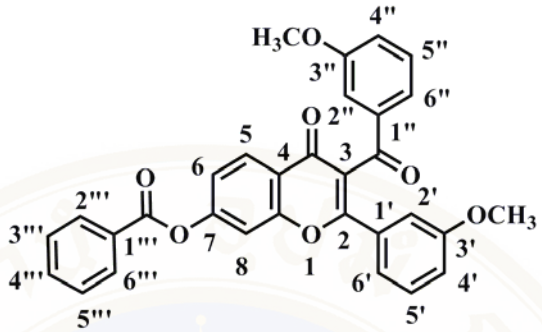

Compound **8d** was synthesized using the same procedure as described for compound **7d** from benzoyl chloride (0.24 mL, 2 mmol) and compound **8** (0.40 g, 1 mmol). After purification by column chromatography (ethyl acetate/hexane [1:2]), the desired compound **8d** was obtained as a white solid (129.9 mg, 25.38 %); m.p. 124-125 ºC; ^{1}H NMR 300 MHz ($CDCl_3$): δ 3.70 (s, 3H, OCH_3), 3.85 (s, 3H, OCH_3), 6.95-7.02 (m, 1H, H4"), 7.12 (dd, *J* = 8.20, 2.59 Hz, 1H, H4'), 7.20 (d, *J* = 1.87 Hz, 1H, H2"), 7.22-7.40 (m, 4H, H6, H5', H5", H6"), 7.46-7.64 (m, 5H, H8, H2', H6', H3"', H5"'), 7.72 (t, *J* = 7.36 Hz, 1H, H4"'), 8.26 (d, *J* = 7.56 Hz, 2H, H2"', H6"'), 8.34 (d, *J* = 8.72 Hz, 1H, H5); FTIR (ATR) (cm^{-1}): 3066 (aromatic C-H st.), 2937, 2834 (aliphatic C-H st.), 1739, 1674, 1636 (C=O st.), 1618, 1565, 1486 (C=C st.), 1436 (bending C-H), 1259, 1147, 1050 (C-O st.); EIMS: m/z (relative intensity) M^+ 506.12(50.91), 477.10(52.96), 475.17(2.43), 401.17(9.04), 373.26(8.92), 344.20 (2.03), 266.24(3.00), 135.19(8.77), 105.06(100.00), 77.06(79.55). TLC (silica gel GF 254, ethyl acetate /hexane [1:2]). R_f of compound **8** = 0.17, compound **8d** = 0.51.

13. 7-(3"'-Methoxy)benzoate-2-(3'-methoxy)phenyl-3-(3"-methoxy)-benzoyl chromone 8e.

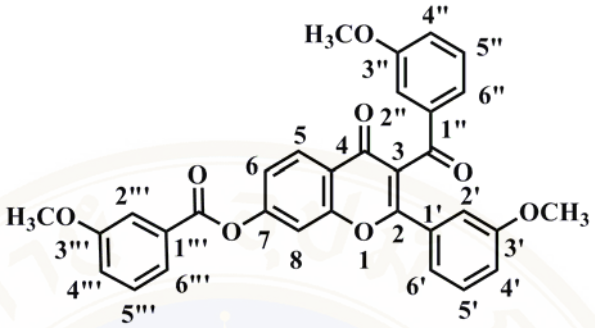

Compound **8e** was synthesized using the same procedure as described for compound **7d** from 3-methoxybenzoyl chloride (0.28 mL, 2 mmol) and compound **8** (0.40 g, 1 mmol). After purification by column chromatography (ethyl acetate/hexane [1:2]), the desired compound **8e** was obtained as a white solid (167.2 mg, 31.19 %); m.p. 143-144 ºC; ^{1}H NMR 300 MHz ($CDCl_3$): δ 3.75 (s, 3H, OCH_3), 3.85 (s, 3H, OCH_3), 3.95 (s, 3H, OCH_3), 6.96-7.01 (m, 1H, H4"), 7.11 (dd, *J* = 8.07, 2.39 Hz, 1H, H4'), 7.19 (d, *J* = 2.12 Hz, 1H, H2"), 7.22-7.39 (m, 5H, H6, H5', H5", H6", H4"'), 7.44-7.56 (m, 3H, H2', H6', H5"'), 7.59 (d, *J* = 2.10 Hz, 1H, H8), 7.74 (d, *J* = 2.18 Hz, 1H, H2"'), 7.86 (d, *J* = 7.66 Hz, 1H, H6"'), 8.32 (d, *J* = 8.69 Hz, 1H, H5); FTIR (ATR) (cm^{-1}): 3072 (aromatic C-H st.), 2940, 2834 (aliphatic C-H st.), 1739, 1674, 1636 (C=O st.), 1615, 1565, 1486 (C=C st.), 1433 (bending C-H), 1271, 1147, 1041 (C-O st.); EIMS: m/z (relative intensity) M^+ 536.13(40.60), 507.21(26.46), 429.06(4.85), 401.13(6.70), 373.20 (10.00), 344.16(1.35), 295.24(0.90), 159.09(6.37), 135.09 (100.00), 107.06(38.07), 77.04(46.08). Anal. Calcd. for $C_{32}H_{24}O_8$ (536.53): C, 71.64; H, 4.51. Found: C, 72.09; H, 4.49. TLC (silica gel GF 254, ethyl acetate/ hexane [1:2]). R_f of compound **8** = 0.17, compound **8e** = 0.51.

14. 7-(4"'-Methoxy)benzoate-2-(3'-methoxy)phenyl-3-(3"-methoxy)-benzoyl chromone 8f.

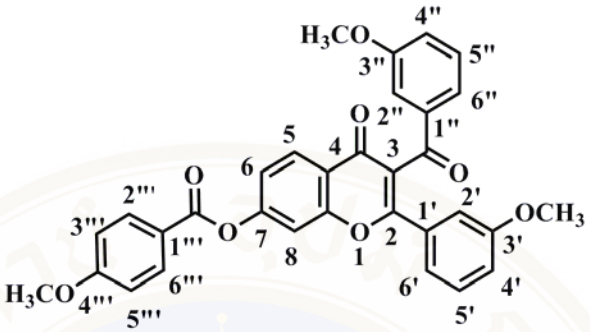

Compound **8f** was synthesized using the same procedure as described for compound **7d** from 4-methoxybenzoyl chloride (0.28 mL, 2 mmol) and compound **8** (0.40 g, 1 mmol). After purification by column chromatography (ethyl acetate/hexane [1:2]), the desired compound **8f** was obtained as a white solid (153.2 mg, 28.54 %); m.p. 123-124 ºC; ^{1}H NMR 300 MHz ($CDCl_3$): δ 3.75 (s, 3H, OCH_3), 3.85 (s, 3H, OCH_3), 3.95 (s, 3H, OCH_3), 6.95-7.01 (m, 1H, H4"), 7.04 (d, *J* = 8.78 Hz, 2H, H3"', H5"'), 7.11 (dd, *J* = 8.06, 2.41Hz, 1H, H4'), 7.19 (d, *J* = 1.99 Hz, 1H, H2"), 7.22-7.38 (m, 4H, H6, H5', H5", H6"), 7.49 (d, *J* = 7.71 Hz, 1H, H6'), 7.54 (s, 1H, H2'), 7.59 (d, *J* = 2.06 Hz, 1H, H8), 8.21 (d, *J* = 8.78 Hz, 2H, H2"', H6"'), 8.31 (d, *J* = 8.68 Hz, 1H, H5); FTIR (ATR) (cm^{-1}): 3072 (aromatic C-H st.), 2937, 2834 (aliphatic C-H st.), 1733, 1671, 1633 (C=O st.), 1600, 1568, 1509, 1483 (C=C st.), 1436 (bending C-H), 1262, 1150, 1053 (C-O st.); EIMS: m/z (relative intensity) M^+ 536.10(13.88), 507.17(3.04), 401.18(1.96), 373.23(4.72), 295.16(0.59), 265.17(0.72), 159.12(2.51), 135.08(100.00), 107.13(11.64), 77.14(23.82). TLC (silica gel GF 254, ethyl acetate /hexane [1:2]). R_f of compound **8** = 0.17, compound **8f** = 0.40.

15. 7-(3"'-Methoxy)benzyloxy-2-(4'-methoxy)phenyl-3-(4"-methoxy)-benzoyl chromone 9b.

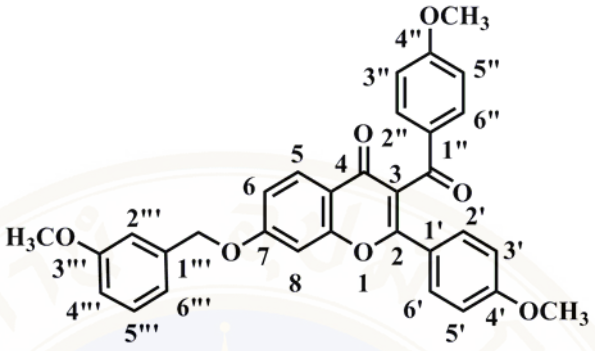

Compound **9b** was synthesized using the same procedure as described for compound **7d** from 3-methoxybenzyl chloride (0.44 mL, 4 mmol) and compound **9** (0.34 g, 1 mmol). After purification by column chromatography (ethyl acetate/hexane [1:2]), the desired compound **9b** was obtained as a white solid (25.9 mg, 4.95 %); m.p. 170-171 ºC; ^{1}H NMR 300 MHz ($CDCl_3$): δ 3.80 (s, 3H, OCH_3), 3.85 (s, 3H, OCH_3), 3.85 (s, 3H, OCH_3), 5.20 (s, 2H, CH_2), 6.82-6.98 (m, 5H, H6, H8, H2"', H4"', H6"'), 7.00-7.15 (m, 4H, H3', H5', H3", H5"), 7.37 (t, *J* = 7.86 Hz, 1H, H5"'), 7.64 (d, *J* = 8.95 Hz, 2H, H2", H6"), 7.93 (d, *J* = 8.94 Hz, 2H, H2', H6'), 8.16 (d, *J* = 8.86 Hz, 1H, H5); FTIR (ATR) (cm^{-1}): 3072 (aromatic C-H st.), 2957, 2834 (aliphatic C-H st.), 1665, 1621 (C=O st.), 1600, 1509 (C=C st.), 1442 (bending C-H), 1256, 1182, 1026 (C-O st.); EIMS: m/z (relative intensity) M^+ 522.00(77.68), 493.14(30.63), 401.08 (31.83), 387.12(4.90), 373.13(51.75), 294.07(43.21), 266.09(6.53), 238.09(3.94), 159.15(15.99), 135.18(71.10), 121.10(100.00), 107.11(8.65), 91.07(74.81), 77.06 (59.26). TLC (silica gel GF 254, ethyl acetate/hexane [1:2]). R_f of compound **9** = 0.08, compound **9b** = 0.20.

16. 7-Benzoate-2-(4'-methoxy)phenyl-3-(4''-methoxy)benzoyl-chromone 9d.

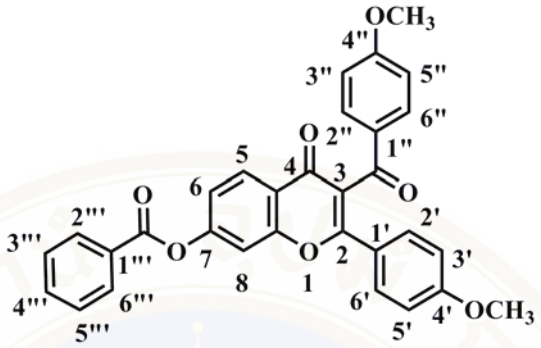

Compound **9d** was synthesized using the same procedure as described for compound **7d** from benzoyl chloride (0.24 mL, 2 mmol) and compound **9** (0.40 g, 1 mmol). After purification by column chromatography (ethyl acetate/hexane [1:2]), the desired compound **9d** was obtained as a white solid (125.1 mg, 24.67 %); m.p. 120-121 ºC; ^{1}H NMR 300 MHz ($CDCl_3$): δ 3.80 (s, 3H, OCH_3), 3.90 (s, 3H, OCH_3), 6.83-6.94 (m, 4H, H3', H5', H3'', H5''), 7.33 (dd, *J* = 8.70, 2.07 Hz, 1H, H6), 7.53-7.62 (m, 3H, H8, H3''', H5'''), 7.62-7.75 (m, 3H, H2'', H6'', H4'''), 7.93 (d, *J* = 8.66 Hz, 2H, H2', H6'), 8.26 (d, *J* = 8.07 Hz, 2H, H2''', H6'''), 8.32 (d, *J* = 8.70 Hz, 1H, H5); FTIR (ATR) (cm^{-1}): 3072 (aromatic C-H st.), 2960, 2837 (aliphatic C-H st.), 1739, 1665, 1636 (C=O st.), 1574, 1509 (C=C st.), 1439 (bending C-H), 1256, 1177, 1024 (C-O st.); EIMS: m/z (relative intensity) M^+ 506.19(22.12), 477.02(10.09), 475.09 (1.30), 401.18(5.38), 373.21(6.41), 344.04(1.51), 266.16(5.98), 238.20(3.31), 159.10(4.81), 135.07(36.06), 105.03(100.00), 77.02(83.37). Anal. Calcd. for $C_{31}H_{22}O_7.0.75H_2O$ (520.02): C, 71.60; H, 4.26. Found: C, 71.65; H, 3.95. TLC (silica gel GF 254, ethyl acetate/hexane [1:2]). R_f of compound **9** = 0.08, compound **9d** = 0.40.

17. 7-(3"'-Methoxy)benzoate-2-(4'-methoxy)phenyl-3-(4"-methoxy)-benzoyl chromone 9e.

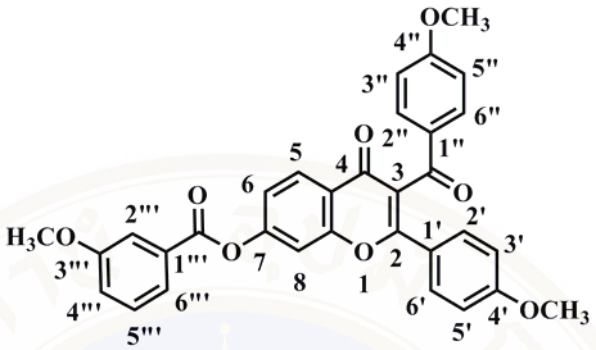

Compound **9e** was synthesized using the same procedure as described for compound **7d** from 3-methoxybenzoyl chloride (0.28 mL, 2 mmol) and compound **9** (0.40 g, 1 mmol). After purification by column chromatography (ethyl acetate/hexane [1:2]), the desired compound **9e** was obtained as a white solid (103.0 mg, 19.21 %); m.p. 144-145 ºC; ^{1}H NMR 300 MHz ($CDCl_3$): δ 3.80 (s, 3H, OCH_3), 3.85 (s, 3H, OCH_3), 3.90 (s, 3H, OCH_3), 6.85-6.95 (m, 4H, H3', H5', H3", H5"), 7.25 (dd, *J* = 7.87, 2.15 Hz, 1H, H4"'), 7.33 (dd, *J* = 8.70, 2.10 Hz, 1H, H6), 7.48 (t, *J* = 7.87 Hz, 1H, H5"'), 7.56 (d, *J* = 2.10 Hz, 1H, H8), 7.66 (d, *J* = 8.89 Hz, 2H, H2", H6"), 7.75 (t, *J* = 2.15 Hz, 1H, H2"'), 7.86 (d, *J* = 7.87 Hz, 1H, H6"'), 7.93 (d, *J* = 8.84 Hz, 2H, H2', H6'), 8.32 (d, *J* = 8.70 Hz, 1H, H5); FTIR (ATR) (cm^{-1}): 3075 (aromatic C-H st.), 2960, 2837 (aliphatic C-H st.), 1739, 1668, 1633 (C=O st.), 1574, 1509 (C=C st.), 1436 (bending C-H), 1262, 1177, 1029 (C-O st.); EIMS: m/z (relative intensity) M^+ 536.10(39.27), 507.22(11.48), 401.14(8.23), 373.19(9.93), 266.18(2.89), 238.28(1.52), 135.09(100.00), 107.08(25.24), 77.05(27.83). Anal. Calcd. for $C_{32}H_{24}O_8$ (536.53): C, 71.64; H, 4.51. Found: C, 72.10; H, 4.40. TLC (silica gel GF 254, ethyl acetate/hexane [1:2]). R_f of compound **9** = 0.08, compound **9e** = 0.34.

18. 7-(4"'-Methoxy)benzoate-2-(4'-methoxy)phenyl-3-(4"- methoxy)-benzoyl chromone 9f.

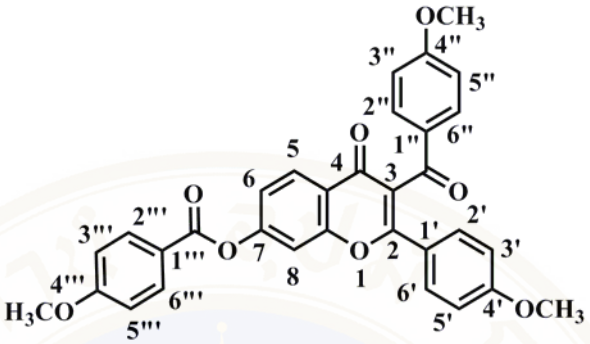

Compound **9f** was synthesized using the same procedure as described for compound **7d** from 4-methoxybenzoyl chloride (0.28 mL, 2 mmol) and compound **9** (0.40 g, 1 mmol). After purification by column chromatography (ethyl acetate/hexane [1:2]), the desired compound **9f** was obtained as a white solid (108.3 mg, 20.18 %); m.p. 167-168 ºC; ^{1}H NMR 300 MHz ($CDCl_3$): δ 3.80 (s, 3H, OCH_3), 3.85 (s, 3H, OCH_3), 3.95 (s, 3H, OCH_3), 6.85-6.94 (m, 4H, H3', H5', H3", H5"), 7.05 (d, *J* = 8.90 Hz, 2H, H3"', H5"'), 7.33 (dd, *J* = 8.74, 2.10 Hz, 1H, H6), 7.56 (d, *J* = 2.10 Hz, 1H, H8), 7.66 (d, *J* = 8.90 Hz, 2H, H2", H6"), 7.93 (d, *J* = 8.85 Hz, 2H, H2', H6'), 8.21 (d, *J* = 8.90 Hz, 2H, H2"', H6"'), 8.30 (d, *J* = 8.74 Hz, 1H, H5); FTIR (ATR) (cm^{-1}): 3075 (aromatic C-H st.), 2963, 2837 (aliphatic C-H st.), 1733, 1665, 1606 (C=O st.), 1577, 1509 (C=C st.), 1440 (bending C-H), 1256, 1163, 1026 (C-O st.); EIMS: m/z (relative intensity) M^+ 536.08(10.35), 507.12(0.46), 401.96(3.21), 373.23(3.84), 295.08(0.76), 266.18(0.68), 239.20(2.11), 135.08(100.00), 107.13(8.39), 77.02(18.71). Anal. Calcd. for $C_{32}H_{24}O_8.3H_2O$ (590.58): C, 65.08; H, 4.10. Found: C, 65.18; H, 4.18. TLC (silica gel GF 254, ethyl acetate/hexane [1:2]). R_f of compound **9** = 0.08, compound **9f** = 0.28.

19. 7-Benzoate-2-(4'-nitro)phenyl-3-(4"-nitro)benzoyl chromone 11b.

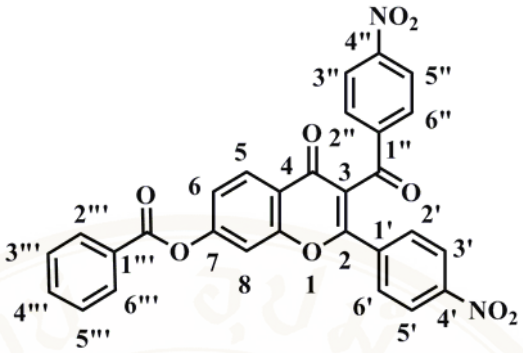

Compound **11b** was synthesized using the same procedure as described for compound **7d** from benzoyl chloride (0.24 mL, 2 mmol) and compound **11** (0.40 g, 1 mmol). After purification by column chromatography (ethyl acetate/hexane [1:2]), the desired compound **11b** was obtained as a yellow solid (58.1 mg, 10.82 %); m.p. 255-256 ºC; ^{1}H NMR 300 MHz ($CDCl_3$): δ 7.45 (dd, *J* = 8.72, 2.03 Hz, 1H ,H6), 7.60 (t, *J* = 8.00, 2H, H3"', H5"'), 7.67 (d, *J* = 2.03, 1H, H8), 7.74 (t, *J* = 8.00, 1H, H4"'), 7.84 (d, *J* = 8.00, 2H, H2"', H6"'), 8.11 (d, *J* = 8.79, 2H, H3", H5"), 8.23-8.39 (m, 7H, H5, H2', H3', H5', H6', H2", H6"); FTIR (ATR) (cm^{-1}): 3108 (aromatic C-H st.), 1742, 1680, 1639 (C=O st.), 1618, 1521 (C=C st.), 1439 (bending C-H), 1344 (C-N st.), 1256, 1109, 1053 (C-O st.); EIMS: m/z (relative intensity) M^{+}-133 403.05(7.86), M^{+} 357.11(3.30), 311.20(1.82), 283.13(1.22), 255.23(1.36), 226.21(3.06), 150.11(12.06), 105.06 (100.00), 77.07(39.97). TLC (silica gel GF 254, ethyl acetate/hexane [1:2]). R_f of compound **11** = 0.21, compound **11b** = 0.51.

20. 7-(3"'-Nitro)benzoate-2-(4'-nitro)phenyl-3-(4"-nitro)benzoyl chromone 11c.

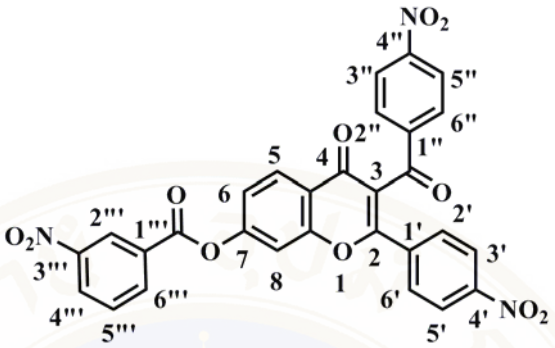

Compound **11c** was synthesized using the same procedure as described for compound **7d** from 3-nitrobenzoyl chloride (0.74 g, 4 mmol) and compound **11** (0.43 g, 1 mmol). After purification by column chromatography (ethyl acetate/hexane [1:2]), the desired compound **11c** was obtained as a yellow solid (453.9 mg, 77.82 %); m.p. 248-249 ºC; ^{1}H NMR 300 MHz ($CDCl_3$): δ 7.48 (dd, *J* = 8.72, 2.10 Hz, 1H ,H6), 7.69 (d, *J* = 2.10 Hz, 1H, H8), 7.78-7.89 (m, 3H, H2", H6", H5"'), 8.11 (d, *J* = 8.88 Hz, 2H, H3", H5"), 8.26-8.40 (m, 5H, H5, H2', H3', H5', H6'), 8.60 (d, *J* = 8.05 Hz, 2H, H4"', H6"'), 9.11 (s, 1H, H2"'); FTIR (ATR) (cm^{-1}): 3102 (aromatic C-H st.), 1748, 1680, 1639 (C=O st.), 1615, 1521 (C=C st.), 1436 (bending C-H), 1344 (C-N st.), 1247, 1112, 1056 (C-O st.); EIMS: m/z (relative intensity) M^+ 581.05(3.67), 552.07(10.23), 402.98(100.00), 357.12(26.44), 311.15(13.04), 236.13(7.79), 150.06(91.18), 104.09(32.19), 76.08 (25.93). Anal. Calcd. for $C_{29}H_{15}N_3O_{11}.4H_2O$ (653.50): C, 53.30; H, 2.31; N, 6.43. Found: C, 53.12; H, 2.30; N 6.25. TLC (silica gel GF 254, ethyl acetate/hexane [1:2]). R_f of compound **11** = 0.21, compound **11c** = 0.60.

CHAPTER V
BIOLOGICAL EXPERIMENTAL

A. Equipment and chemicals

1. Equipments

Analytical balance model CP225D	Sartorius, Germany
Camptothecin	Topogen, USA
Electrophoresis cell	Beijing liuyi, China
Electrophoresis power supply	GE healthcare, UK
ImageMaster VDS CL	GE healthcare, UK
Microcentrifuge	ALC, Italy
Microcentrifuge tube 0.5 mL	Biologix, France
Micropipettes 0.1-2.5 µL, 0.5-10 µL, 2-20 µL	Biohit oyj, Finland
Micropipette 20-200 µL	Biohit oyj, Finland
Micropipette tips 10 µL, 200 µL	Biologix, France
Shaker	Taitec corporation, Japan
Vortex	Taitec corporation, Japan
Water bath	Stuart, UK

2. Chemicals

Agarose gel	Axygen biosciences, Spain
Dimethyl sulfoxide	Sigma, USA
EDTA	Sigma, USA
Ethidium bromide	Bio basic, Canada
Eukaryotic topoisomerase I drug screening kit	Topogen, USA
Glacial acetic acid	Lab scan, Thailand
Recombinant human topoisomerase I	Topogen, USA
Tris base	Fischer sciencetific, UK

3. Software

ImageQuant TL Amersham, UK

B. Methods

The ability of synthesized compounds to stabilize the formation of the DNA-TOP covalent binary complex was determined using eukaryotic TOP drug screening kit. Supercoiled DNA (125 ng) was incubated in the presence of TOP I (2.5 Units), TOP I assay buffer (1.5 µL) and synthesized compounds (with varying concentrations) at 37 ºC. After 30 minutes the reactions were terminated by adding 10% sodium dodecyl sulfate (0.1 volume), and digested with 0.5 mg/ml proteinase K at 37 ºC for 30 minutes. Gel loading buffer (1/10 volume) was added into the reaction mixture. Then DNA was separated by loading on 1% agarose gel. Relaxed DNA was included in the electrophoresis run as markers for DNA topology (Figure 5.1). CPT (100 µM) was used as positive control. Electrophoresis was conducted at 100 V for 1.5 hours in TAE buffer (Tris-acetate, EDTA, pH 8.0). After electrophoresis the gels were stained with 0.5 µg/ml ethidium bromide, and photographed under UV light. The amount of nicked DNA was calculated using ImageQuant TL (Image analysis software version 2003). All determinations were performed in triplicate. The IC_{50} values (the concentration of tested compound required to stabilize 50% of nicked DNA) were determined from the calibration curve plotted between inhibition percentage (relative to the intensity of the band produced by 100 µM CPT) and log samples concentration. The percentage of TOP I inhibition was calculated using the formula given below:

Inhibition (%) = (Amount of nicked DNA_{sample} x 100) / Amount of nicked $DNA_{control}$

where amount of nicked DNA_{sample} was calculated from the band produced by synthesized compound and amount of nicked $DNA_{control}$ was calculated from the band produced by 100 µM CPT.

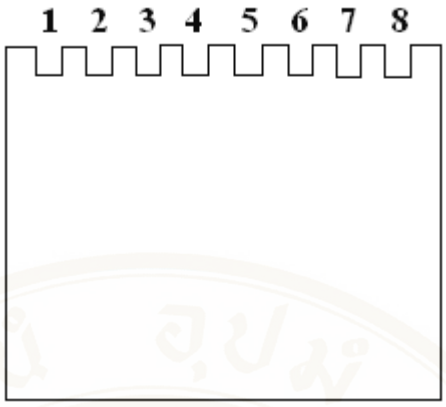

Lane	Substance
1-4	DNA supercoiled + enzyme + synthesized compound
5	Relaxed DNA
6	DNA supercoiled
7	DNA supercoiled + enzyme
8	DNA supercoiled + enzyme + CPT

Figure 5.1. Substance loading on agarose gel of gel electrophoresis.

Dimethyl sulfoxide (DMSO) at 5% final concentration was used as solvent. To ensure that DMSO was not affecting the activity of purify enzyme, the reactions containing DNA supercoiled and enzyme in the presence and absence DMSO were tested. The DNA cleavage pattern of both assay reactions was not different, consequently DMSO (5% final concentration) was suitable for this assay.

All compounds at the concentration of 20 μM, which is a cutoff value of the lowest soluble compound, were investigated for their inhibitory activities. Six compounds (compounds 7d, 7e, 7f, 8e, 11b and 11c) with the superior activity and solubility were selected for further evaluation of IC_{50} values.

CHAPTER VI
RESULTS AND DISCUSSION

A. Molecular modeling

Several flavonoids, for examples, myricetin, quercetin, fisetin, and morin demonstrated potent TOP I inhibition (82). In this study, the flavonoid-based structure, chromone derivatives, were subjected to docking simulation study for preliminary screening of TOP I inhibitory activity. Table 6.1 summarizes the result of the docking study presented as binding energy.

Table 6.1. Structures of chromone derivatives (compounds **1-12**) and their binding energy.

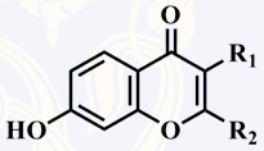

Compd	R_1	R_2	Binding energy (kcal/mole)
1	H	phenyl	-5.01
2	H	3'-(OCH_3)-phenyl	-5.81
3	H	4'-(OCH_3)-phenyl	-5.86
4	H	3'-(NO_2)-phenyl	-5.43
5	H	4'-(NO_2)-phenyl	-5.88
6	H	3',5'-(diNO_2)-phenyl	-5.90
7	benzoyl	phenyl	-5.97
8	3"-(OCH_3)-benzoyl	3'-(OCH_3)-phenyl	-6.16
9	4"-(OCH_3)-benzoyl	4'-(OCH_3)-phenyl	-6.68
10	3"-(NO_2)-benzoyl	3'-(NO_2)-phenyl	-7.09
11	4"-(NO_2)-benzoyl	4'-(NO_2)-phenyl	-6.36
12	3",5"-(diNO_2)-benzoyl	3',5'-(diNO_2)-phenyl	-7.14

As seen from Table 6.1, compounds with substitution at benzoyl (R_1) and phenyl (R_2) rings exhibited higher binding energy than unsubstituted ones. For example, compound **12** with R_1 = 3,5-dinitrobenzoyl and R_2 = 3,5-dinitrophenyl groups revealed better binding energy than compound **7**. To obtain tighter binding chromone derivatives, compounds **7-12** were used as starting template molecules for further structural modification by adding steric group at 7-OH group. The modified chromone structures and binding energy are shown in Table 6.2. Introduction of steric group at 7-OH led to higher binding energy. Compounds **7e**, **8e**, **9f**, **10d**, **11c** and **12c** possessed better binding energy values than their corresponding unmodified compounds (compounds **7-12**). Compound **11c** was the best dock ligand for TOP I with binding energy = -11.39 kcal/mole.

Based on this docking result, sixteen chromone derivatives, compounds **7a**, **7d-7g**, **8a-8b**, **8d-8f**, **9b**, **9d-9f**, **11b** and **11c** were synthesized and evaluated for their DNA TOP I inhibitory activity. Table 6.3 summarizes binding energy of these sixteen derivatives and the contacting amino acid residues of DNA TOP I obtained from the docking study. Amino acid residues located at the binding sites of DNA TOP I are Asn325, Arg364, Lys425, Tyr426, Met428, Lys436, Asp533, Thr718 and Asn722. Figure 6.1 showed the hydrogen bonding interactions between DNA TOP I and compounds **7d**, **7e**, **7f**, **8e**, **11b** and **11c**.

Table 6.2. Structures of the modified chromone derivatives (compounds in series 7-12) and their binding energy.

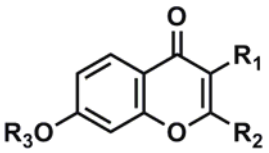

Compd	R_1	R_2	R_3	Binding energy (kcal/mole)
7a	benzoyl	phenyl	benzyl	-8.26
7b	benzoyl	phenyl	3‴-(OCH_3)-benzyl	-8.33
7c	benzoyl	phenyl	4‴-(OCH_3)-benzyl	-8.21
7d	benzoyl	phenyl	3‴-(OCH_3)-benzoyl	-8.77
7e	benzoyl	phenyl	4‴-(OCH_3)-benzoyl	-8.82
7f	benzoyl	phenyl	3‴-(NO_2)-benzoyl	-8.62
7g	benzoyl	phenyl	4‴-(NO_2)-benzoyl	-8.56
7h	benzoyl	phenyl	3‴,5‴-(diNO_2)-benzoyl	-7.25
8a	3″-(OCH_3)-benzoyl	3′-(OCH_3)-phenyl	benzyl	-7.62
8b	3″-(OCH_3)-benzoyl	3′-(OCH_3)-phenyl	3‴-(OCH_3)-benzyl	-7.50
8c	3″-(OCH_3)-benzoyl	3′-(OCH_3)-phenyl	4‴-(OCH_3)-benzyl	-7.64
8d	3″-(OCH_3) benzoyl	3′-(OCH_3)-phenyl	benzoyl	-8.42
8e	3″-(OCH_3)-benzoyl	3′-(OCH_3)-phenyl	3‴-(OCH_3)-benzoyl	-8.72
8f	3″-(OCH_3)-benzoyl	3′-(OCH_3)-phenyl	4‴-(OCH_3)-benzoyl	-6.91
9a	4″-(OCH_3)-benzoyl	4′-(OCH_3)-phenyl	benzyl	-7.50
9b	4″-(OCH_3)-benzoyl	4′-(OCH_3)-phenyl	3‴-(OCH_3)-benzyl	-7.95
9c	4″-(OCH_3)-benzoyl	4′-(OCH_3)-phenyl	4‴-(OCH_3)-benzyl	-7.86
9d	4″-(OCH_3)-benzoyl	4′-(OCH_3)-phenyl	benzoyl	-8.11
9e	4″-(OCH_3)-benzoyl	4′-(OCH_3)-phenyl	3‴-(OCH_3)-benzoyl	-7.97
9f	4″-(OCH_3)-benzoyl	4′-(OCH_3)-phenyl	4‴-(OCH_3)-benzoyl	-8.93
10a	3″-(NO_2)-benzoyl	3′-(NO_2)-phenyl	benzyl	-7.30
10b	3″-(NO_2)-benzoyl	3′-(NO_2)-phenyl	benzoyl	-7.70
10c	3″-(NO_2)-benzoyl	3′-(NO_2)-phenyl	3‴-(NO_2)-benzoyl	-9.35
10d	3″-(NO_2)-benzoyl	3′-(NO_2)-phenyl	4‴-(NO_2)-benzoyl	-9.39
10e	3″-(NO_2)-benzoyl	3′-(NO_2)-phenyl	3‴,5‴-(diNO_2)-benzoyl	-6.94
11a	4″-(NO_2)-benzoyl	4′-(NO_2)-phenyl	benzyl	-8.81
11b	4″-(NO_2)-benzoyl	4′-(NO_2)-phenyl	benzoyl	-9.29
11c	4″-(NO_2)-benzoyl	4′-(NO_2)-phenyl	3‴-(NO_2)-benzoyl	-11.39
11d	4″-(NO_2)-benzoyl	4′-(NO_2)-phenyl	4‴-(NO_2)-benzoyl	-10.54
11e	4″-(NO_2)-benzoyl	4′-(NO_2)-phenyl	3‴,5‴-(diNO_2)-benzoyl	-6.67
12a	3″,5″-(diNO_2)-benzoyl	3′,5′-(diNO_2)-phenyl	benzyl	-6.92
12b	3″,5″-(diNO_2)-benzoyl	3′,5′-(diNO_2)-phenyl	benzoyl	-6.75
12c	3″,5″-(diNO_2)-benzoyl	3′,5′-(diNO_2)-phenyl	3‴-(NO_2)-benzoyl	-8.87
12d	3″,5″-(diNO_2)-benzoyl	3′,5′-(diNO_2)-phenyl	4‴-(NO_2)-benzoyl	-7.56
12e	3″,5″-(diNO_2)-benzoyl	3′,5′-(diNO_2)-phenyl	3‴,5‴-(diNO_2)-benzoyl	-5.56

Table 6.3. Binding energy and the contacting amino acid residues of DNA TOP I from docking study.

Compd	Binding energy (kcal/mole)	Contacting amino acid residues
7a	-8.26	Arg364
7d	-8.77	Arg364
7e	-8.82	Arg364
7f	-8.62	Arg364
7g	-8.56	Arg364
8a	-7.62	Arg364
8b	-7.50	Arg364, Met428
8d	-8.42	Arg364, Lys425
8e	-8.72	Arg364, Lys425, Tyr426
8f	-6.91	Lys425
9b	-7.95	Arg364, Met428
9d	-8.11	Asp533
9e	-7.97	Arg364, Met428
9f	-8.93	Arg364, Lys425, Met428, Asn722
11b	-9.29	Arg364, Met428
11c	-11.39	Arg364, Lys425, Thr718

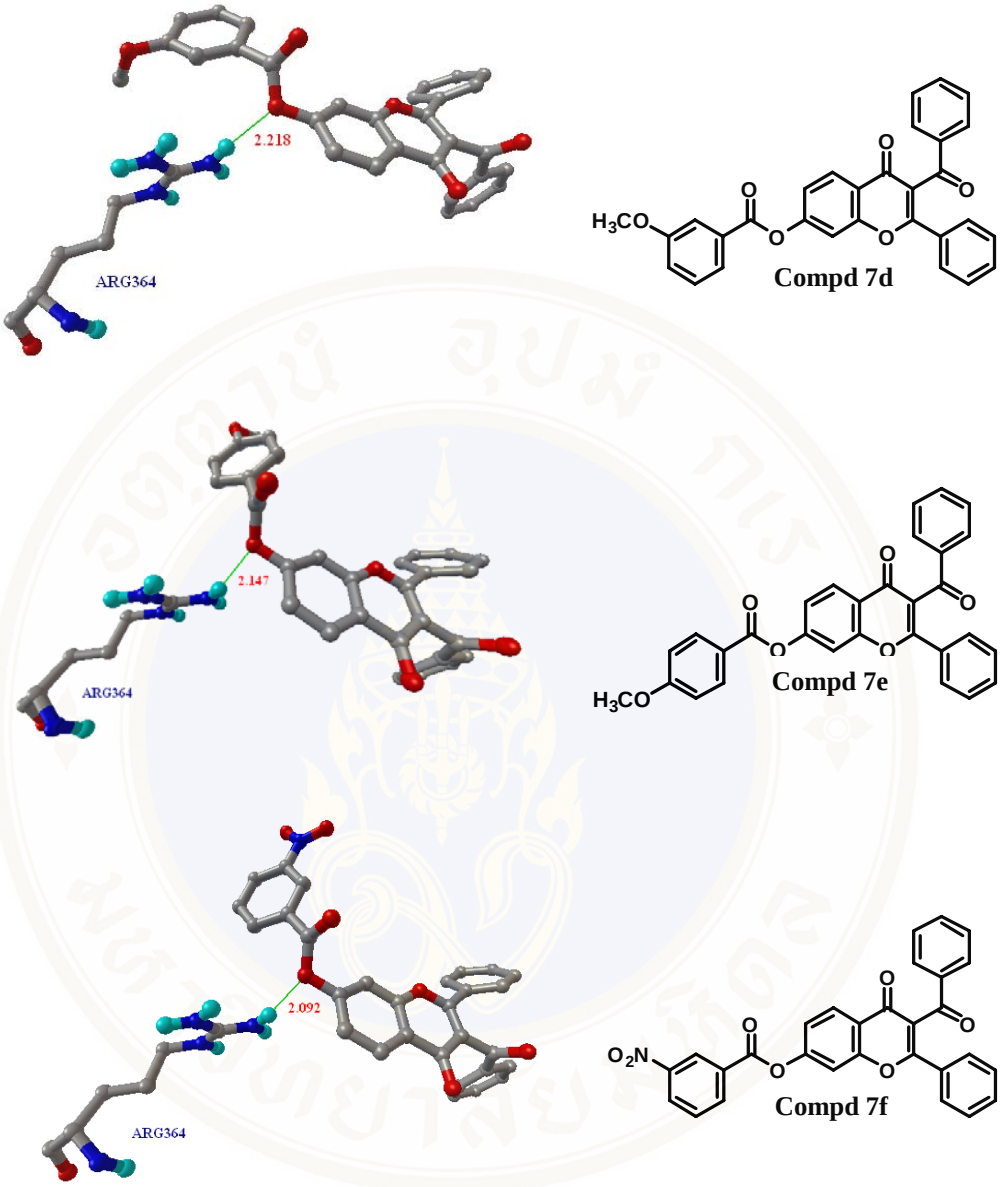

Figure 6.1. Hydrogen bonding interaction between DNA TOP I (1T8I) and compounds **7d**, **7e**, **7f**, **8e**, **11b** and **11c**.

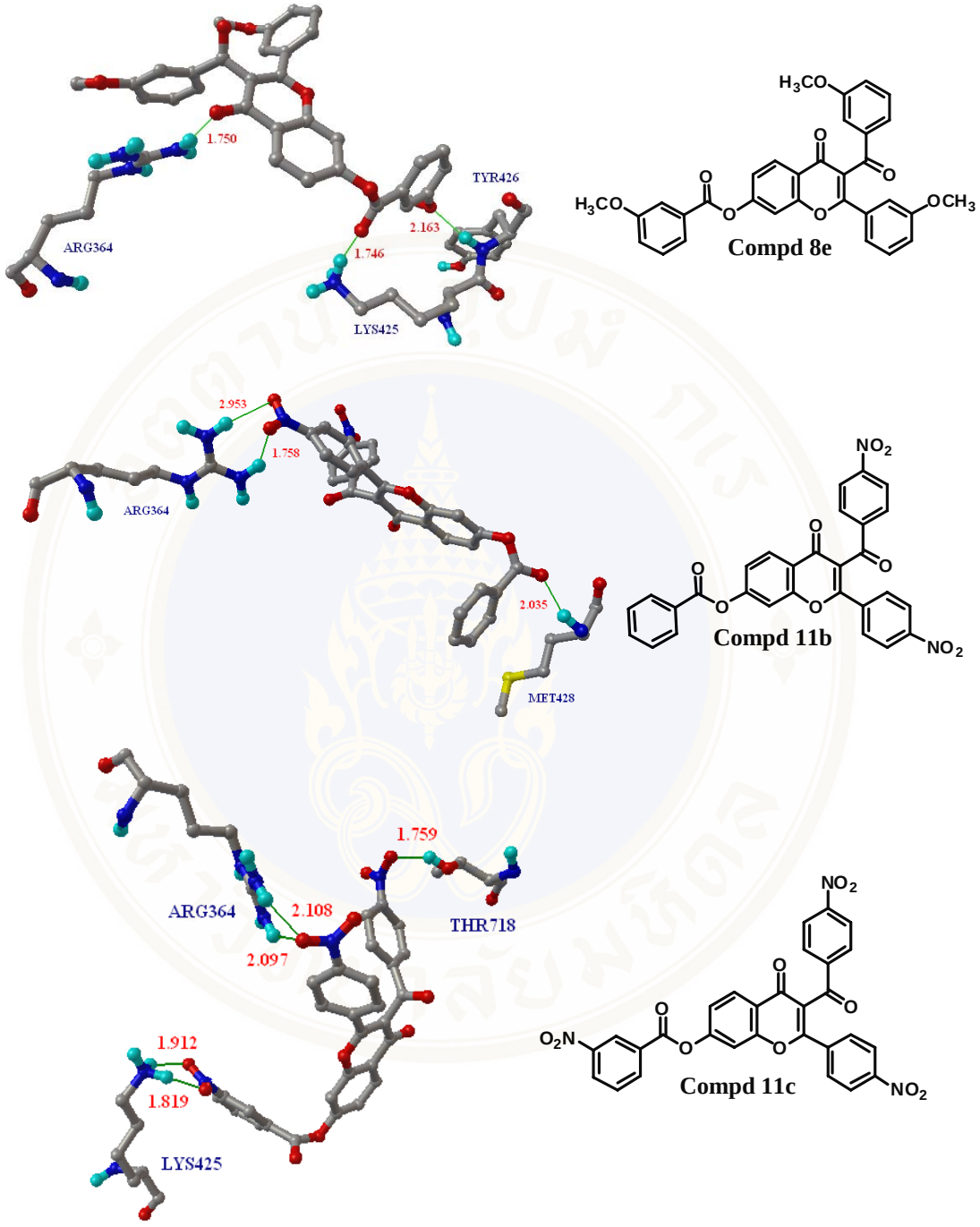

Figure 6.1. Hydrogen bonding interaction between DNA TOP I (1T8I) and compounds **7d**, **7e**, **7f**, **8e**, **11b** and **11c** (cont.).

B. Synthesis

The synthetic pathway was carried out in two main steps. The first step was the one-pot cyclization. The second step was for adding steric group to the chromone via esterification or etherification (O-alkylation) reaction. The synthetic pathway of substituted chromone compounds is outlined in Figure 6.2. The commercially available phenolic ketones reacted with aroyl chloride in the presence of 1,8-diazabicyclo[5,4,0]undec-7-ene (DBU) to generate the intermediate substituted chromone esters intermediates in one step. These intermediates were then submitted to hydrolysis to yield the desired chromone compounds.

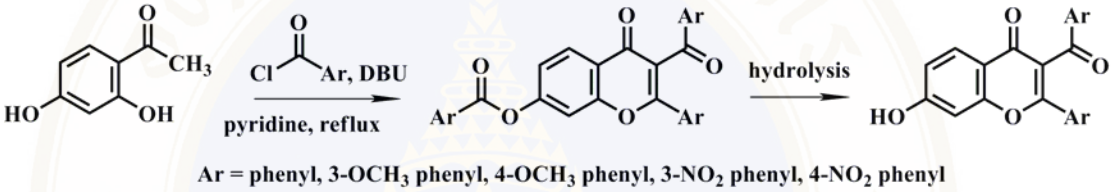

Figure 6.2. Synthesis of chromone derivatives.

Addition of steric group at 7-OH of chromones was performed via esterification or Williamson etherification. Esterification of chromone derivatives with the appropriate acid chloride provided the chromone compounds **7d-7g**, **8d-8f**, **9d-9f**, **11b** and **11c** (Figure 6.3). Etherification was carried out by using substituted benzyl chloride (outline as shown in Figure 6.4), giving compounds **7a**, **8a**, **8b** and **9b**.

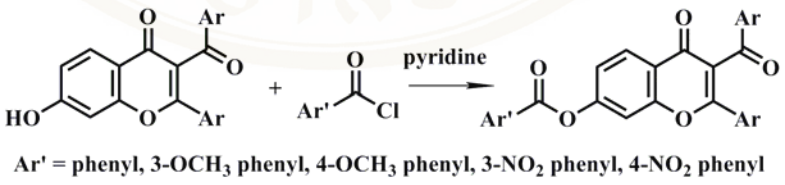

Figure 6.3. Esterification of chromone derivatives.

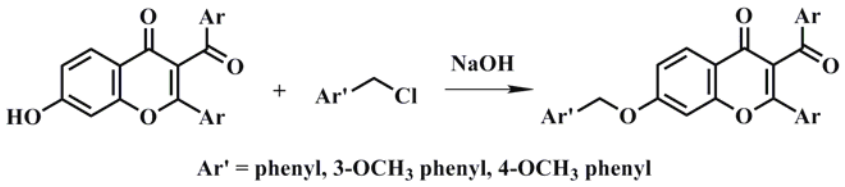

Figure 6.4. The Williamson ether synthesis of chromone derivatives.

Melting point and % yield of synthesized compounds were summarized in Table 6.4.

Table 6.4. Melting point (m.p.) and % yield of chromome derivatives.

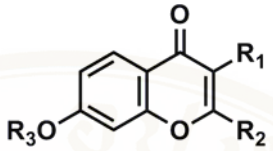

Compd	R_1	R_2	R_3	m.p. (ºC)	% yield
7a	benzoyl	phenyl	benzyl	129-130	11.13
7d	benzoyl	phenyl	3'''-(OCH_3)-benzoyl	145-146	73.76
7e	benzoyl	phenyl	4'''-(OCH_3)-benzoyl	144-145	61.60
7f	benzoyl	phenyl	3'''-(NO_2)-benzoyl	174-175	18.07
7g	benzoyl	phenyl	4'''-(NO_2)-benzoyl	220-221	35.75
8a	3''-(OCH_3)-benzoyl	3'-(OCH_3)-phenyl	benzyl	163-164	19.17
8b	3''-(OCH_3)-benzoyl	3'-(OCH_3)-phenyl	3'''-(OCH_3)-benzyl	128-129	10.16
8d	3''-(OCH_3)-benzoyl	3'-(OCH_3)-phenyl	benzoyl	124-125	25.38
8e	3''-(OCH_3)-benzoyl	3'-(OCH_3)-phenyl	3'''-(OCH_3)-benzoyl	143-144	31.19
8f	3''-(OCH_3)-benzoyl	3'-(OCH_3)-phenyl	4'''-(OCH_3)-benzoyl	123-124	28.54
9b	4''-(OCH_3)-benzoyl	4'-(OCH_3)-phenyl	3'''-(OCH_3)-benzyl	170-171	18.48
9d	4''-(OCH_3)-benzoyl	4'-(OCH_3)-phenyl	benzoyl	120-121	24.67
9e	4''-(OCH_3)-benzoyl	4'-(OCH_3)-phenyl	3'''-(OCH_3)-benzoyl	144-145	19.21
9f	4''-(OCH_3)-benzoyl	4'-(OCH_3)-phenyl	4'''-(OCH_3)-benzoyl	167-168	20.18
11b	4''-(NO_2)-benzoyl	4'-(NO_2)-phenyl	benzoyl	255-256	10.82
11c	4''-(NO_2)-benzoyl	4'-(NO_2)-phenyl	3'''-(NO_2)-benzoyl	248-249	77.82

The IR spectrum of the obtained ether linkage chromone derivatives showed the similar pattern e.g., IR spectrum of compound **8b** (Figure 6.5) showed the frequency of aromatic C-H stretching at 3069 cm^{-1}, aliphatic C-H stretching at 2940 and 2834 cm^{-1}, carbonyl C=O stretching at 1674 and 1624 cm^{-1}, C=C stretching at 1600 and 1497 cm^{-1}.

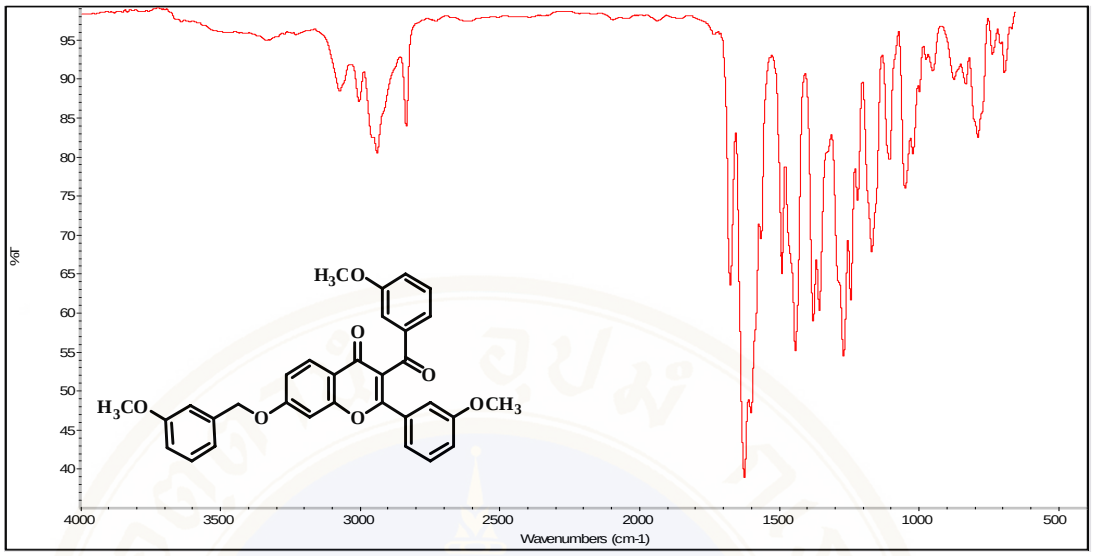

Figure 6.5. IR spectrum of compound **8b**.

The ^{1}H NMR and ^{1}H-^{1}H COSY spectrum are shown in Figures 6.6 and 6.7. Table 6.5 summarizes the details of ^{1}H NMR data and ^{1}H-^{1}H correlation of compound **8b**.

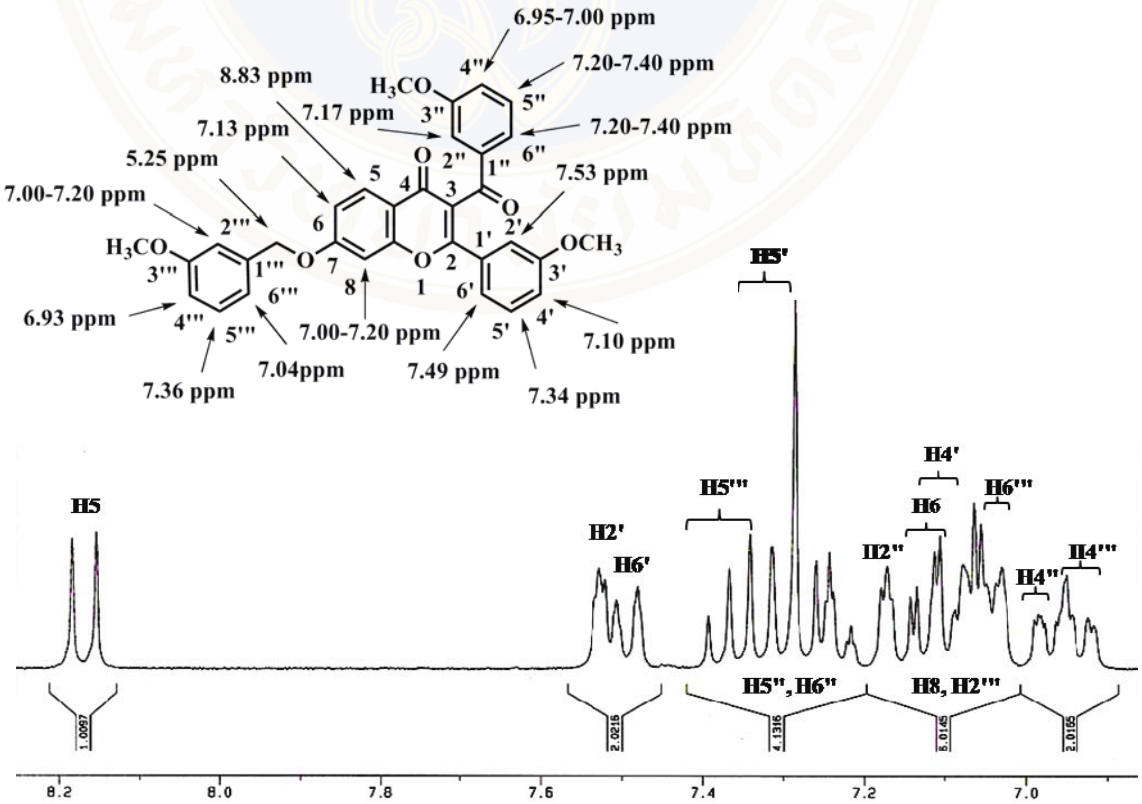

Figure 6.6. ^{1}H NMR spectra (300 MHz, $CDCl_3$) of compound **8b**.

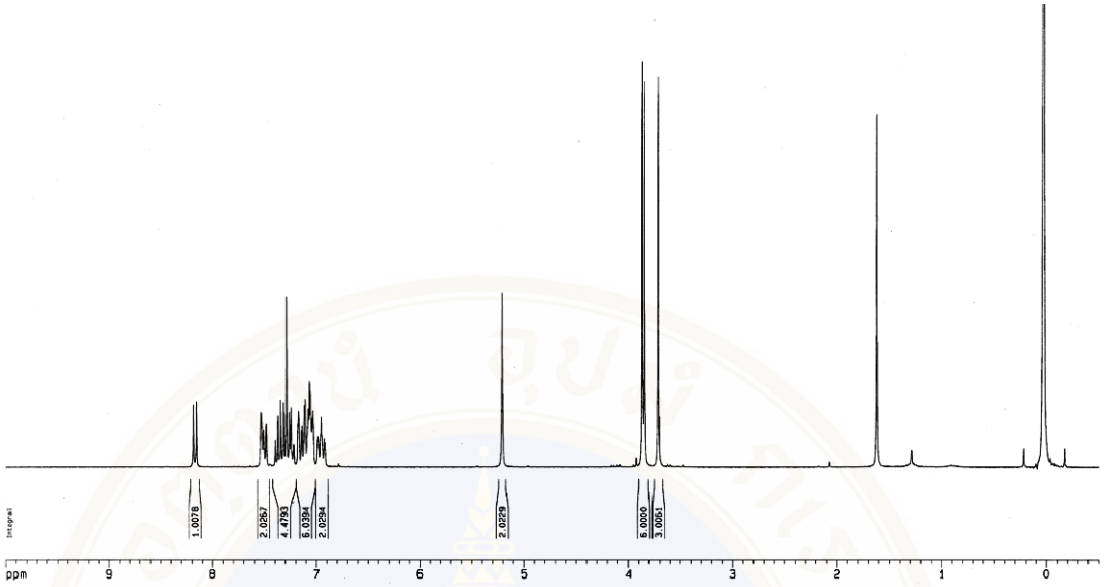

Figure 6.6. ^{1}H NMR spectra (300 MHz, $CDCl_3$) of compound **8b** (cont.).

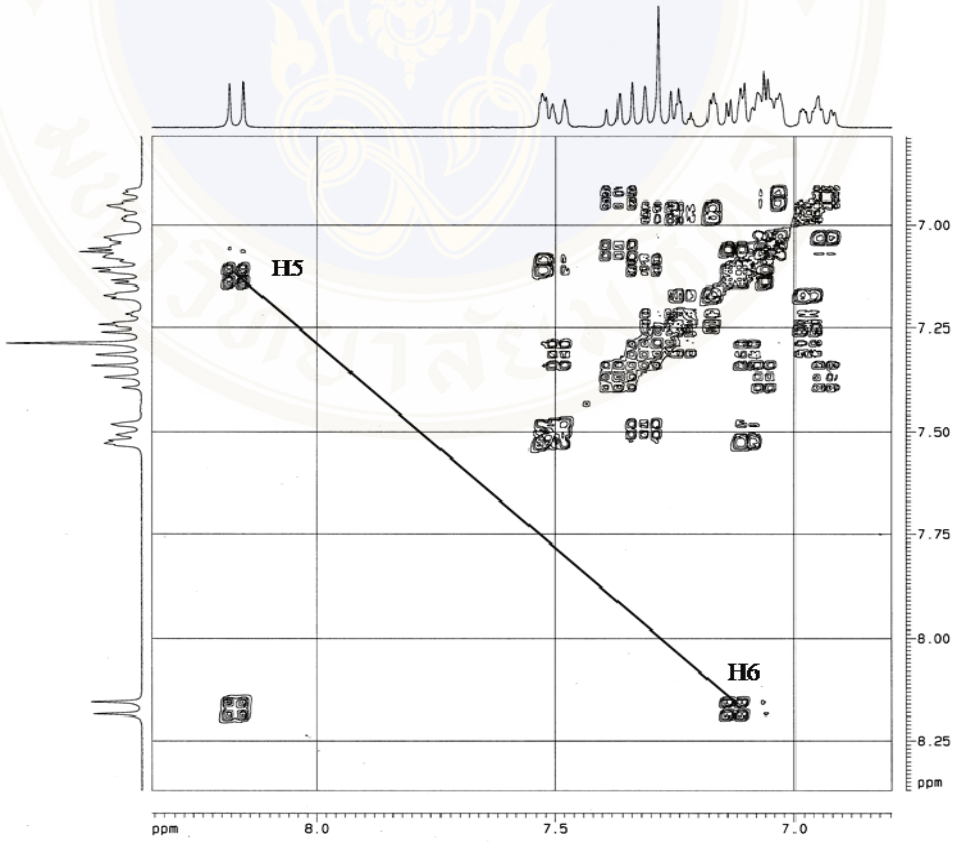

Figure 6.7. ^{1}H-^{1}H COSY spectra (300 MHz, $CDCl_3$) of compound **8b**.

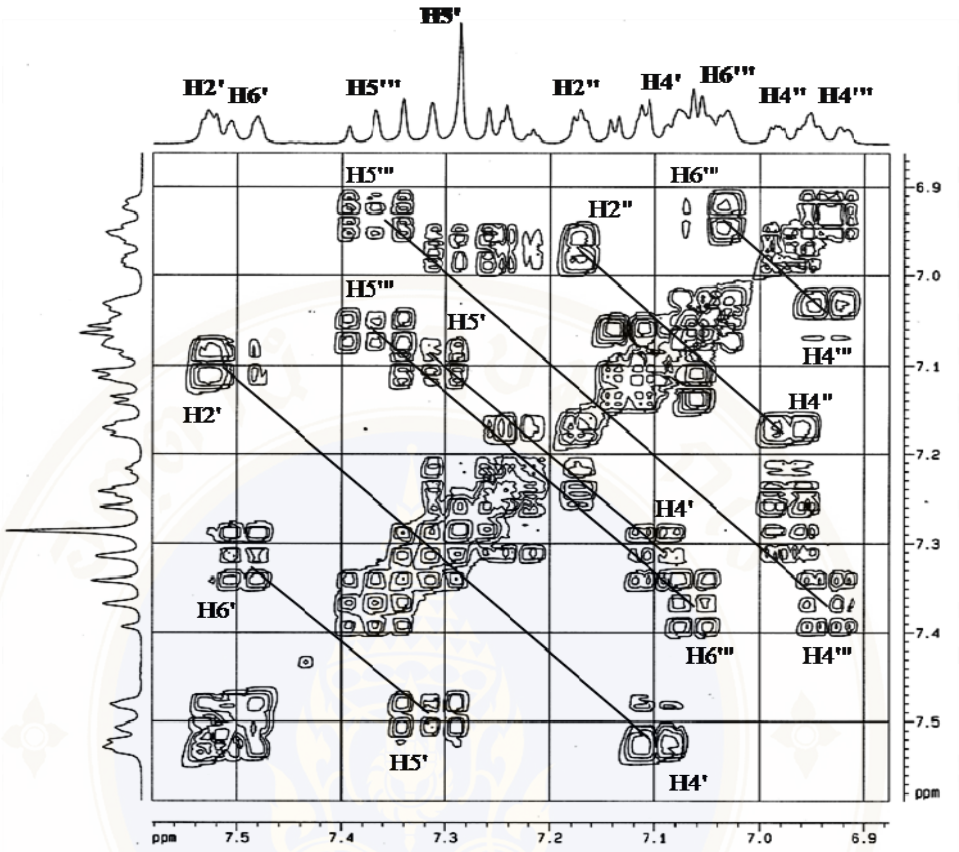

Figure 6.7. ^{1}H-^{1}H COSY spectra (300 MHz, $CDCl_3$) of compound **8b** (cont.).

Table 6.5. ^{1}H NMR data and ^{1}H-^{1}H correlation of compound **8b**.

H	δ (ppm)	Multiplicity (coupling protons)	*J* (Hz)	^{1}H-^{1}H COSY
OCH_3	3.75, 3.85, 3.90	s		
CH_2	5.25	s		
4'''	6.93	dd (5''', 6''')	7.93, 2.18	5''', 6'''
4''	6.95-7.00	m		
6'''	7.04	dd (5''', 4''')	7.73, 2.18	5''', 4'''
8, 2'''	7.00-7.20	m		
4'	7.10	dd (5', 2')	8.05, 2.49	5', 2'
6	7.13	dd (5, 8)	8.83, 2.38	
2''	7.17	d (4'')	2.18	4''
5'', 6''	7.20-7.40	m		
5'	7.34	t (4', 6')	8.05	4', 6'
5'''	7.36	t (4''', 6''')	7.93	4''', 6'''
6'	7.49	d (5')	8.05	5'
2'	7.53	d (4')	2.49	4'
5	8.17	d (6)	8.83	6

The EI mass spectrum of compound **8b** had characteristic peaks at m/z M^+ 522, 493, 415, 401, 373, 295, 266, 238, 159, 135, 121, 107, 91 and 77 as shown in Figure 6.8. The proposed fragmentation mechanism was illustrated in Figure 6.9.

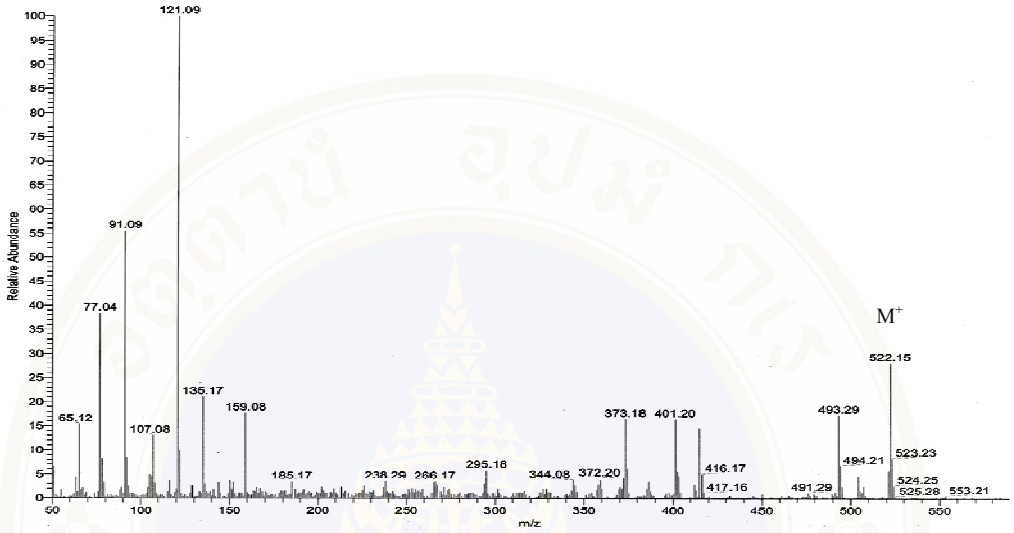

Figure 6.8. EI mass spectra of compound **8b**.

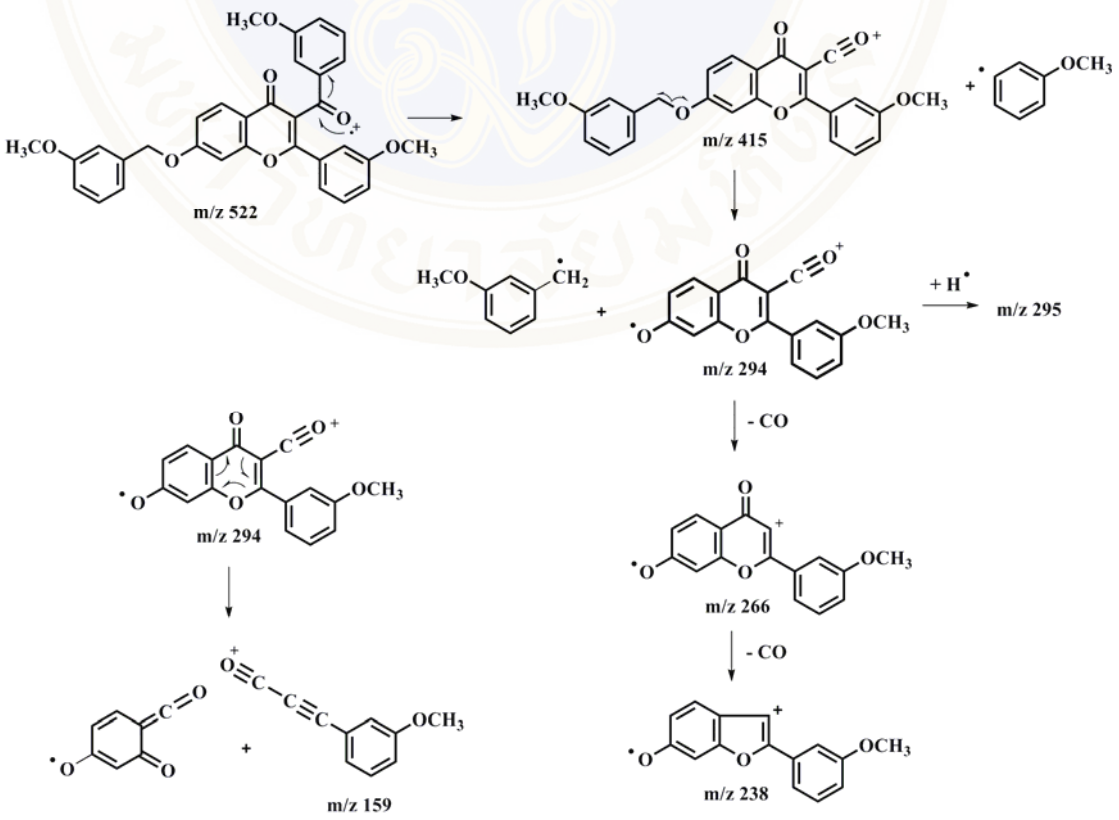

Figure 6.9. Proposed fragmentation mechanism of compound **8b**.

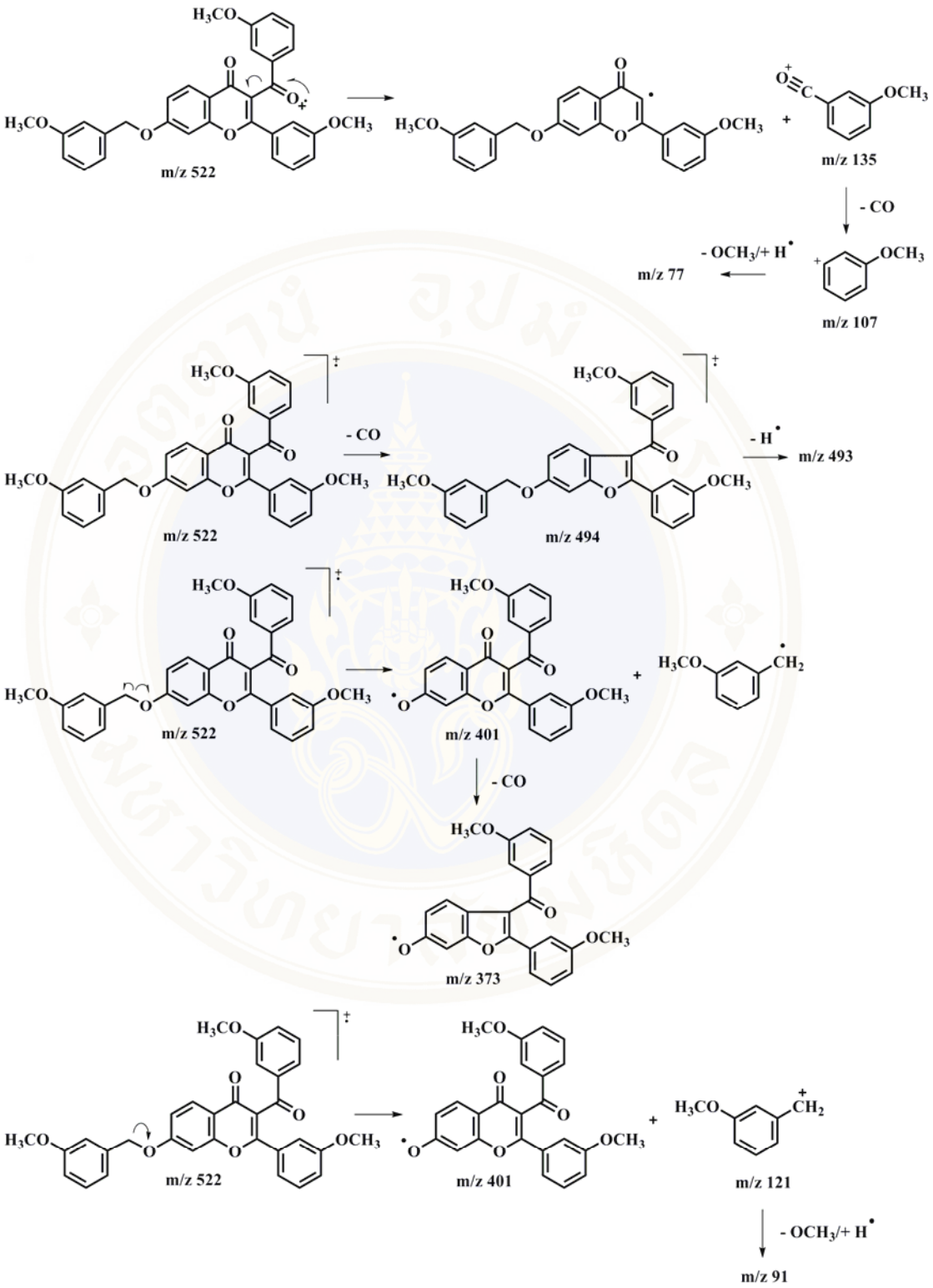

Figure 6.9. Proposed fragmentation mechanism of compound **8b** (cont.).

The IR spectrum of the obtained ester linkage chromone derivatives showed aromatic C-H stretching at 3075 cm^{-1}, aliphatic C-H stretching at 2963 and 2837 cm^{-1}, carbonyl C=O stretching at 1733, 1665 and 1606 cm^{-1}, C=C stretching at 1577 and 1509 cm^{-1} (Figure 6.10).

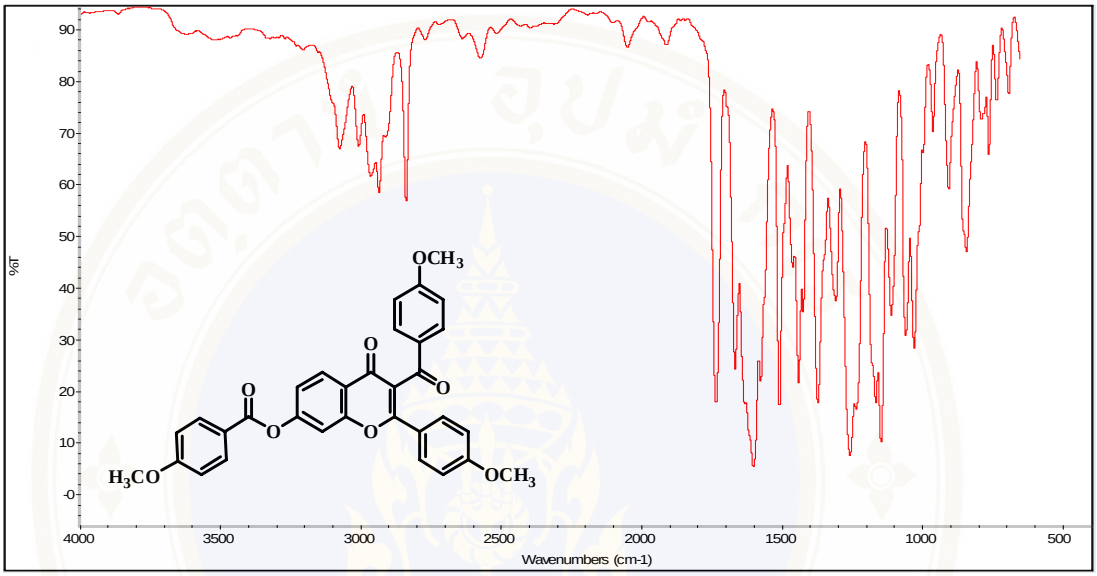

Figure 6.10. IR spectrum of compound **9f**.

The ^{1}H NMR spectrum and the details of the ^{1}H NMR interpretation data of compound **9f** are shown in Figure 6.11 and Table 6.6, respectively.

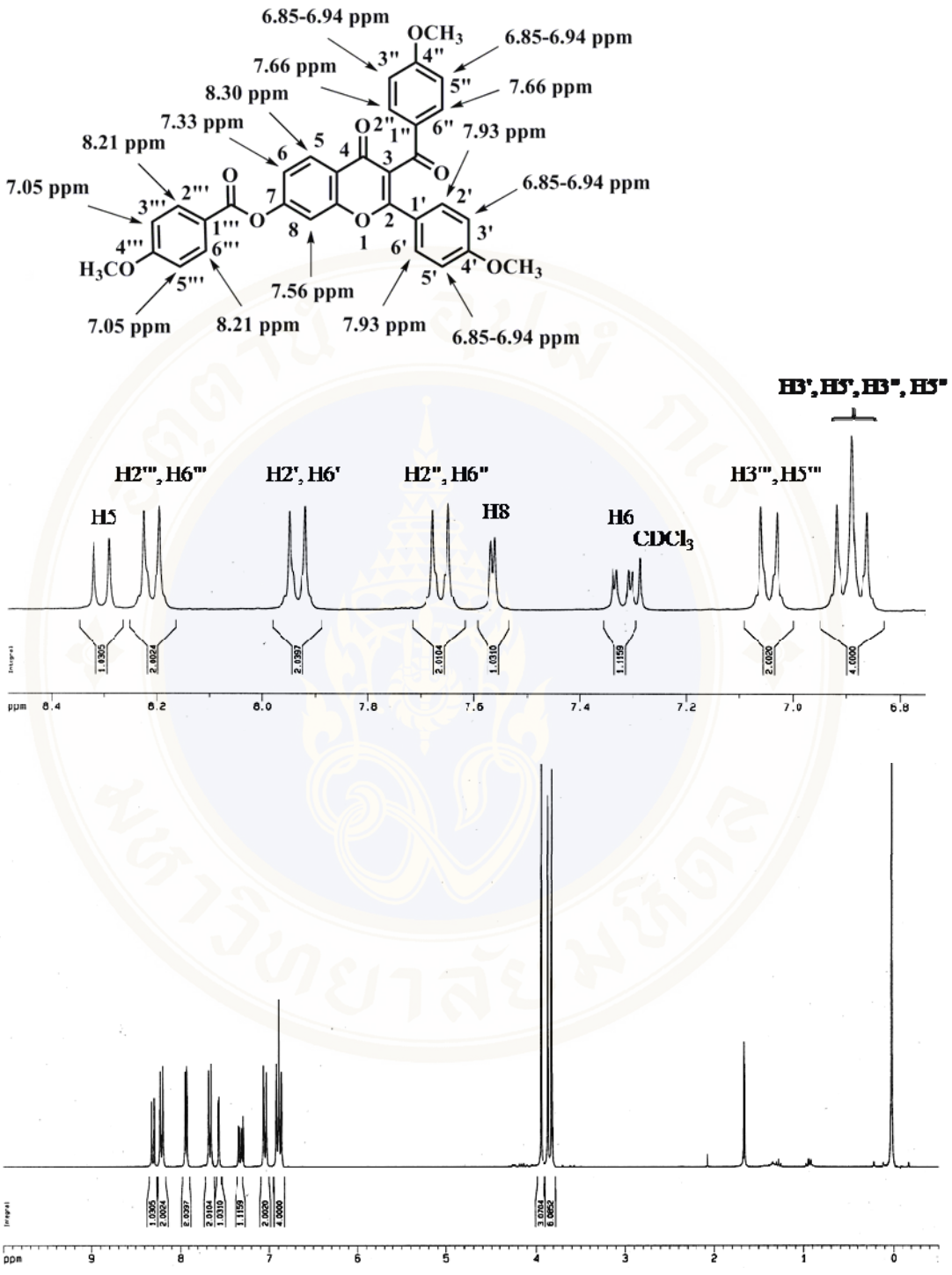

Figure 6.11. ^{1}H NMR spectra (300 MHz, $CDCl_3$) of compound **9f**.

Table 6.6. ^{1}H NMR data of compound **9f**.

H	δ (ppm)	Multiplicity (coupling protons)	*J* (Hz)
OCH_3	3.80, 3.85, 3.95	s	
3', 5', 3", 5"	6.85-6.94	m	
3"', 5"'	7.05	d (2"', 6"')	8.90
6	7.33	dd (5, 8)	8.74, 2.10
8	7.56	d (6)	2.10
2", 6"	7.66	d (3", 5")	8.90
2', 6'	7.93	d (3', 5')	8.85
2"', 6"'	8.21	d (3"', 5"')	8.90
5	8.30	d	8.74

The EI mass spectrum of compound **9f** showed characteristic peaks at m/z M^+ 536, 507, 401, 373, 295, 266, 239, 135, 107 and 77 as shown in Figure 6.12. The proposed fragmentation mechanism was illustrated in Figure 6.13.

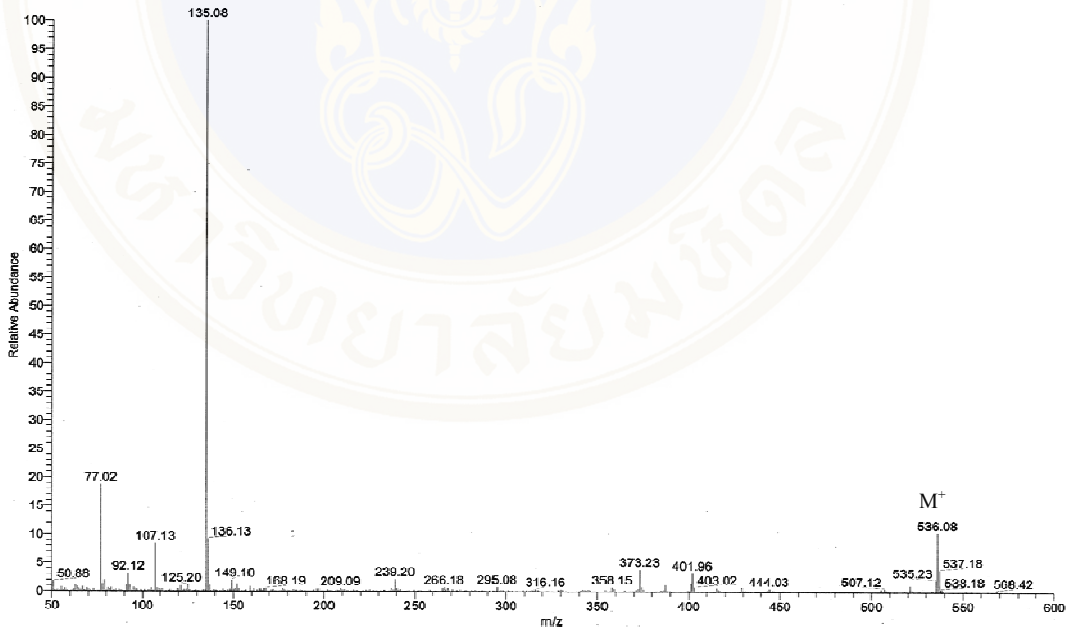

Figure 6.12. EI mass spectra of compound **9f**.

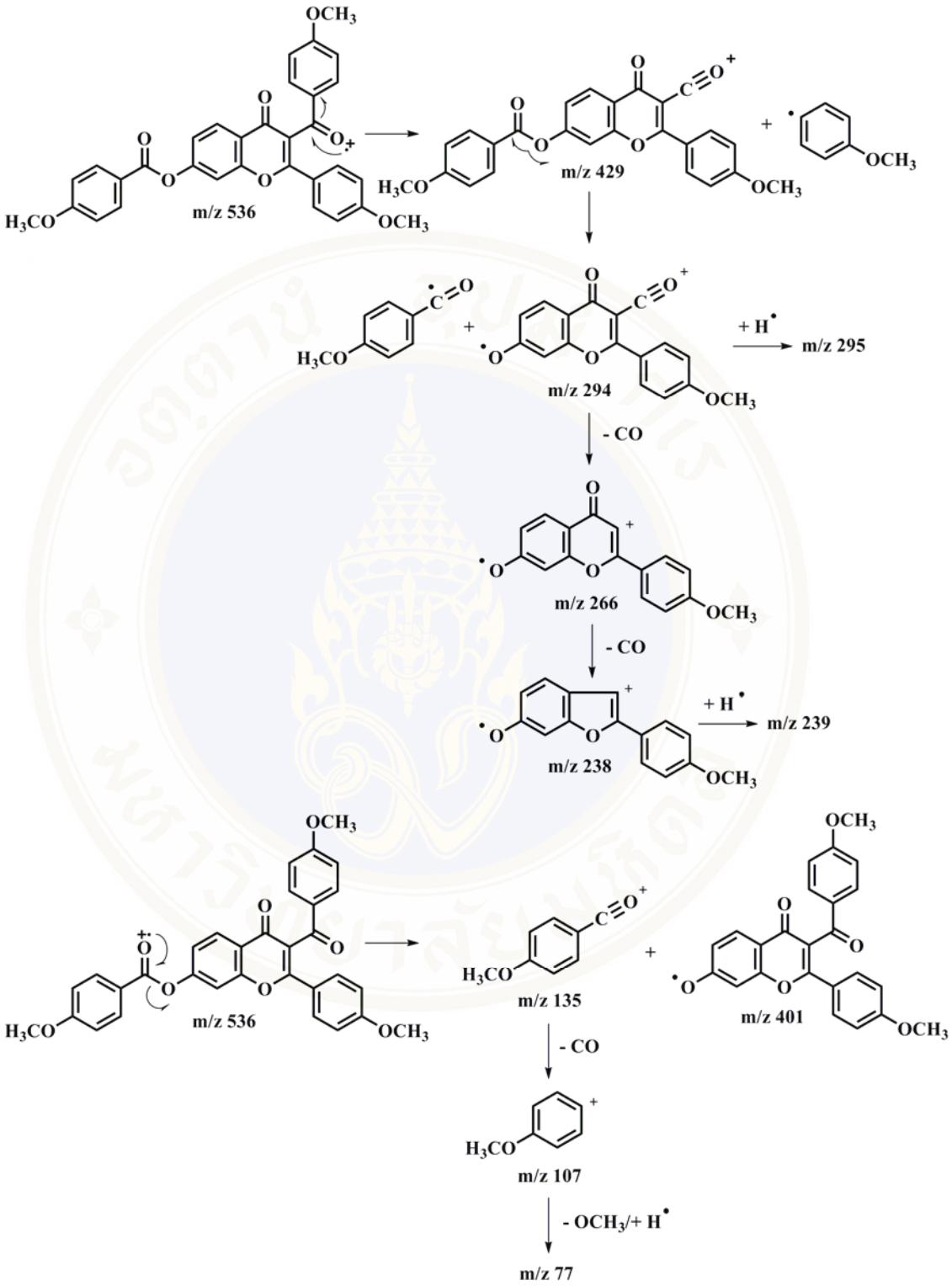

Figure 6.13. Proposed fragmentation mechanism of compound **9f.**

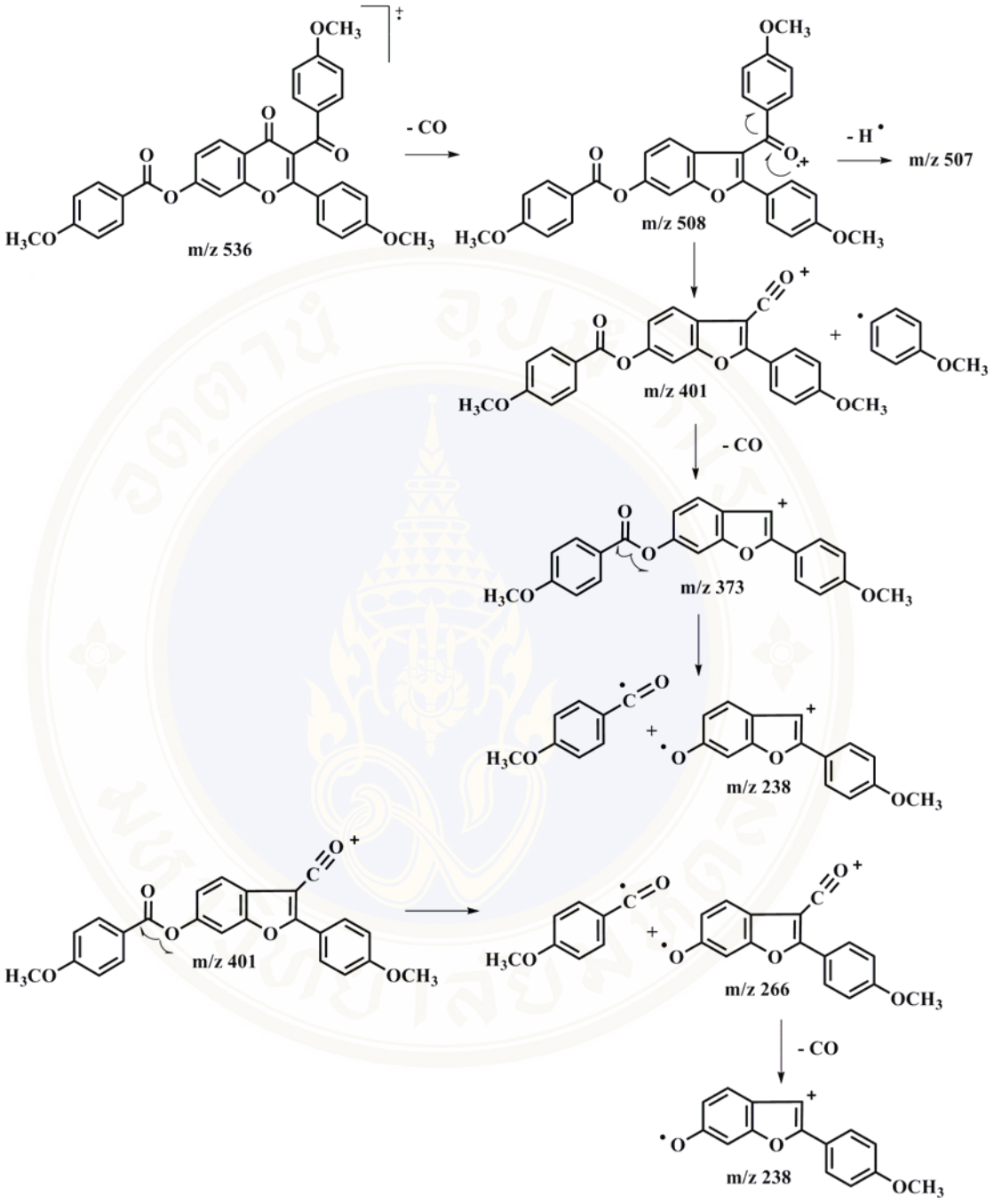

Figure 6.13. Proposed fragmentation mechanism of compound **9f** (cont.).

C. Topoisomerase I inhibitory activity testing

The ability of chromone derivatives to inhibit TOP I was determined using eukaryotic DNA TOP I drug screening kit (TopoGen, Inc., USA). The percentage of TOP I inhibition was calculated as follows:

Inhibition (%) = (Amount of nicked DNA_{sample} x 100) / Amount of nicked $DNA_{control}$

where amount of nicked DNA_{sample} was calculated from the band produced by synthesized compound and amount of nicked $DNA_{control}$ was calculated from the band produced by 100 μM CPT.

TOP I causes transient nicks in DNA at specific sites. Detection of the transient DNA nicks requires trapping the enzyme on DNA in a nicked intermediate complex using protein denaturants (SDS). The resulting covalent DNA/TOP I complexes contain nicked open circular DNA which can be detected by agarose gel electrophoresis (with ethidium bromide). The process to trap the nicked intermediates is relatively inefficient since the half life of this cleavage complex is rather short. However, CPT can stabilize the intermediate and increases in the nicked DNA product. Therefore, detection of agents that affect TOP I by stabilizing the cleaved intermediate complex can be performed.

Sixteen chromone derivatives were evaluated for inhibitory activity against DNA TOP I at concentration of 20 μM which is the cutoff value of the lowest DMSO soluble derivative. Results were reported as percentage inhibition as shown in Table 6.7. CPT was used as a positive control which exhibited 100 % inhibition at 100 μM. The tested chromone derivatives were found to show the inhibitory activity between 33.41 to 66.03 %. Compound **11b** exhibited highest activity with 66.03 % inhibition.

Figure 6.14 illustrated the stabilization of TOP I-DNA complex obtained from agarose gel electrophoresis. In the presence of chromone compounds, the nicked DNA bands were more intense. These results imply that chromone compounds can inhibit TOP I by stabilizing TOP I-DNA cleavage complex. Compounds **7a, 7d-7g, 8e, 8f, 9d, 11b** and **11c** exhibited inhibitory activities greater than 50 % inhibition. Structure-activity relationships could be deduced that R_1 and R_2 preferred no substituent at benzoyl and phenyl respectively, with the exception that electron

withdrawing group, e.g., NO_2 was allowed at *para* position of both rings. On the contrary, substituent at R_3 could be varied.

Table 6.7. The inhibitory activities of the synthesized chromone derivatives (at 20 μM).

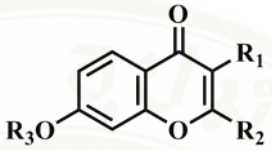

Compd	R_1	R_2	R_3	% Inhibition ± S.E.*
7a	benzoyl	phenyl	benzyl	52.03 ± 4.53
7d	benzoyl	phenyl	3'''-(OCH_3)-benzoyl	62.63 ± 1.74
7e	benzoyl	phenyl	4'''-(OCH_3)-benzoyl	52.37 ± 1.26
7f	benzoyl	phenyl	3'''-(NO_2)-benzoyl	63.96 ± 2.33
7g	benzoyl	phenyl	4'''-(NO_2)-benzoyl	50.63 ± 2.28
8a	3''-(OCH_3)-benzoyl	3'-(OCH_3)-phenyl	benzyl	44.54 ± 1.94
8b	3''-(OCH_3)-benzoyl	3'-(OCH_3)-phenyl	3'''-(OCH_3)-benzyl	33.41 ± 2.30
8d	3''-(OCH_3)-benzoyl	3'-(OCH_3)-phenyl	benzoyl	48.68 ± 2.46
8e	3''-(OCH_3)-benzoyl	3'-(OCH_3)-phenyl	3'''-(OCH_3)-benzoyl	58.76 ± 2.83
8f	3''-(OCH_3)-benzoyl	3'-(OCH_3)-phenyl	4'''-(OCH_3)-benzoyl	50.23 ± 1.95
9b	4''-(OCH_3)-benzoyl	4'-(OCH_3)-phenyl	3'''-(OCH_3)-benzyl	47.76 ± 0.95
9d	4''-(OCH_3)-benzoyl	4'-(OCH_3)-phenyl	benzoyl	55.77 ± 1.26
9e	4''-(OCH_3)-benzoyl	4'-(OCH_3)-phenyl	3'''-(OCH_3)-benzoyl	39.78 ± 3.08
9f	4''-(OCH_3)-benzoyl	4'-(OCH_3)-phenyl	4'''-(OCH_3)-benzoyl	42.66 ± 3.02
11b	4''-(NO_2)-benzoyl	4'-(NO_2)-phenyl	benzoyl	66.03 ± 1.36
11c	4''-(NO_2)-benzoyl	4'-(NO_2)-phenyl	3'''-(NO_2)-benzoyl	64.73 ± 1.64

* relative to the intensity of the band produced by 100 μM CPT

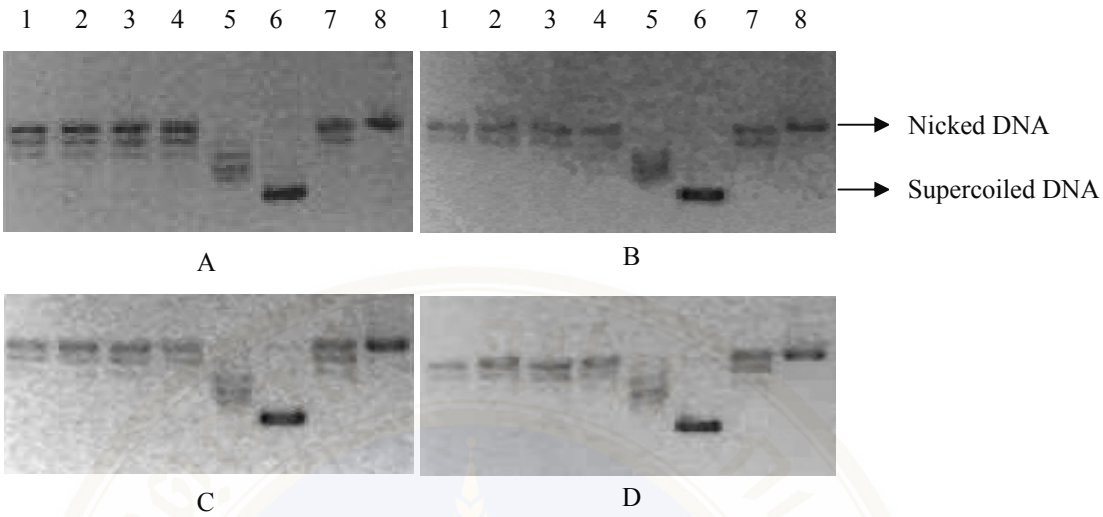

Figure 6.14. Stabilization of recombinant human TOP I-DNA complex by chromone compounds, measured after agarose gel electrophoresis. A) Lanes 1-4 = supercoiled DNA + TOP I + 20 μM of compounds **7d**, **7f**, **7g** and **11b**, respectively. B) Lanes 1-4 = supercoiled DNA + TOP I + 20 μM of compounds **8b**, **8a**, **9b** and **7a**, respectively. C) Lanes 1-4 = supercoiled DNA + TOP I + 20 μM of compounds **9e**, **9d**, **8f** and **8d**, respectively. D) Lanes 1-4 = supercoiled DNA + TOP I + 20 μM of compounds **9f**, **8e**, **7e** and **11c**, respectively. For A, B, C and D, lane 5 = relaxed plasmid DNA marker; lane 6 = supercoiled DNA; lane7 = supercoiled DNA + TOP I; lane 8 = supercoiled DNA + TOP I + 100 μM of CPT.

Due to the DMSO solubility limitation, only compounds **7d**, **7e**, **7f**, **8e**, **11b** and **11c** were selected for further IC_{50} evaluation (Tables 6.8-6.13). The IC_{50} was determined from the calibration curve plotted between percentage inhibition and log concentration (Figures 6.15-6.20). Table 6.14 summarizes the binding energy from docking study and IC_{50} of compounds **7d**, **7e**, **7f**, **8e**, **11b** and **11c**.

1. IC_{50} determination of 7-(3"'-Methoxy)benzoyl-2-phenyl-3-benzoyl-chromone 7d

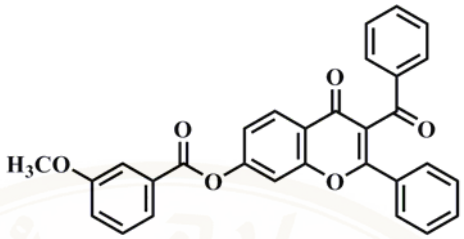

Table 6.8. IC_{50} determination result of compound **7d**.

Conc (μM)	logC (concentration in nM)	% inhibition	S.E.	intercept	slope	R^2	IC_{50} (μM)
1	3.00000	39.58	3.00	-25.575	21.583	0.9911	3.17
4	3.60206	50.86	0.14				
7	3.84510	58.15	0.96				
10	4.00000	60.92	2.58				

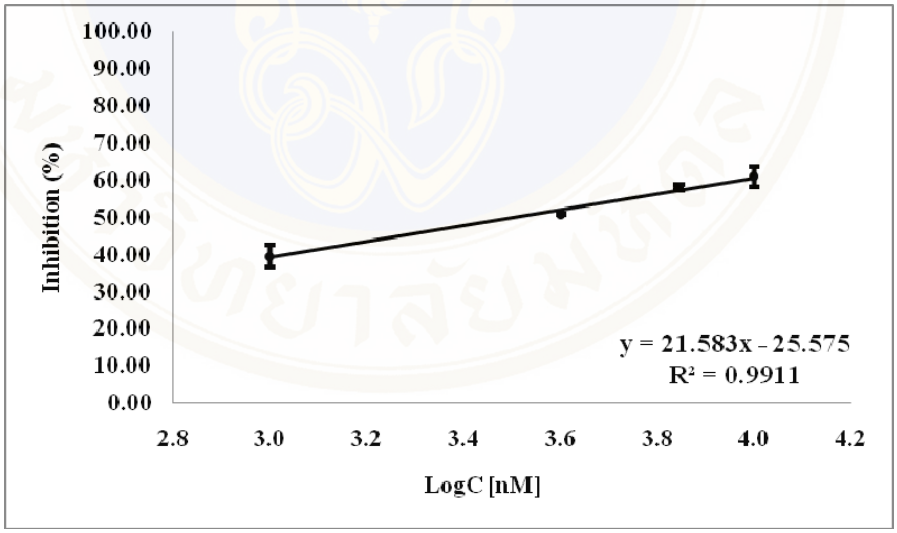

Figure 6.15. The percentage of inhibition and log concentration profile of compound **7d**.

2. IC_{50} determination of 7-(4"'-Methoxy)benzoyl-2-phenyl-3-benzoyl-chromone 7e

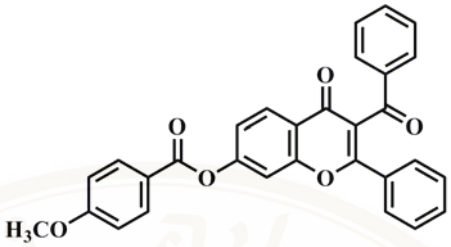

Table 6.9. IC_{50} determination result of compound **7e**.

Conc (μM)	logC (concentration in nM)	% Inhibition	S.E.	intercept	slope	R^2	IC_{50} (μM)
10	4.00000	43.35	4.50	-87.44	32.391	0.9202	17.50
15	4.17609	45.41	0.53				
20	4.30103	52.37	1.26				
25	4.39794	55.71	1.46				

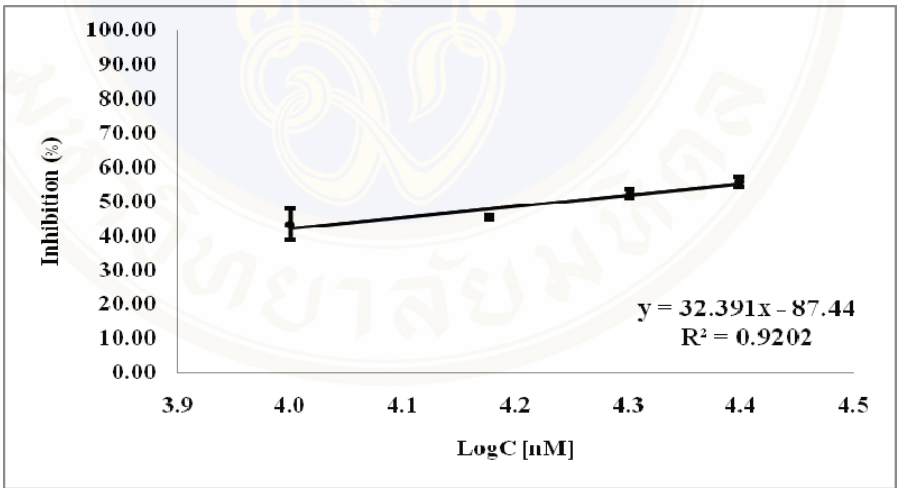

Figure 6.16. The percentage of inhibition and log concentration profile of compound **7e**.

3. IC_{50} determination of 7-(3"'-Nitro)benzoyl-2-phenyl-3-benzoyl-chromone 7f

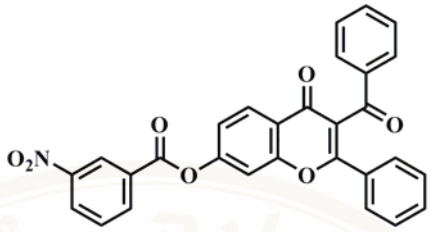

Table 6.10. IC_{50} determination result of compound **7f**.

Conc (μM)	logC (concentration in nM)	% inhibition	S.E.	intercept	slope	R^2	IC_{50} (μM)
0.5	2.69897	32.32	1.57	-19.381	19.179	0.9897	4.15
5	3.69897	52.68	1.45				
10	4.00000	55.44	0.72				
20	4.30103	63.96	2.33				

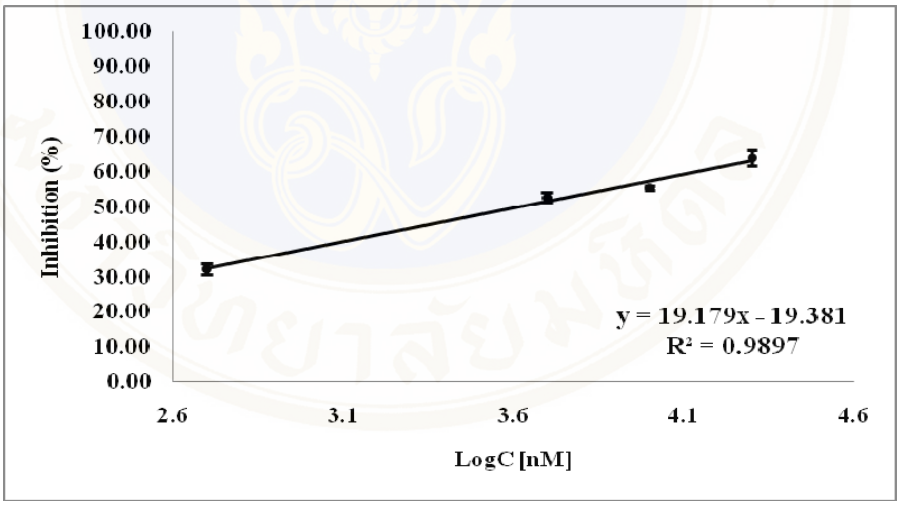

Figure 6.17. The percentage of inhibition and log concentration profile of compound **7f**.

4. IC_{50} determination of 7-(3"'-Methoxy)benzoyl-2-(3'-methoxy)-phenyl-3-(3"-methoxybenzoyl) chromone 8e

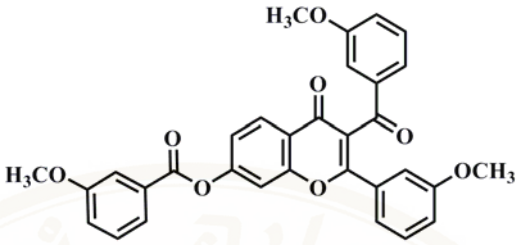

Table 6.11. IC_{50} determination result of compound **8e**.

Conc. (μM)	logC (concentration in nM)	% inhibition	S.E.	intercept	slope	R^2	IC_{50} (μM)
10	4.00000	44.14	0.93	-124.02	42.331	0.9784	12.91
15	4.17609	54.17	0.74				
20	4.30103	58.76	2.83				
30	4.47712	64.52	1.29				

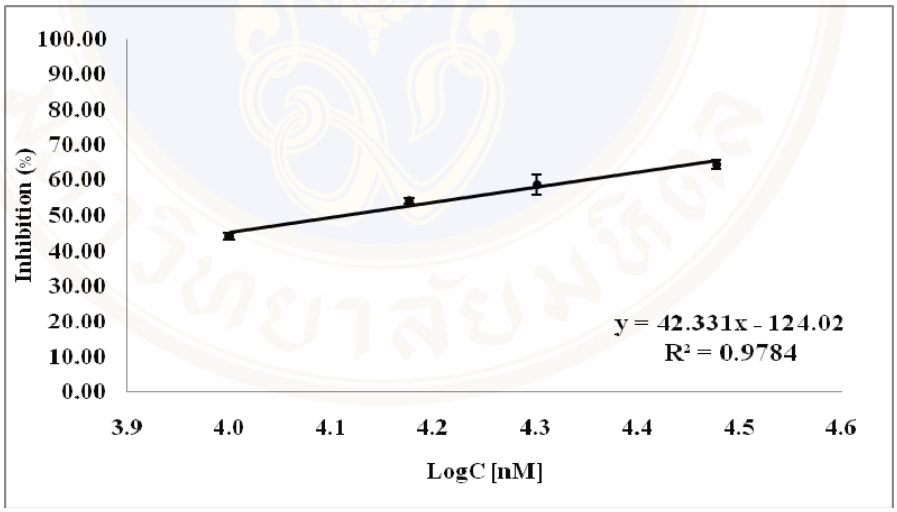

Figure 6.18. The percentage of inhibition and log concentration profile of compound **8e**.

5. IC_{50} determination of 7-Benzoyl-2-(3'-nitro)phenyl-3-(3"-nitro)-benzoyl chromone 11b

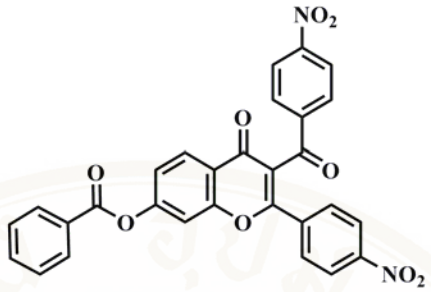

Table 6.19. IC_{50} determination result of compound **11b**.

Conc (μM)	logC (concentration in nM)	% inhibition	S.E.	intercept	slope	R^2	IC_{50} (μM)
0.1	2.00000	36.10	3.89	10.076	12.622	0.9841	1.46
1	3.00000	47.48	3.70				
5	3.69897	54.78	1.10				
20	4.30103	66.03	1.36				

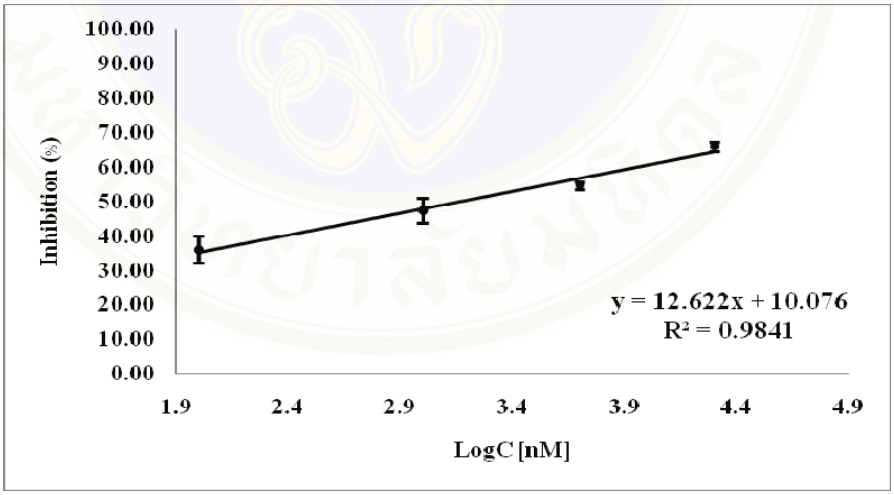

Figure 6.16. The percentage of inhibition and log concentration profile of compound **11b**.

6. IC_{50} determination of 7-(3"'-Nitro)benzoyl-2-(3'-nitro)phenyl-3-(3"-nitro)benzoyl chromone 11c

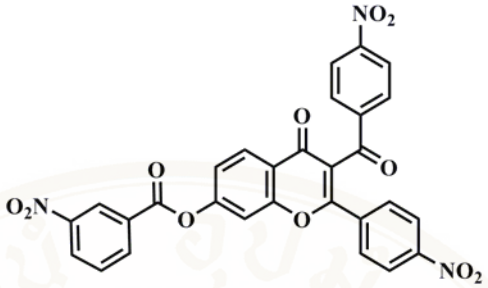

Table 6.13. IC_{50} determination result of compound **11c**.

Conc (μM)	logC (concentration in nM)	% inhibition	S.E.	intercept	slope	R^2	IC_{50} (μM)
5	3.69897	46.71	1.60	-68.69	31.321	0.9803	6.16
10	4.00000	56.91	2.23				
15	4.17609	63.54	1.56				
20	4.30103	64.73	1.64				

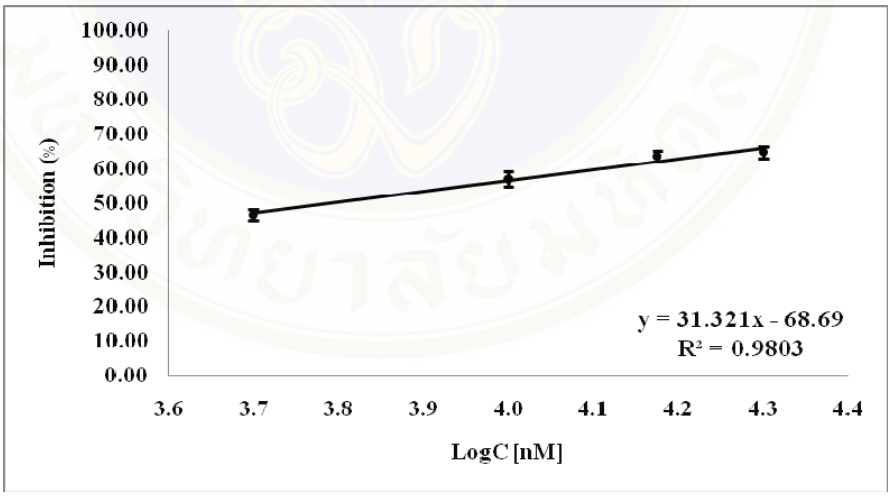

Figure 6.20. The percentage of inhibition and log concentration profile of compound **11c**.

Table 6.14. The IC_{50} (μM) of six compounds and their binding energy.

Compd	Binding energy	IC_{50} (μM)
7d	-8.77	3.17
7e	-8.82	17.50
7f	-8.62	4.15
8e	-8.72	12.91
11b	-9.29	1.46
11c	-11.39	6.16

The three most potent inhibitors were compounds **11b**, **7d** and **7f** with IC_{50} = 1.46, 3.17 and 4.15 μM, respectively. All chromones listed in Table 6.14 showed higher potency than the known potent TOP I inhibitor, CPT, which possessed IC_{50} = 18.85 μM (95). Furthermore, these chromones also showed more potency than the structurally related flavonoids, i.e., fisetin (IC_{50} = 20.6 μM) and morin (IC_{50} = 42.1 μM) (5).

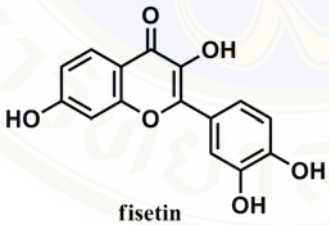

fisetin

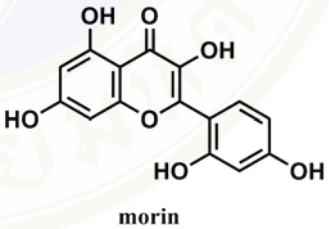

morin

CHAPTER VII
CONCLUSION

In this study, a new series of chromone derivatives have been designed and synthesized for TOP I inhibitors. The general structure of molecules in this series consists of benzopyran-4-one (chromone) nucleus with different substituents at positions 2 and 3 and varied OH substitution at ring C. AutoDock 4.0 was used to predict the inhibitory activity against the target macromolecule. Docking results indicated that introduction of steric group at 7-OH led to the higher binding energy. From docking study, the 2-substituted phenyl-3-substituted benzoyl chromones, compounds **7-12** showed good binding energy, therefore compounds **7-12** were selected for further modification by adding steric group at the 7-OH group. The structure-modified compounds **7a-7h, 8a-8f, 9a-9f, 10a-10e, 11a-11e and 12a-12e** exhibited binding energy in the range of -5.56 to -11.39 kcal/mole. Compound **11c** was the best docked ligand with the binding energy -11.39 kcal/mole. Sixteen compounds whose structures were designed based on compounds **7-12** were synthesized and evaluated for their inhibitory activity using eukaryotic TOP drug screening kit at concentration of 20 µM. The synthesized chromone derivatives showed 33.41 % - 66.03 % inhibition. Structure-activity relationships indicated that R_1 and R_2 preferred no substituent at benzoyl and phenyl rings respectively but electron withdrawing group, e.g., NO_2 was allowed at *para*- position and substituent at R_3 could be varied. Six compounds were selected for further determination of IC_{50} values. The IC_{50} values of compounds **7d**, **7e**, **7f**, **8e**, **11b** and **11c** were 3.17 μM, 17.50 μM, 4.15 μM, 12.91 μM, 1.46 μM and 6.16 μM, respectively. All these six derivatives exhibited higher potency than the known TOP I inhibitor, CPT. The most potent inhibitor, compound **11b** showed greater potency than the structurally-related flavonoids, fisetin and morin which reportedly exhibited TOP I inhibitory activity.

REFERENCES

1 Allan YC, Hak C, Mace LR. DNA topoisomerase I-targetting drug as radiation sensitizer. Oncol. 1999: 13.

2 Hertzberg RP, Busby RW, Caranfa MJ, Holden KG, Johnson RK, Hecht SM, et al. Irreversible trapping of the DNA-topoisomerase I covalent complex. Affinity labeling of the camptothecin binding site. J Biol Chem. 1990; 265 (31): 19287-95.

3 Chan A, Chang WS, Chen LM, Lee CM, Chen CE, Lin CM, et al. Evodiamine stabilizes topoisomerase I-DNA cleavable complex to inhibit topoisomerase I activity. Molecules. 2009; 14 (4): 1342-52.

4 Phosrithong N, Ungwitayatorn J. Molecular docking study on anticancer activity of plant-derived natural products. Med Chem Res. 2009; 19 (8): 817-35.

5 Constantinou A, Mehta R, Runyan C, Rao K, Vaughan A, Moon R. Flavonoids as DNA topoisomerase antagonists and poisons: structure-activity relationships. J Nat Prod. 1995; 58 (2): 217-25.

6 Huey R, Morris G. Using autodock with autodocktools: A tutorial. Available from: http://autodock.scripps.edu/faqs-help/tutorial/using-autodock-4-with-autodocktools/UsingAutoDock4WithADT_1.4.5d.pdf [Accessed 2010 March 26]

7 Riva C, De Toma C, Donadel L, Boi C, Pennini R, Motta G, et al. New DBU (1,8-Diazabicyclo(5.4.0)undec-7-ene) assisted one-pot synthesis of 2,8-disubstituted 4*H*-1-benzopyran-4-ones. Synthesis. 1997: 195-201.

8 L.G. Wade J. Carboxylic acids. In: Organic chemistry. 6 ed. USA: Pearson Education Inc 2006: 966-7.

9 L.G. Wade J. Ether, Epoxides, and Sulfides. In: Organic chemistry. 6 ed. USA: Pearson Education Inc 2006: 633.

10 McNulty J, Krishnamoorthy V, Robertson A. Direct formation of esters and amides from carboxylic acids using diethyl chlorophosphate in pyridine. Tetrahedron Lett. 2008; 49 (44): 6344-47.

11 Stabile RG, Dicks AP. Semi-microscale Williamson ether synthesis and simultaneous isolation of an expectorant from cough tablets. J Chem Educ. 2003; 80 (3): 313.

12 William A R. Antineoplastic agents. In: Wilson and Gisvold 's textbook of organic medicinal and pharmaceutical chemistry. 11 ed. 2004: 390-453.

13 Graham L P. Anticancer agents. In: An introduction to medicinal chemistry. 4 ed. New York: Oxford University Press Inc 2008: 519-78.

14 Chinnaswamy G, Errington J, Foot A, Boddy AV, Veal GJ, Cole M. Pharmacokinetics of cyclophosphamide and its metabolites in paediatric patients receiving high-dose myeloablative therapy. Eur J Cancer. 2011; 47 (10): 1556-63.

15 Thomas LL, David AW, Victoria FR. Cancer and chemotherapy. In: Foye 's principles of medicinal chemistry. 6 ed. USA: Lippincott Williams and Wilkins 2008: 1147-92.

16 Akutsu M, Kano Y, Tsunoda S, Suzuki K, Yazawa Y, Miura Y. Schedule-dependent interaction between paclitaxel and doxorubicin in human cancer cell lines in vitro. Eur J Cancer. 1995; 31 (13): 2341-46.

17 Marchetti P, Urien SK, Antonini Cappellini G, Ronzino G, Ficorella C. Weekly administration of paclitaxel: theoretical and clinical basis. Crit Rev Oncol Hemat. 2002; 44: 3-13.

18 Fu Y, Ye D, Chen H, Lu W, Ye F, Xie X. Weakened spindle checkpoint with reduced BubR1 expression in paclitaxel-resistant ovarian carcinoma cell line SKOV3-TR30. Gynecol Oncol. 2007; 105 (1): 66-73.

19 Sjoblom T, Parvinen M, Lahdetie J. Stage-specific DNA synthesis of rat spermatogenesis as an indicator of genotoxic effects of vinblastine, mitomycin C and ionizing radiation on rat spermatogonia and spermatocytes. Mutat Res Fundam Mol Mech Mugag. 1995; 331 (2): 181-90.

20 Genestier L, Paillot R, Quemeneur L, Izeradjene K, Revillard JP. Mechanisms of action of methotrexate. Immunopharmacol. 2000; 47(2): 247-57.

21 Clemons M, Danson S, Howell A. Tamoxifen (Nolvadex): a review antitumour treatment. Cancer Treat Rev. 2002; 28 (4): 165-80.

22 Burden DA, Osheroff N. Mechanism of action of eukaryotic topoisomerase II and drugs targeted to the enzyme. Biochim Biophys Acta Gene Struct Expr. 1998; 1400 (1): 139-54.

23 Minotti G, Menna P, Salvatorelli E, Cairo G, Gianni L. Anthracyclines: molecular advances and pharmacologic developments in antitumor activity and cardiotoxicity. Pharmacol Rev. 2004; 56 (2): 185-229.

24 George JW. Rituximab: mechanism of action. Semin Hematol. 2010; 47 (2): 115-23.

25 Bonavida B, Vega MI. Rituximab-mediated chemosensitization of AIDS and non-AIDS non-Hodgkin's Lymphoma. Drug Resist Update. 2005; 8 (1): 27-41.

26 Miyamoto S, Yagi H, Yotsumoto F, Kawarabayashi T, Mekada E. Heparin-binding epidermal growth factor-like growth factor as a novel targeting molecule for cancer therapy. Cancer Sci. 2006; 97 (5): 341-47.

27 Kataoka H, Joh T, Kasugai K, Okayama N, Moriyama A, Asai K, et al. Expression of mRNA for heregulin and its receptor, ErbB-3 and ErbB-4, in human upper gastrointestinal mucosa. Life Sci. 1998; 63 (7): 553-64.

28 Hynes NE, Lane HA. ERBB receptors and cancer: the complexity of targeted inhibitors. Nat Rev Cancer. 2005; 5 (5): 341-54.

29 Herbst RS, Shin DM. Monoclonal antibodies to target epidermal growth factor receptor–positive tumors. Cancer. 2002; 94 (5):1593-611.

30 Kataoka H. EGFR ligands and their signaling scissors, ADAMs, as new molecular targets for anticancer treatments. J Dermatol Sci. 2010.

31 Bellone S, Frera G, Landolfi G, Romani C, Bandiera E, Tognon G, et al. Overexpression of epidermal growth factor type-1 receptor (EGF-R1) in cervical cancer: implications for Cetuximab-mediated therapy in recurrent/metastatic disease. Gynecol Oncol. 2007; 106 (3): 513-20.

32 Tabernero J, Van CE, Diaz RE, Cervantes A, Humblet Y, Andre T, et al. Phase II trial of cetuximab in combination with fluorouracil, leucovorin, and oxaliplatin in the first-line treatment of metastatic colorectal cancer. J Clin Oncol. 2007; 25 (33): 5225-32.

33 Vincenzi B, Santini D, Rabitti C, Coppola R, Beomonte ZB, Trodella L, et al. Cetuximab and irinotecan as third-line therapy in advanced colorectal cancer patients: a single centre phase II trial. Br J Cancer. 2006; 94 (6): 792-97.

34 Amado RG, Wolf M, Peeters M, Van Cutsem E, Siena S, Freeman DJ, et al. Wild-type KRAS is required for panitumumab efficacy in patients with metastatic colorectal cancer. J Clin Oncol. 2008; 26 (10): 1626-34.

35 Yang CH. EGFR tyrosine kinase inhibitors for the treatment of NSCLC in East Asia: present and future. Lung Cancer. 2008; 60: 23-30.

36 Kopper L. Lapatinib: a sword with two edges. Pathol Oncol Res. 2008; 14 (1): 1-8.

37 Andrea AD, Grompe M. The fanconi anaemia/BRCA pathway. Nat Rev Cancer. 2003; 3 (1): 23-34.

38 Michelson RJ, Weinert T. Closing the gaps among a web of DNA repair disorders. Bioessays. 2000; 22 (11): 966-9.

39 Montagnoli A, Tenca P, Sola F, Carpani D, Brotherton D, Albanese C, et al. Cdc7 inhibition reveals a p53-dependent replication checkpoint that is defective in cancer cells. Cancer Res. 2004; 64 (19): 7110-16.

40 Vanotti E, Amici R, Bargiotti A, Berthelsen J, Bosotti R, Ciavolella A, et al. Cdc7 kinase inhibitors: pyrrolopyridinones as potential antitumor agents synthesis and structure–activity relationships. J Med Chem. 2008; 51 (3): 487-501.

41 Giaever G, Chu AM, Ni L, Connelly C, Riles L, Veronneau S, et al. Functional profiling of the saccharomyces cerevisiae genome. Nature. 2002; 418 (6896): 387-91.

42 Eissenberg J, Shilatifard A, Dorokhov N, Michener D. Cdk9 is an essential kinase in *Drosophila* that is required for heat shock gene expression, histone methylation and elongation factor recruitment. Mol Genet Genomics. 2007; 277 (2): 101-14.

43 Salerno D, Hasham MG, Marshall R, Garriga J, Tsygankov AY, Grana X. Direct inhibition of CDK9 blocks HIV-1 replication without preventing T-cell

activation in primary human peripheral blood lymphocytes. Gene. 2007; 405 (1): 65-78.

44 Cai D, Byth KF, Shapiro GI. AZ703, an imidazo[1,2-α]pyridine inhibitor of cyclin-dependent kinases 1 and 2, induces E2F-1-dependent apoptosis enhanced by depletion of cyclin-dependent kinase 9. Cancer Res. 2006; 66 (1): 435-44.

45 Shapiro GI. Cyclin-dependent kinase pathways as targets for cancer treatment. J Clin Oncol. 2006; 24 (11): 1770-83.

46 Montagnoli A, Valsasina B, Croci V, Menichincheri M, Rainoldi S, Marchesi V, et al. A cdc7 kinase inhibitor restricts initiation of DNA replication and has antitumor activity. Nat Chem Biol. 2008; 4 (6): 357-65.

47 Benakanakere I, Besch WC, Schnell J, Brandt S, Ellersieck MR, Molinolo A, et al. Natural and synthetic progestins accelerate 7,12-dimethylbenz[a]-anthracene-initiated mammary tumors and increase angiogenesis in sprague-dawley rats. Clin Cancer Res. 2006; 12 (13): 4062-71.

48 Suggitt M, Bibby MC. 50 years of preclinical anticancer drug screening: empirical to target-driven approaches. Clin Cancer Res. 2005; 11 (3): 971-81.

49 Duffy MJ, Donovan N, Brennan DJ, Gallagher WM, Ryan BM. Survivin: a promising tumor biomarker. Cancer Lett. 2007; 249 (1): 49-60.

50 Grossman D, Kim PJ, Blanc OP, Brash DE, Tognin S, Marchisio PC, et al. Transgenic expression of survivin in keratinocytes counteracts UVB-induced apoptosis and cooperates with loss of p53. J Clin Invest. 2001; 108 (7): 991-99.

51 Yamamoto T, Manome Y, Nakamura M, Tanigawa N. Downregulation of survivin expression by induction of the effector cell protease receptor-1 reduces tumor growth potential and results in an increased sensitivity to anticancer agents in human colon cancer. Eur J Cancer. 2002; 38 (17): 2316-24.

52 Dean EJ, Ranson M, Blackhall F, Holt SV, Dive C. Novel therapeutic targets in lung cancer: inhibitor of apoptosis proteins from laboratory to clinic. Cancer Treat Rev. 2007; 33 (2): 203-12.

53 Chantalat L, Skoufias DA, Kleman JP, Jung B, Dideberg O, Margolis RL. Crystal structure of human survivin reveals a bow tie shaped dimer with two unusual alpha-helical extensions. Mol Cell. 2000; 6 (1): 183-89.

54 Biroccio A, Leonetti C, Zupi G. The future of antisense therapy: combination with anticancer treatments. Oncogene. 2003; 22 (42): 6579-88.

55 Pennati M, Folini M, Zaffaroni N. Targeting survivin in cancer therapy: fulfilled promises and open questions. Carcinogenesis. 2007; 28 (6): 1133-39.

56 Kim KW, Mutter RW, Willey CD, Subhawong TK, Shinohara ET, Albert JM, et al. Inhibition of survivin and aurora B kinase sensitizes mesothelioma cells by enhancing mitotic arrests. Int J Rad Oncol Biol Phys. 2007; 67 (5): 1519-25.

57 Sah NK, Munshi A, Hobbs M, Carter BZ, Andreeff M, Meyn RE. Effect of downregulation of survivin expression on radiosensitivity of human epidermoid carcinoma cells. Int J Rad Oncol Biol Phys. 2006; 66 (3): 852-59.

58 Kanwar JR, Shen WP, Kanwar RK, Berg RW, Krissansen GW. Effects of survivin antagonists on growth of established tumors and B7-1 immunogene Therapy. J Natl Cancer Inst. 2001; 93 (20): 1541-52.

59 Tu SP, Jiang XH, Lin MCM, Cui JT, Yang Y, Lum CT, et al. Suppression of survivin expression inhibits *in vivo* tumorigenicity and angiogenesis in gastric cancer. Cancer Res. 2003; 63 (22): 7724-32.

60 Puerta FE, Romero LC, Barroso DA, Berzal HA. Ribozymes: recent advances in the development of RNA tools. FEMS Microbiol Rev. 2003; 27 (1): 75-97.

61 Pennati M, Colella G, Folini M, Citti L, Daidone MG, Zaffaroni N. Ribozyme-mediated attenuation of survivin expression sensitizes human melanoma cells to cisplatin-induced apoptosis. J Clin Invest. 2002; 109 (2): 285-86.

62 Pennati M, Binda M, Colella G, Zoppe M, Folini M, Vignati S, et al. Ribozyme-mediated inhibition of survivin expression increases spontaneous and drug-induced apoptosis and decreases the tumorigenic potential of human prostate cancer cells. Oncogene. 2004; 23 (2): 386-94.

63 Aagaard L, Rossi JJ. RNAi therapeutics: principles, prospects and challenges. Adv Drug Deliv Rev. 2007; 59 (2): 75-86.

64 Carvalho A, Carmena M, Sambade C, Earnshaw WC, Wheatley SP. Survivin is required for stable checkpoint activation in taxol-treated HeLa cells. J Cell Sci. 2003; 116 (14): 2987-98.

65 Croci DO, Cogno IS, Vittar NBR, Salvatierra E, Trajtenberg F, Podhajcer OL, et al. Silencing survivin gene expression promotes apoptosis of human breast cancer cells through a caspase-independent pathway. J Cell Biochem. 2008; 105 (2): 381-90.

66 Paduano F, Villa R, Pennati M, Folini M, Binda M, Daidone MG, et al. Silencing of survivin gene by small interfering RNAs produces supra-additive growth suppression in combination with 17-allylamino-17-demethoxygeldanamycin in human prostate cancer cells. Mol Cancer Therapeut. 2006; 5 (1): 179-86.

67 Nakao K, Hamasaki K, Ichikawa T, Arima K, Eguchi K, Ishii N. Survivin downregulation by siRNA sensitizes human hepatoma cells to TRAIL-induced apoptosis. Oncol Rep. 2006; 16 (2): 389-92.

68 Gaofeng J, Jinlong L, Zhaolei Z, Lijian X. Lentivirus-mediated gene therapy by suppressing survivin in BALB/c nude mice bearing oral squamous cell carcinoma. Cancer Biol Ther. 2006; 5 (4): 435-40.

69 Staker BL, Feese MD, Cushman M, Pommier Y, Zembower D, Stewart L, et al. Structures of three classes of anticancer agents bound to the human topoisomerase I DNA covalent complex. J Med Chem. 2005; 48 (7): 2336-45.

70 Liu LF. DNA topoisomerase poisons as antitumor drugs. Annu Rev Biochem. 1989; 58 (1): 351-75.

71 Lauria A, Ippolito M, Almerico A. Molecular docking approach on the topoisomerase I inhibitors series included in the NCI anti-cancer agents mechanism database. J Mol Model. 2007; 13 (3): 393-400.

72 Redinbo MR, Stewart L, Kuhn P, Champoux JJ, Hol WGJ. Crystal structures of human topoisomerase I in covalent and noncovalent complexes with DNA. Science. 1998; 279 (5356): 1504-13.

73 Rothenberg ML. Topoisomerase I inhibitors: review and update. Ann Oncol. 1997; 8 (9): 837-55.

74 Wang LK, Rogers BD, Hecht SM. Inhibition of topoisomerase I function by coralyne and 5,6-dihydrocoralyne. Chem Res Toxicol. 1996; 9 (1): 75-83.

75 Palumbo M, Gatto B, Moro S, Sissi C, Zagotto G. Sequence-specific interactions of drugs interfering with the topoisomerase-DNA cleavage complex. Biochim Biophys Acta. 2002; 1587 (2): 145-54.

76 Pommier Y. Topoisomerase I inhibitors: camptothecins and beyond. Nat Rev Cancer. 2006; 6 (10): 789-802.

77 Pommier Y. DNA topoisomerase I inhibitors: chemistry, biology, and interfacial inhibition. Chem Rev. 2009; 109 (7): 2894-902.

78 Bailly C. Homocamptothecins: potent topoisomerase I inhibitors and promising anticancer drugs. Crit Rev Oncol Hematol. 2003; 45 (1): 91-108.

79 Das BB, Sen N, Roy A, Dasgupta SB, Ganguly A, Mohanta BC, et al. Differential induction of leishmania donovani bi-subunit topoisomerase I-DNA cleavage complex by selected flavones and camptothecin: activity of flavones against camptothecin-resistant topoisomerase I. Nucleic Acids Res. 2006; 34 (4): 1121-32.

80 Champoux JJ. Strand breakage by the DNA untwisting enzyme results in covalent attachment of the enzyme to DNA. P Natl Acad Sci. 1977; 74 (9): 3800-04.

81 Marchand C, Antony S, Kohn KW, Cushman M, Ioanoviciu A, Staker BL, et al. A novel norindenoisoquinoline structure reveals a common interfacial inhibitor paradigm for ternary trapping of the topoisomerase I-DNA covalent complex. Mol Cancer Ther. 2006; 5 (2): 287-95.

82 Boege F, Straub T, Kehr A, Boesenberg C, Christiansen K, Andersen A, et al. Selected novel flavones inhibit the DNA binding or the DNA religation step of eukaryotic topoisomerase I. J Biol Chem. 1996; 271 (4): 2262-70.

83 Wenying R, Zhenhua Q, Hongwei W, Lei Z, Li Z. Flavonoids: promising anticancer agents. Med Res Rev. 2003; 23: 519-34.

84 Lopez LM, Willmore E, Austin CA. The dietary flavonoids myricetin and fisetin act as dual inhibitors of DNA topoisomerases I and II in cells. Mutat Res Genet Toxicol Environ Mutagen. 2010; 696 (1): 41-47.

85 Paola F, Christine LH, Piero B, Mary AB. Drug-induced stabilization of covalent DNA topoisomerase I-DNA intermediates. In: DNA topoisomerase procols. Totowa: Humana Press Inc 2008: 291-301.

86 Hsiang YH, Hertzberg R, Hecht S, Liu LF. Camptothecin induces protein-linked DNA breaks via mammalian DNA topoisomerase I. J Biol Chem. 1985; 260 (27): 14873-78.

87 James J C. DNA topoisomerase I-mediated nicking of circular duplex DNA. In: DNA topoisomerase procols. Totowa: Humana Press Inc 2008: 81-87.

88 Hertzberg RP, Caranfa MJ, Hecht SM. On the mechanism of topoisomerase I inhibition by camptothecin: evidence for binding to an enzyme-DNA complex. Biochemistry. 1989; 28 (11): 4629-38.

89 Hajime K, Yusuke K, Kimiyoshi K, Takamitsu O, Takatsu N. Synthetic inhibitors of DNA topoisomerase I and II. Chem Pharm Bull. 1999; 47 (1): 48-53.

90 Kitchen DB, Decornez H, Furr JR, Bajorath J. Docking and scoring in virtual screening for drug discovery: methods and applications. Nat Rev Drug Discov. 2004; 3 (11): 935-49.

91 Taylor RD, Jewsbury PJ, Essex JW. A review of protein-small molecule docking methods. J Comput Aided Mol Des. 2002; 16 (3): 151-66.

92 Graham LP. Drug design: optimizing target interaction. In: an introduction to medicinal chemistry. 4 ed. New York: Oxford University Press Inc; 2008: 212-41.

93 Schulz GT, Stahl M. Scoring functions for protein-ligand interactions: a critical perspective. Drug Discov Today. 2004; 1 (3): 231-9.

94 David CY. Docking. In: computational drug design. John Wiley and Sons 2009: 133-60.

95 Vladu B, Woynarowski JM, Manikumar G, Wani MC, Wall ME, Von Hoff DD, et al. 7- and 10-Substituted camptothecins: dependence of topoisomerase

I-DNA cleavable complex formation and stability on the 7- and 10-substituents. Mol Pharmacol. 2000; 57 (2): 243-51.

APPENDIX
PROTON NMR SPECTRA

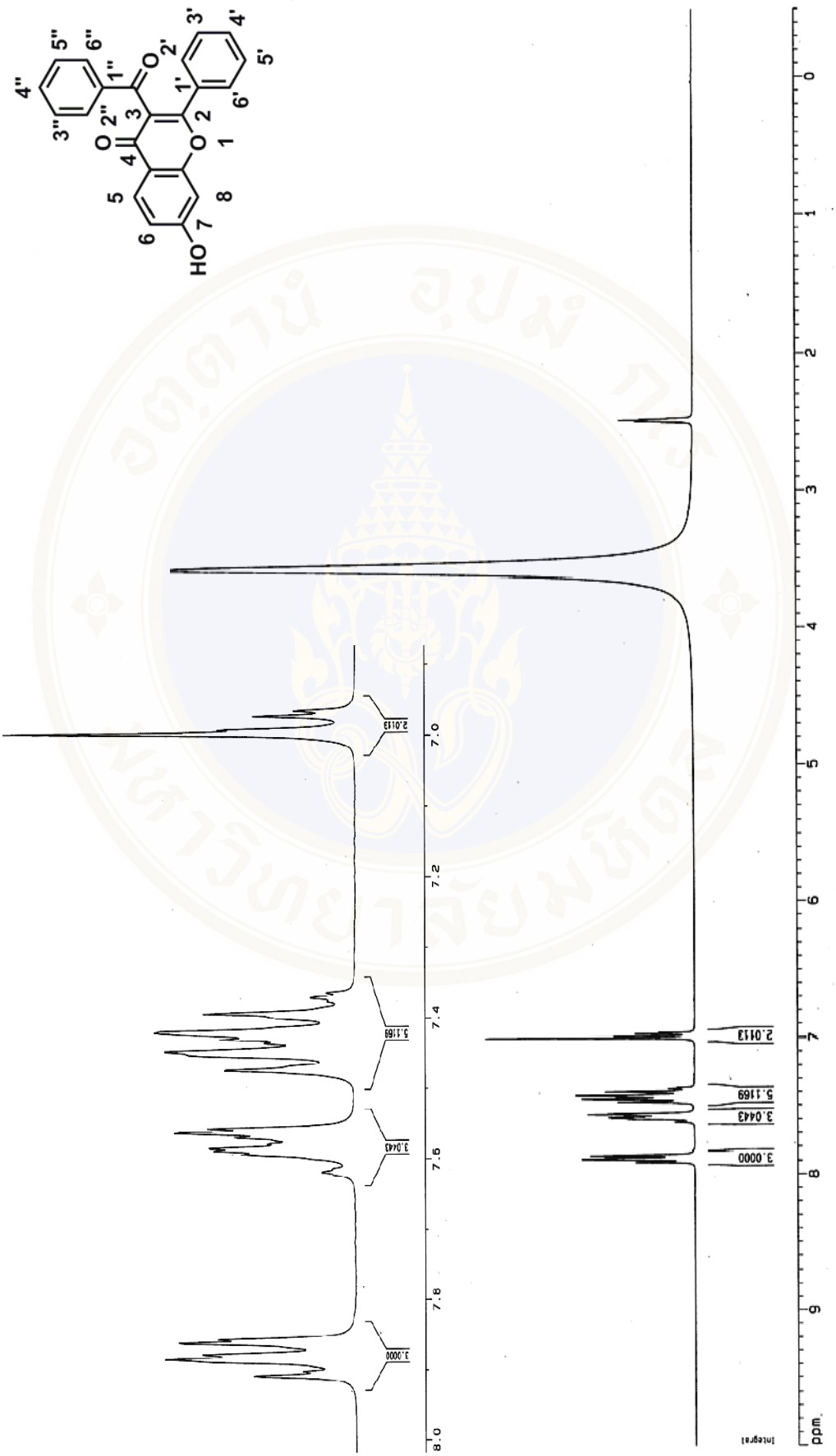

7-Hydroxy-2-phenyl-3-benzoyl chromone **7**

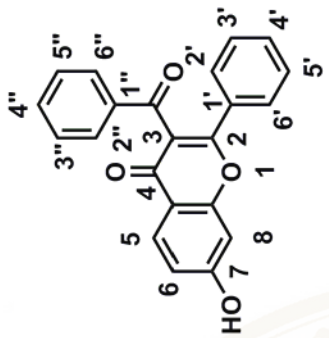

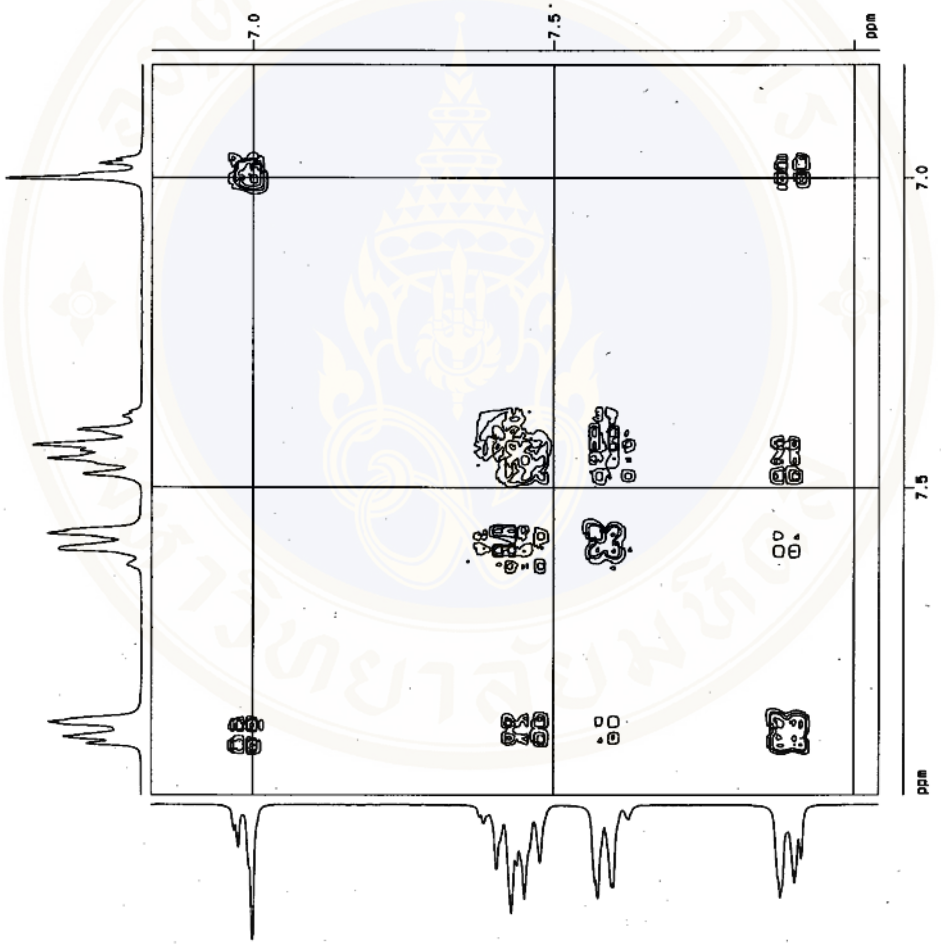

7-Hydroxy-2-phenyl-3-benzoyl chromone **7** (continued)

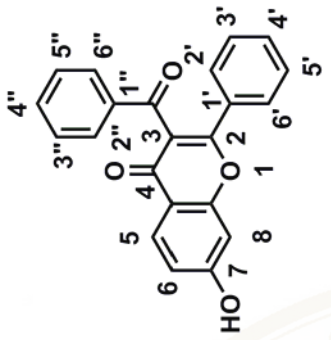

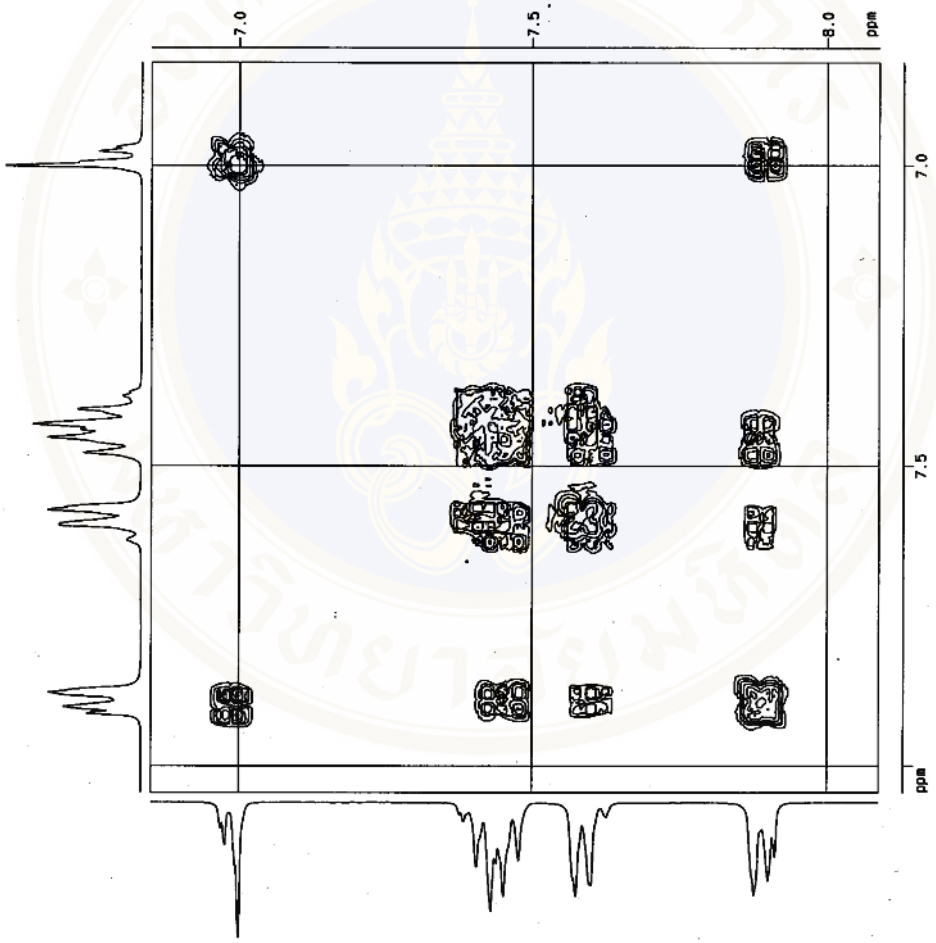

7-Hydroxy-2-phenyl-3-benzoyl chromone **7** (cont.)

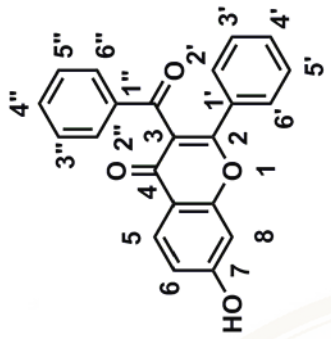

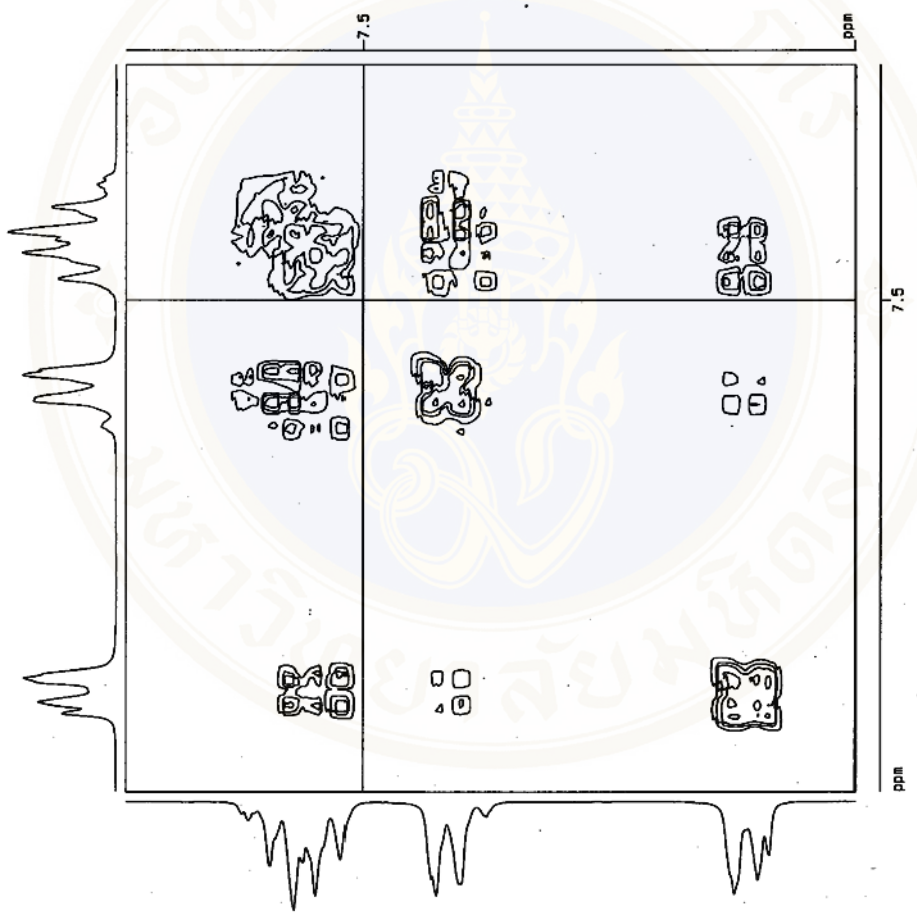

7-Hydroxy-2-phenyl-3-benzoyl chromone **7** (cont.)

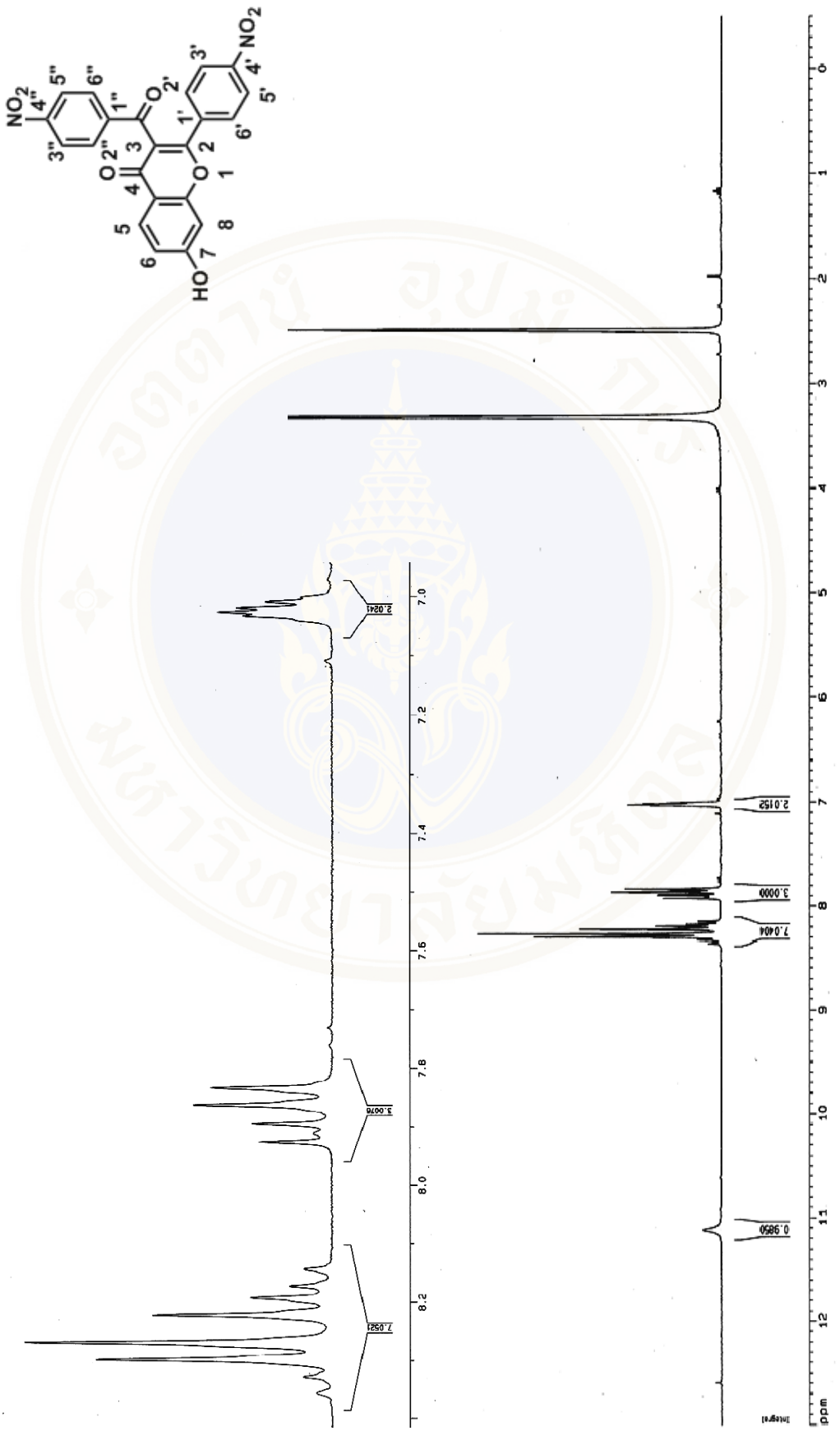

7-Hydroxy-2-(4'-nitro)phenyl-3-(4''-nitro)benzoyl chromone **11**

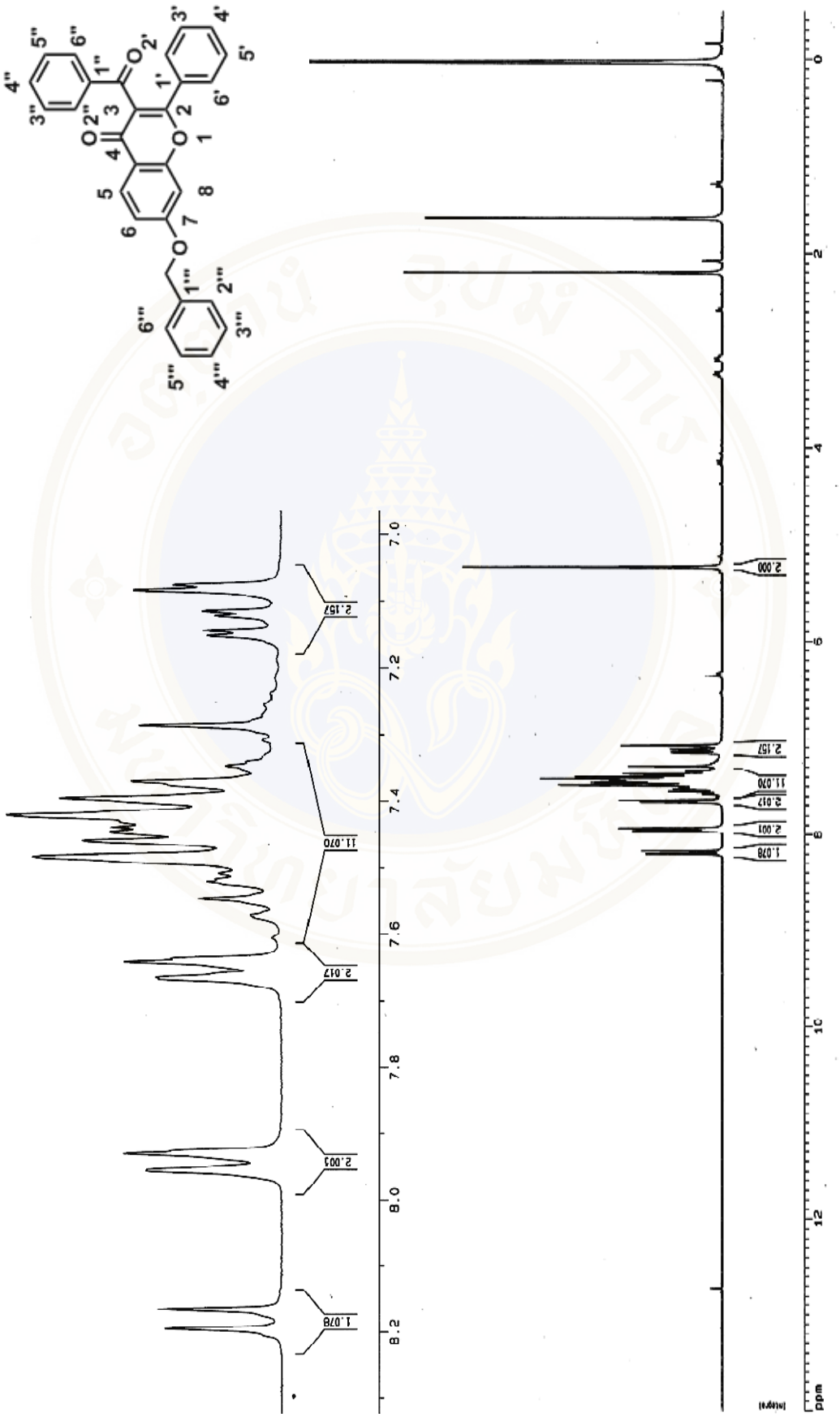

7-Benzyloxy-2-phenyl-3-benzoyl chromone **7a**

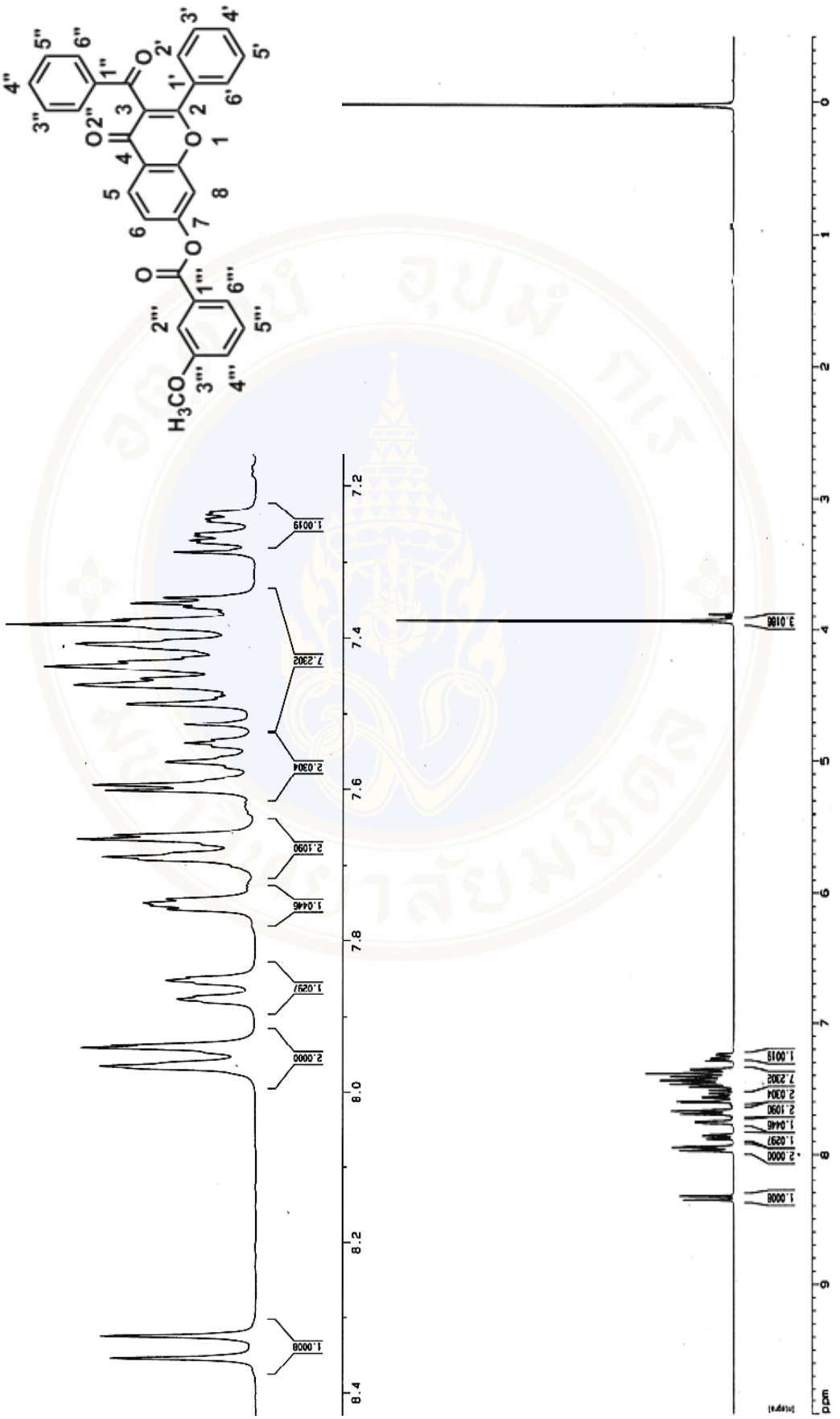

7-(3'''-Methoxy)benzoate-2-phenyl-3-benzoyl chromone **7d**

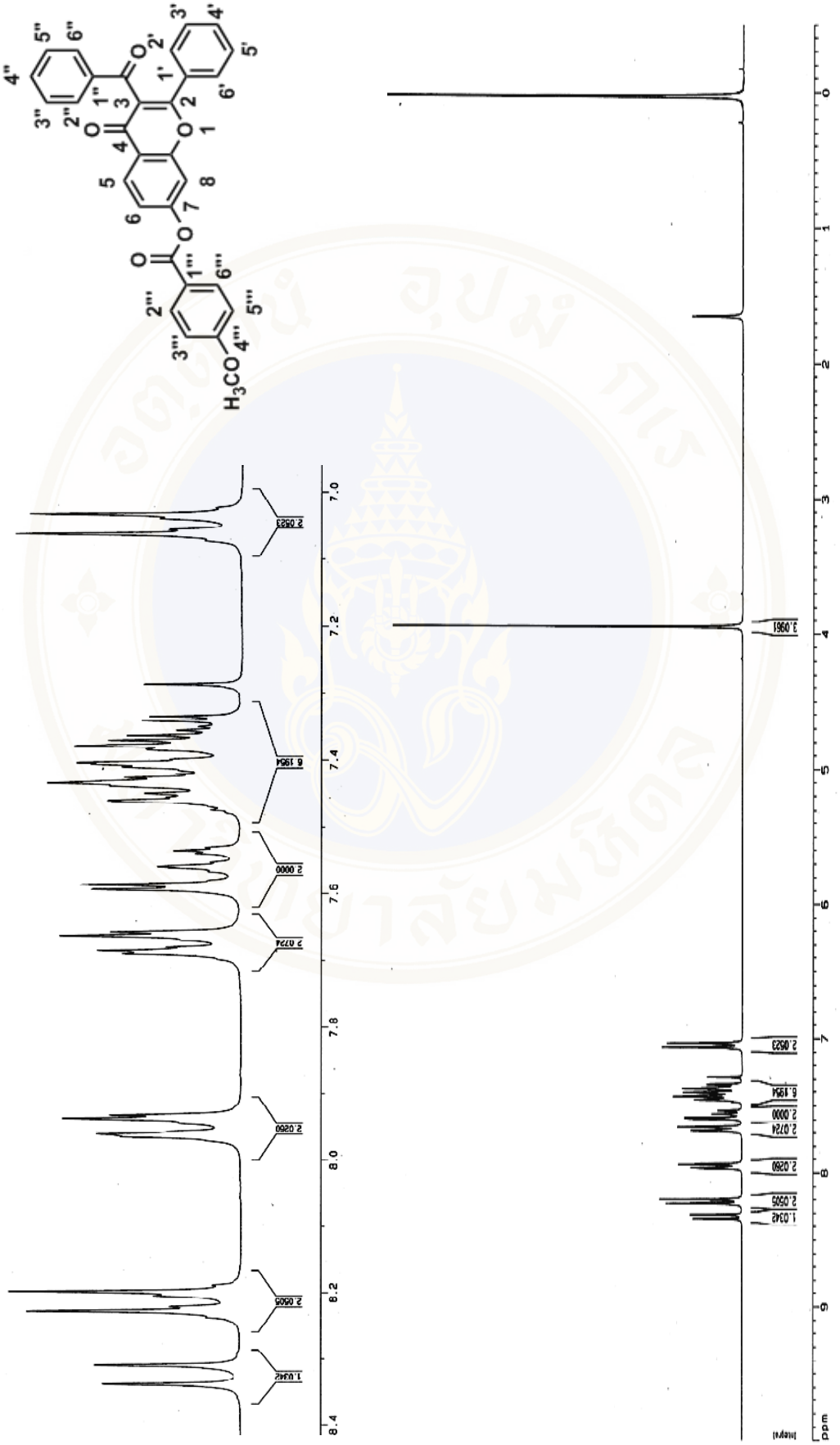

7-(4'''-Methoxy)benzoate-2-phenyl-3-benzoyl chromone **7e**

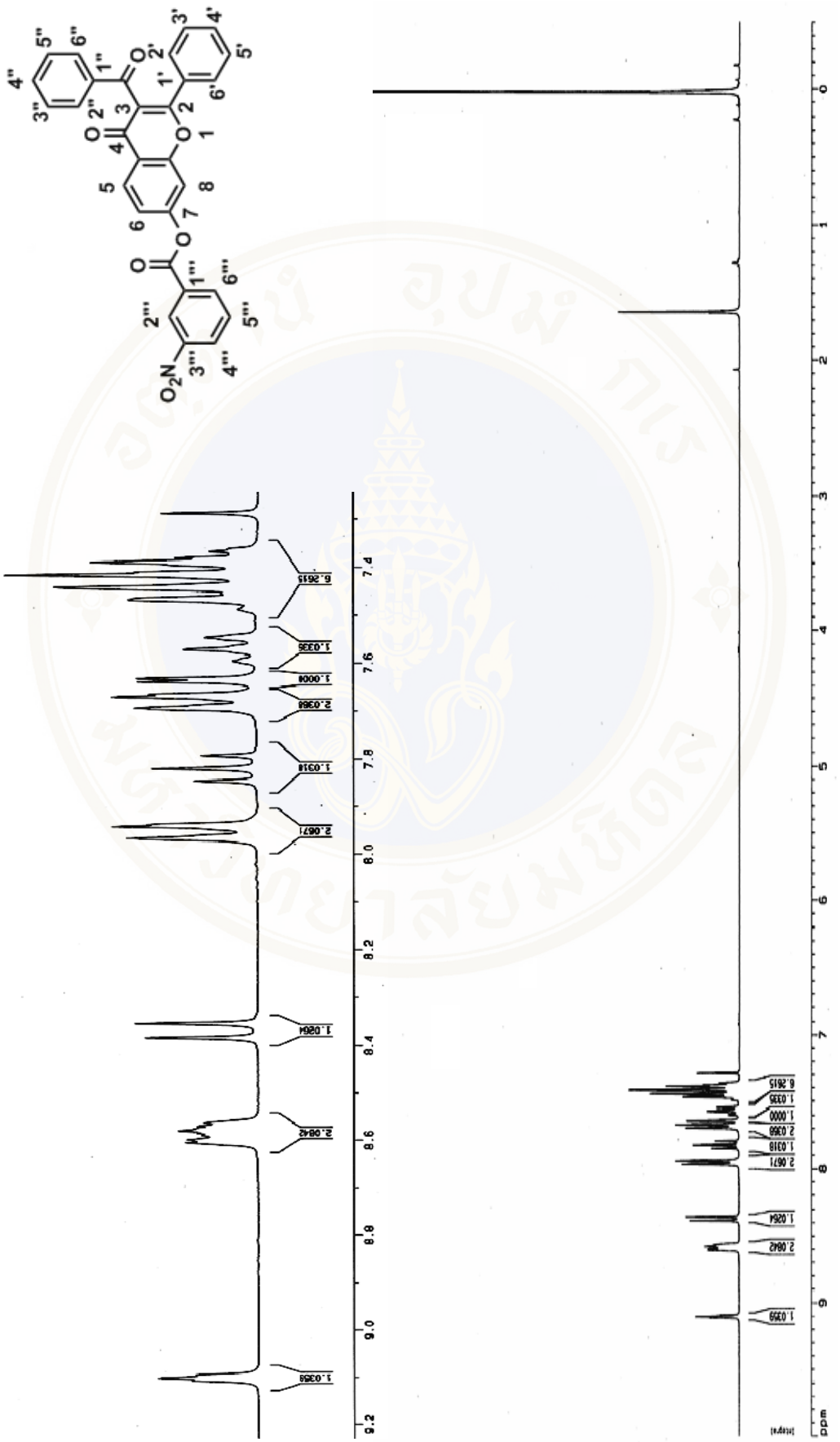

7-(3'''-Nitro)benzoate-2-phenyl-3-benzoyl chromone **7f**

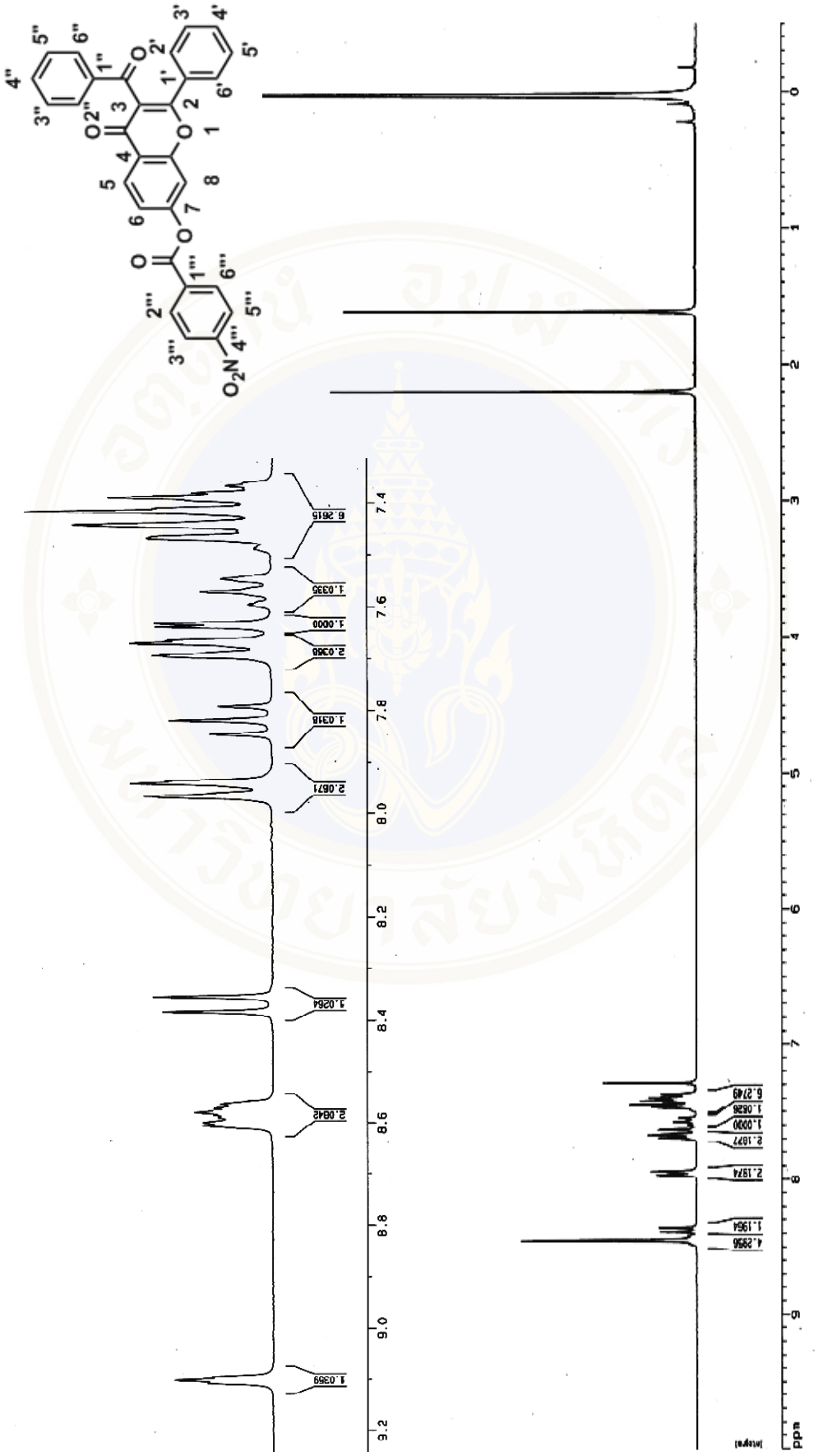

7-(4'''-Nitro)benzoate-2-phenyl-3-benzoyl chromone **7g**

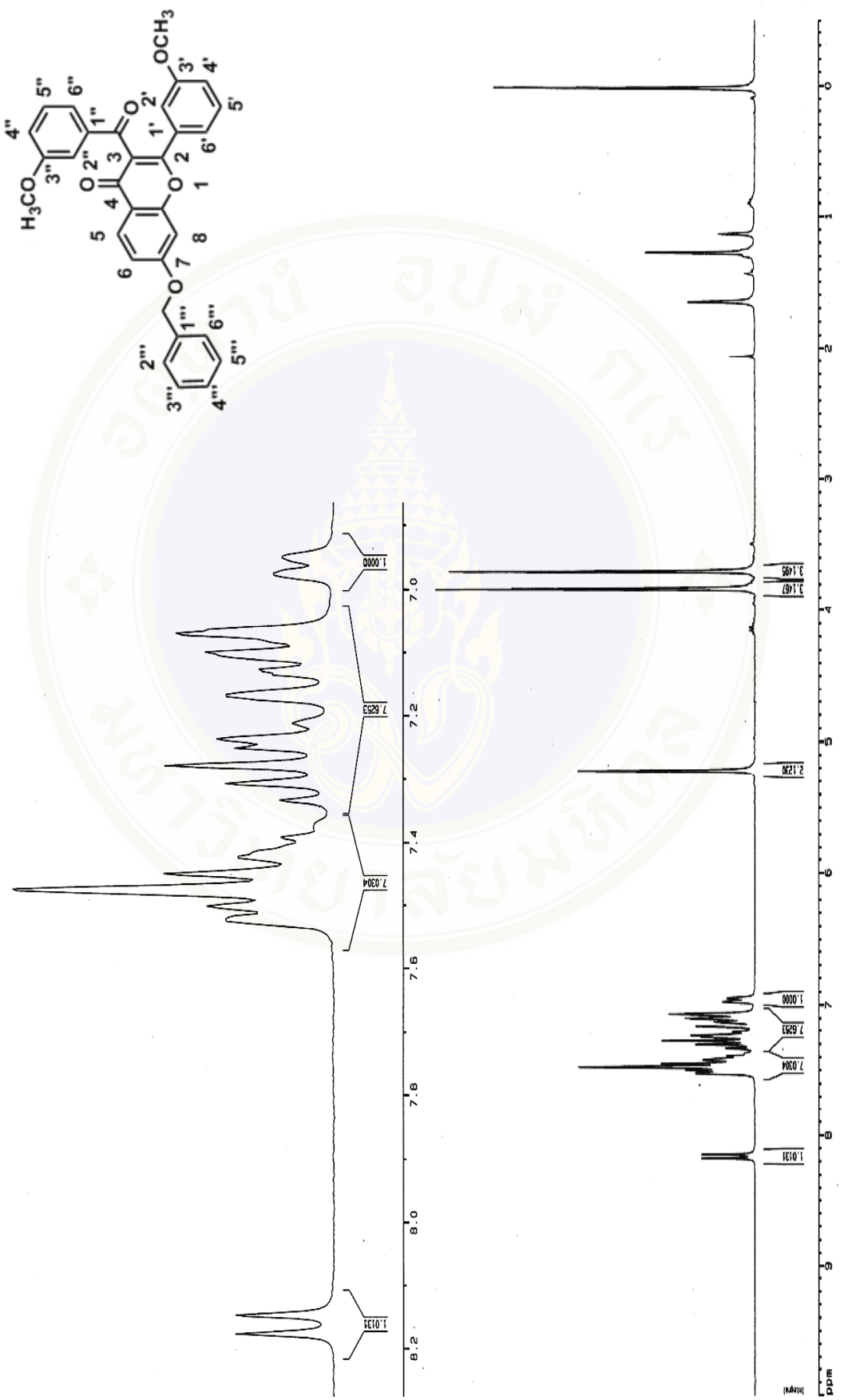

7-Benzyloxy-2-(3'-methoxy)phenyl-3-(3"-methoxy)benzoyl chromone **8a**

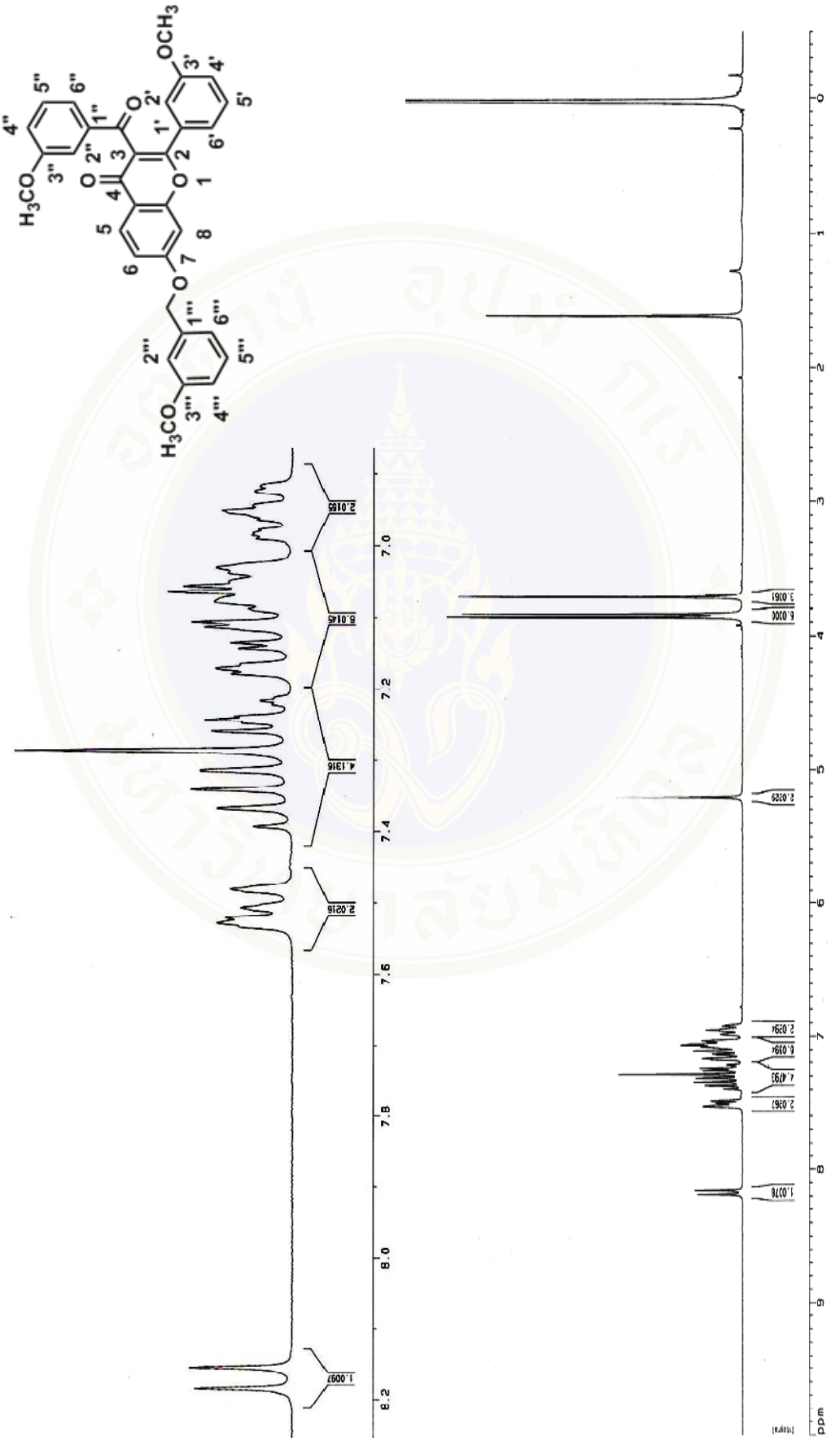

7-(3'''-Methoxy)benzyloxy-2-(3'-methoxy)phenyl-3-(3''-methoxy)benzoyl chromone **8b**

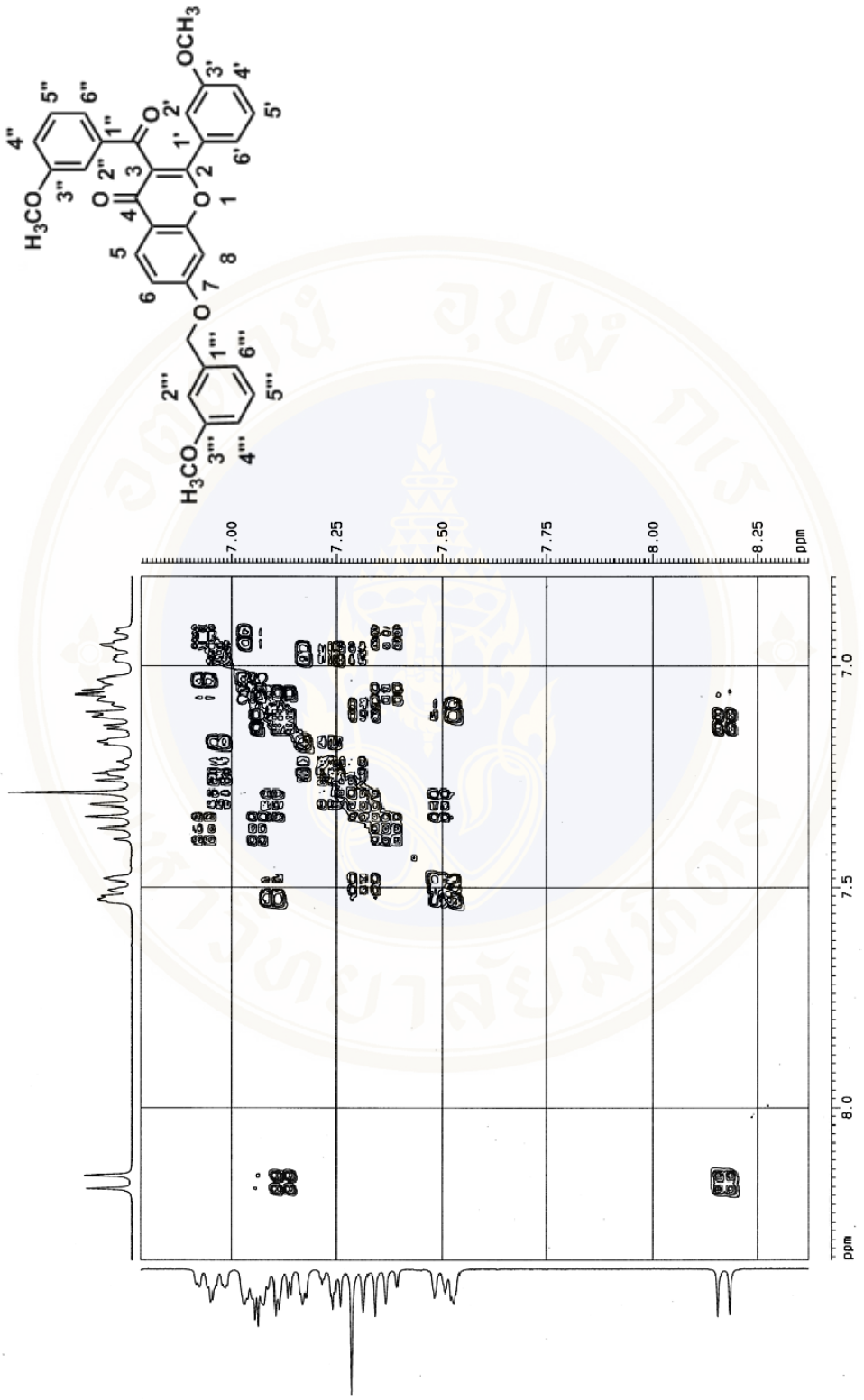

7-(3'''-Methoxy)benzyloxy-2-(3'-methoxy)phenyl-3-(3''-methoxy)benzoyl chromone **8b** (cont.)

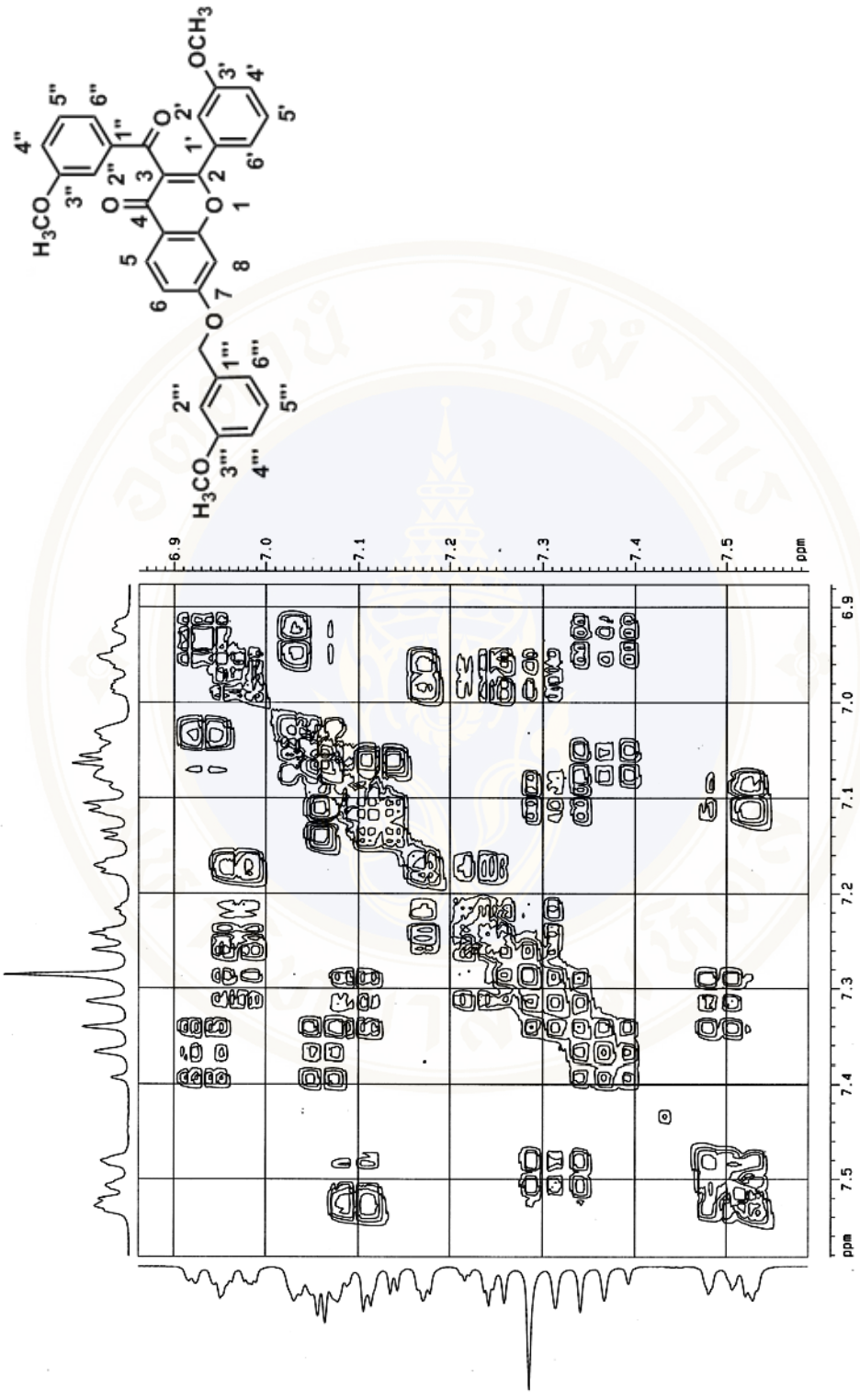

7-(3'''-Methoxy)benzyloxy-2-(3'-methoxy)phenyl-3-(3''-methoxy)benzoyl chromone 8b (continued)

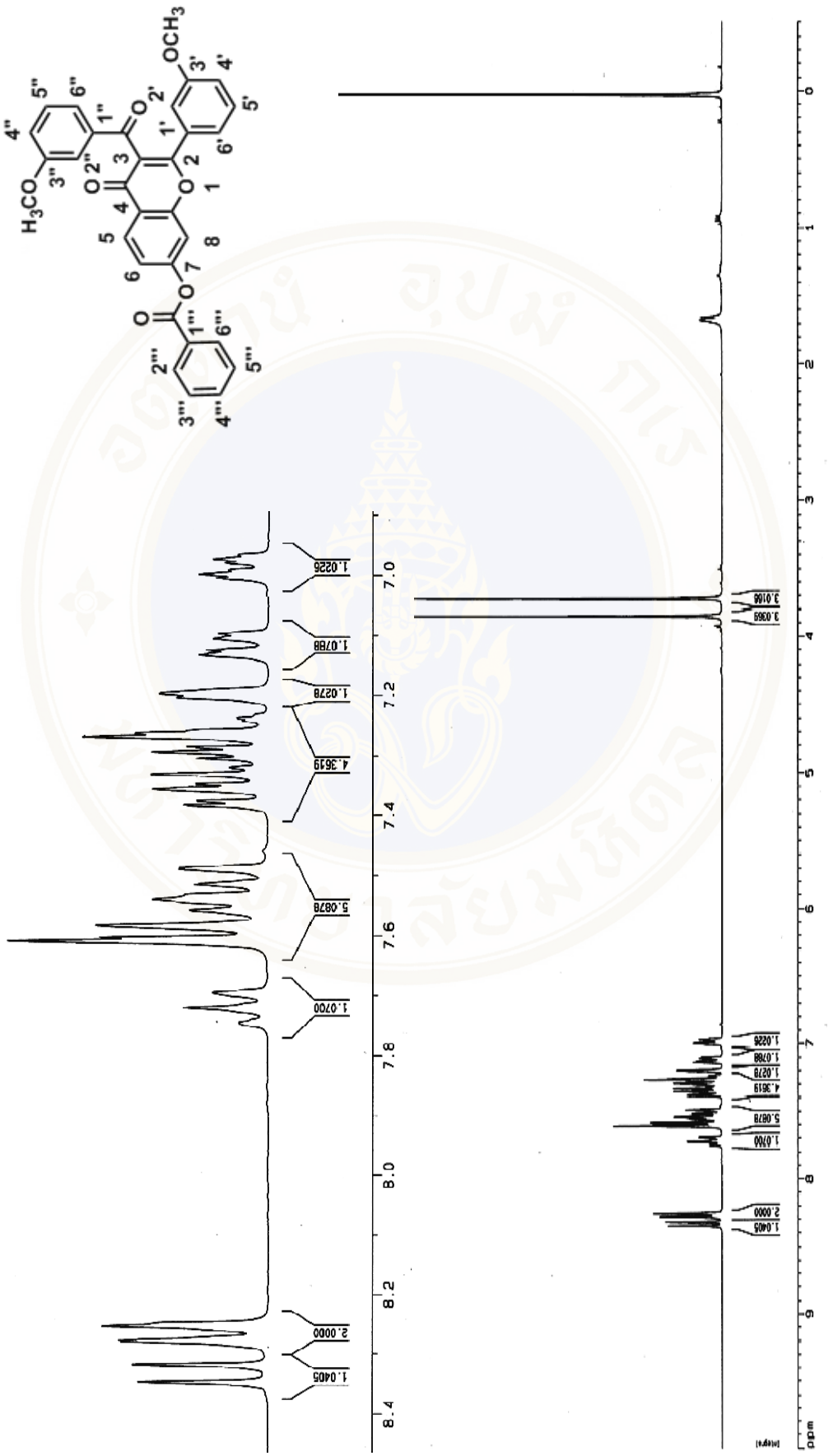

7-Benzoate-2-(3'-methoxy)phenyl-3-(3''-methoxy)benzoyl chromone **8d**

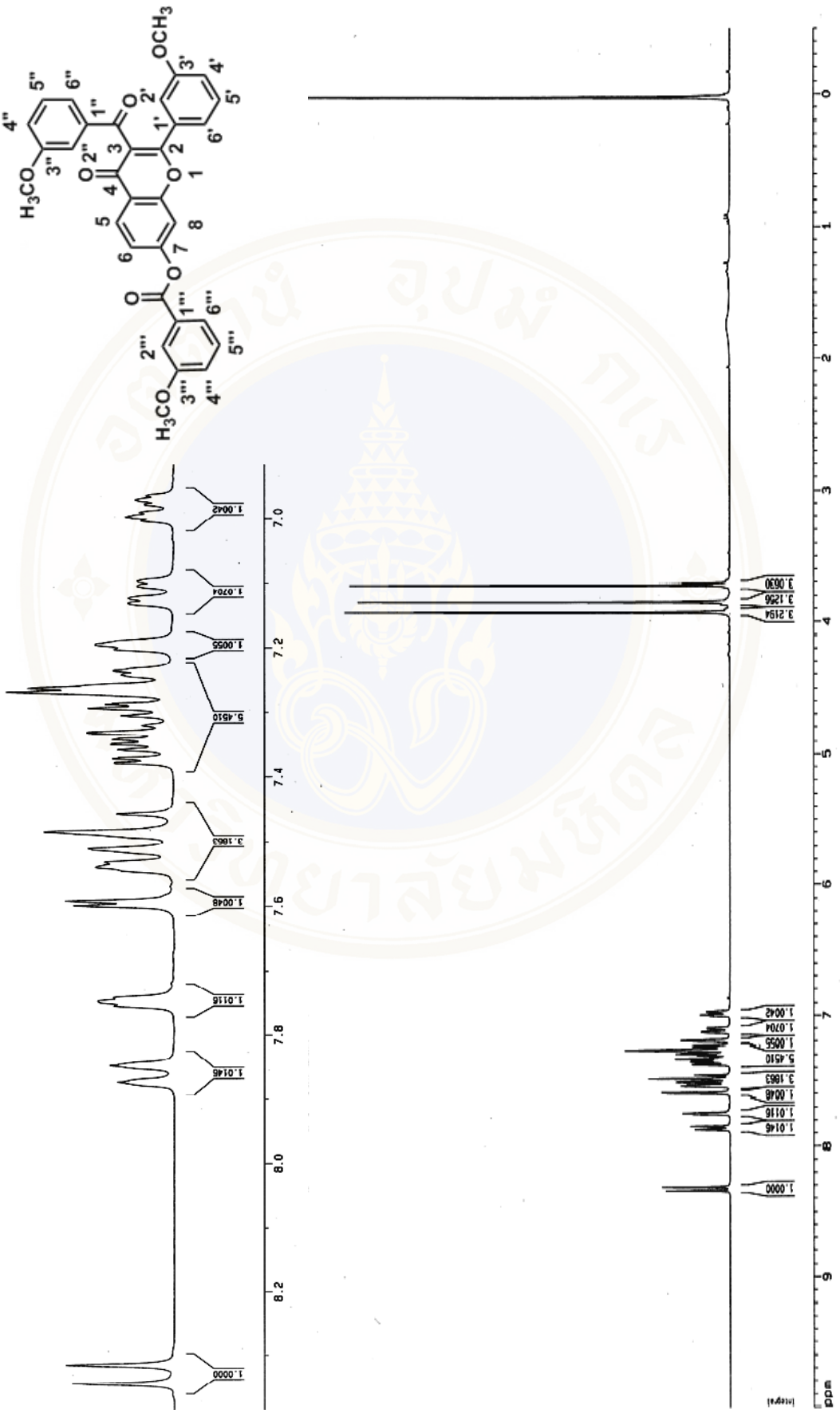

7-(3'''-Methoxy)benzoate-2-(3'-methoxy)phenyl-3-(3''-methoxy)benzoyl chromone **8e**

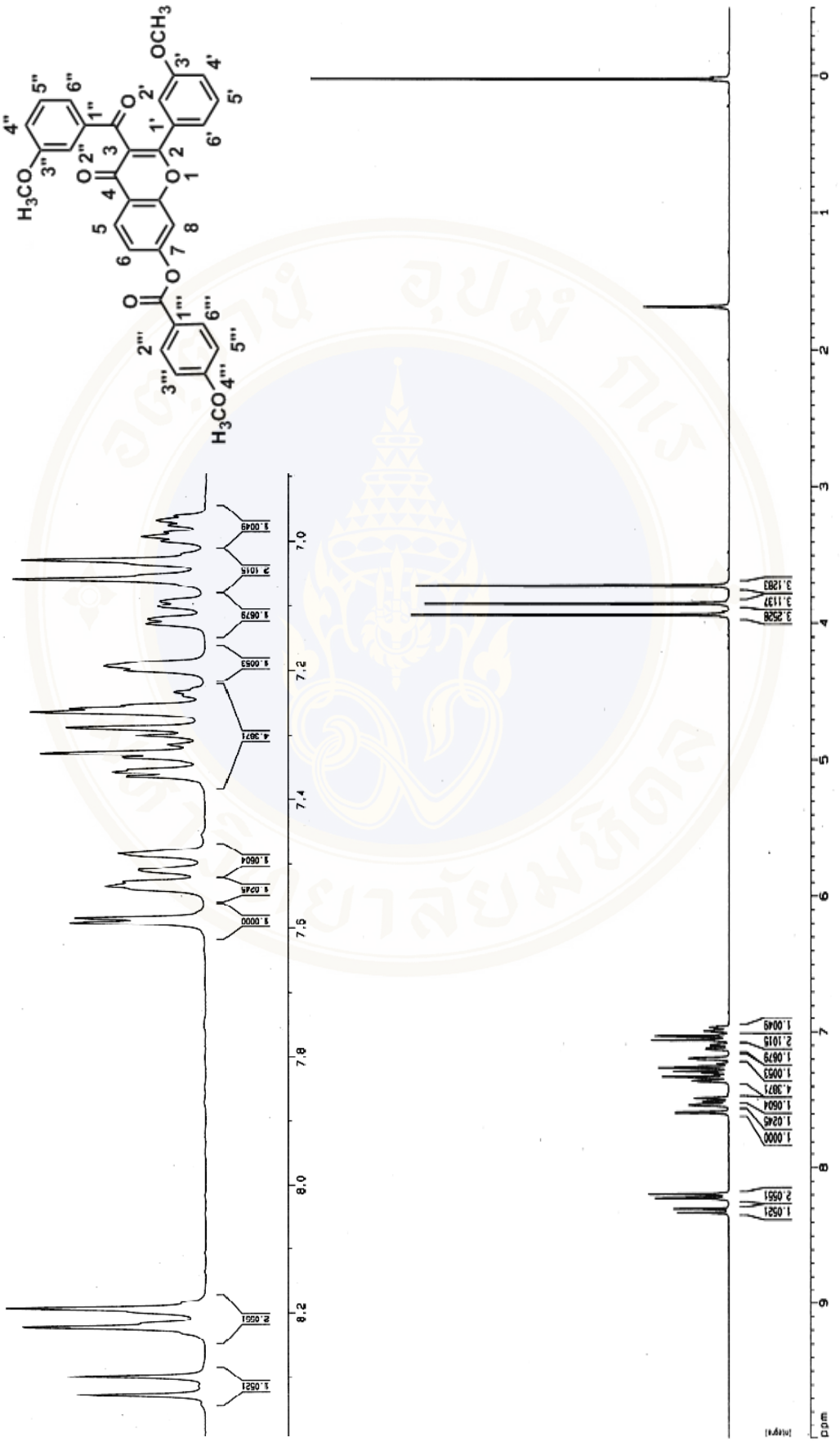

7-(4'''-Methoxy)benzoate-2-(3'-methoxy)phenyl-3-(3''-methoxy)benzoyl chromone **8f**

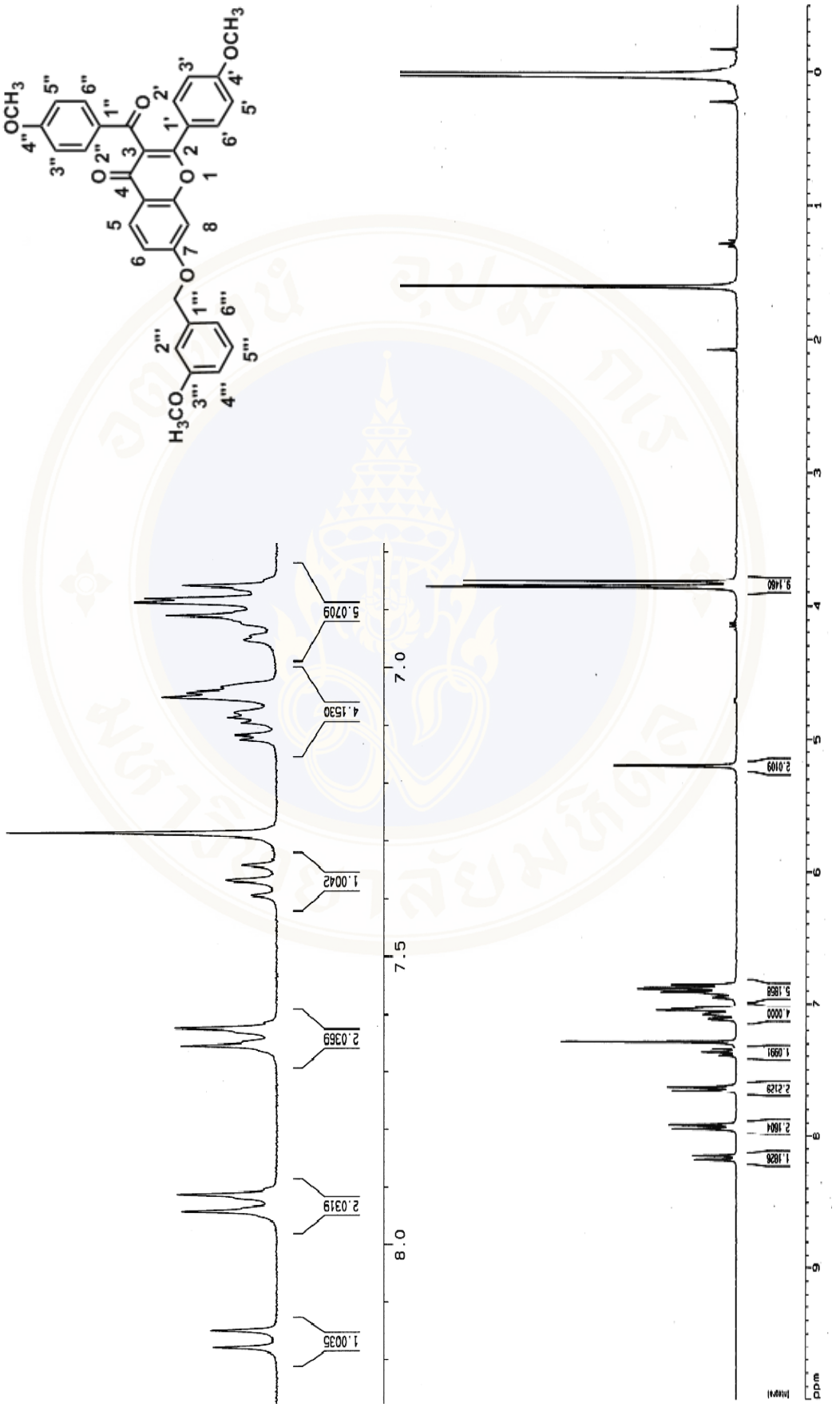

7-(3'''-Methoxy)benzyloxy-2-(4'-methoxy)phenyl-3-(4''-methoxy)benzoyl chromone **9b**

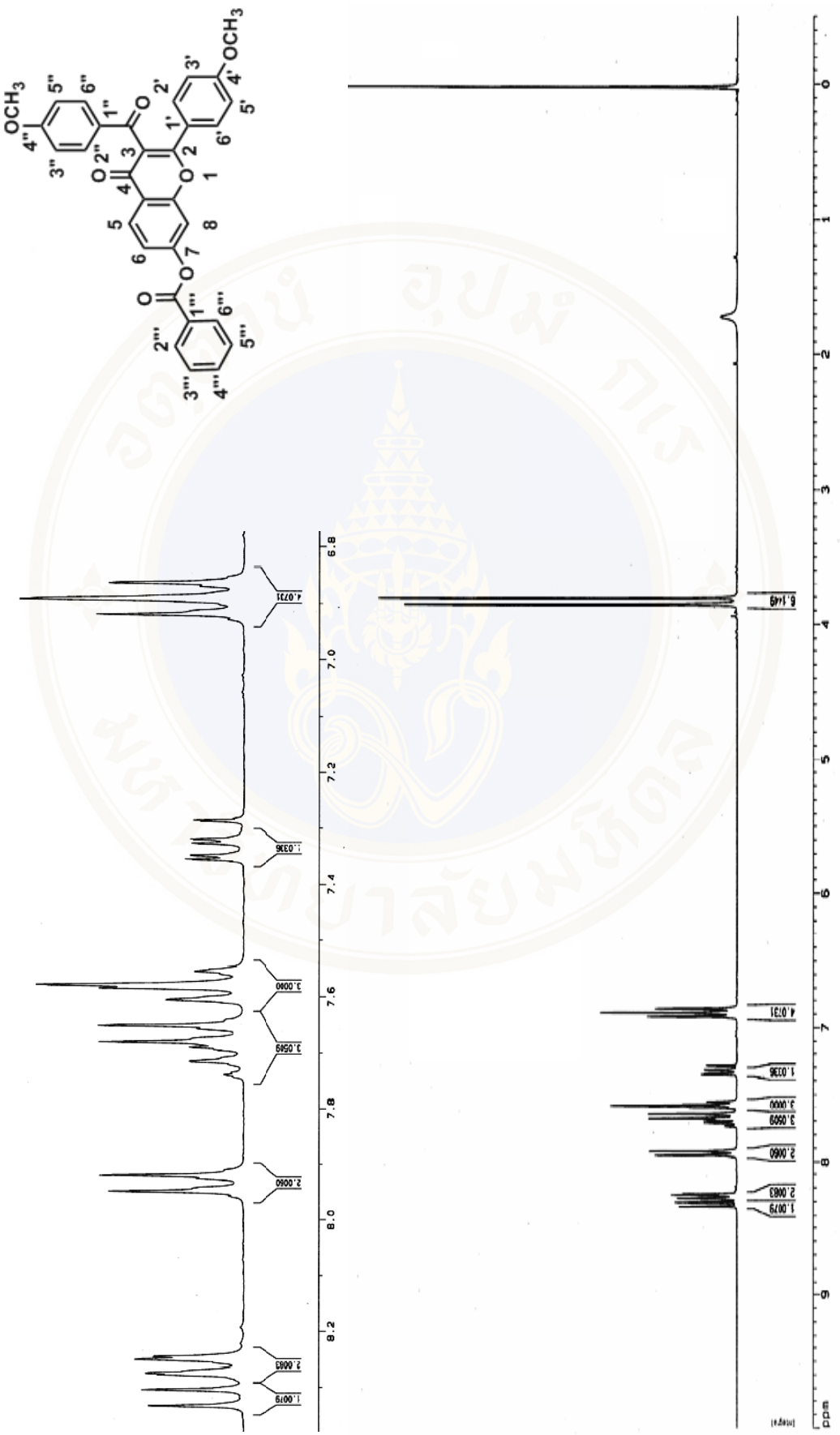

7-Benzoate-2-(4'-methoxy)phenyl-3-(4''-methoxy)benzoyl chromone **9d**

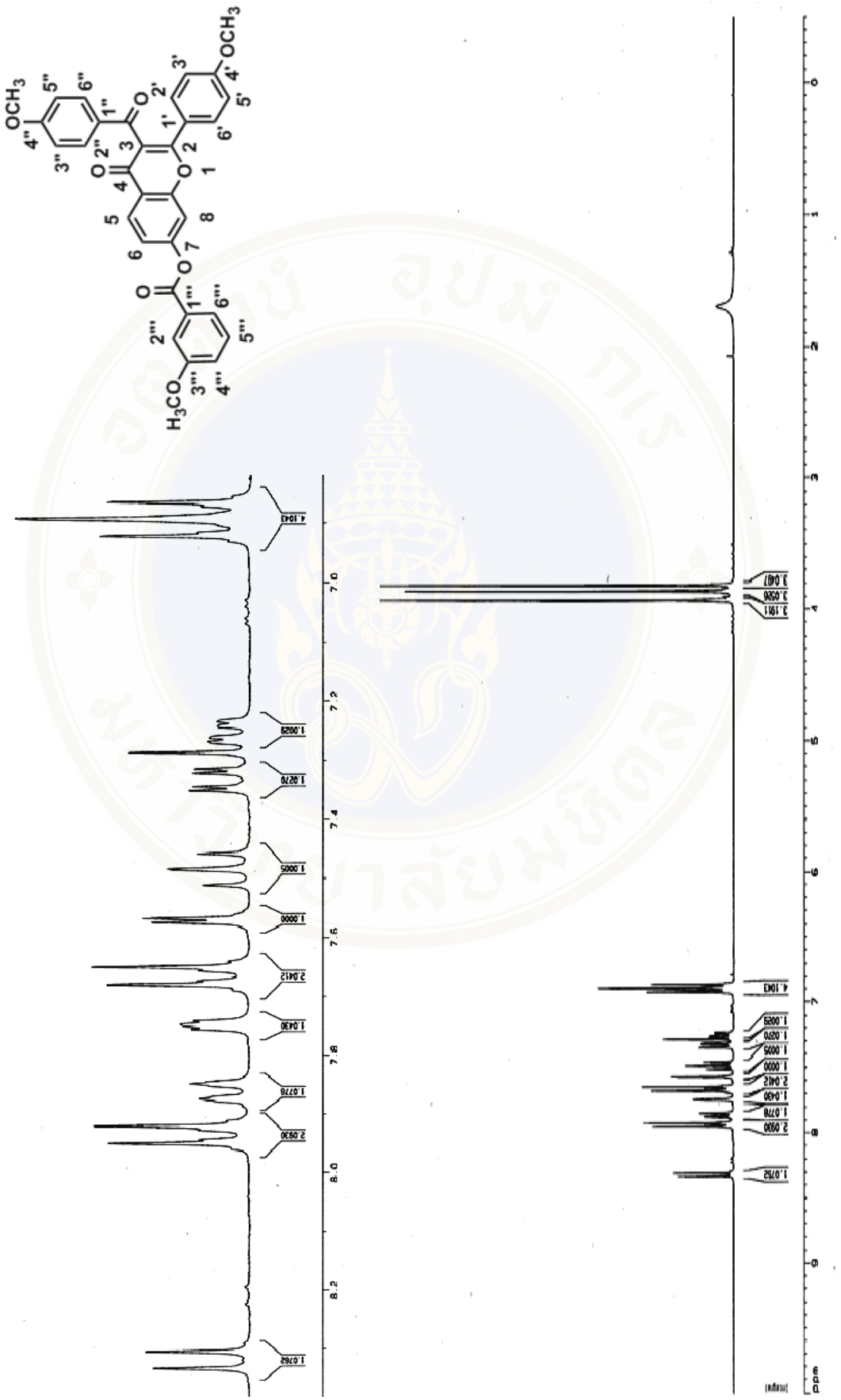

7-(3'''-Methoxy)benzoate-2-(4'-methoxy)phenyl-3-(4''-methoxy)benzoyl chromone **9e**

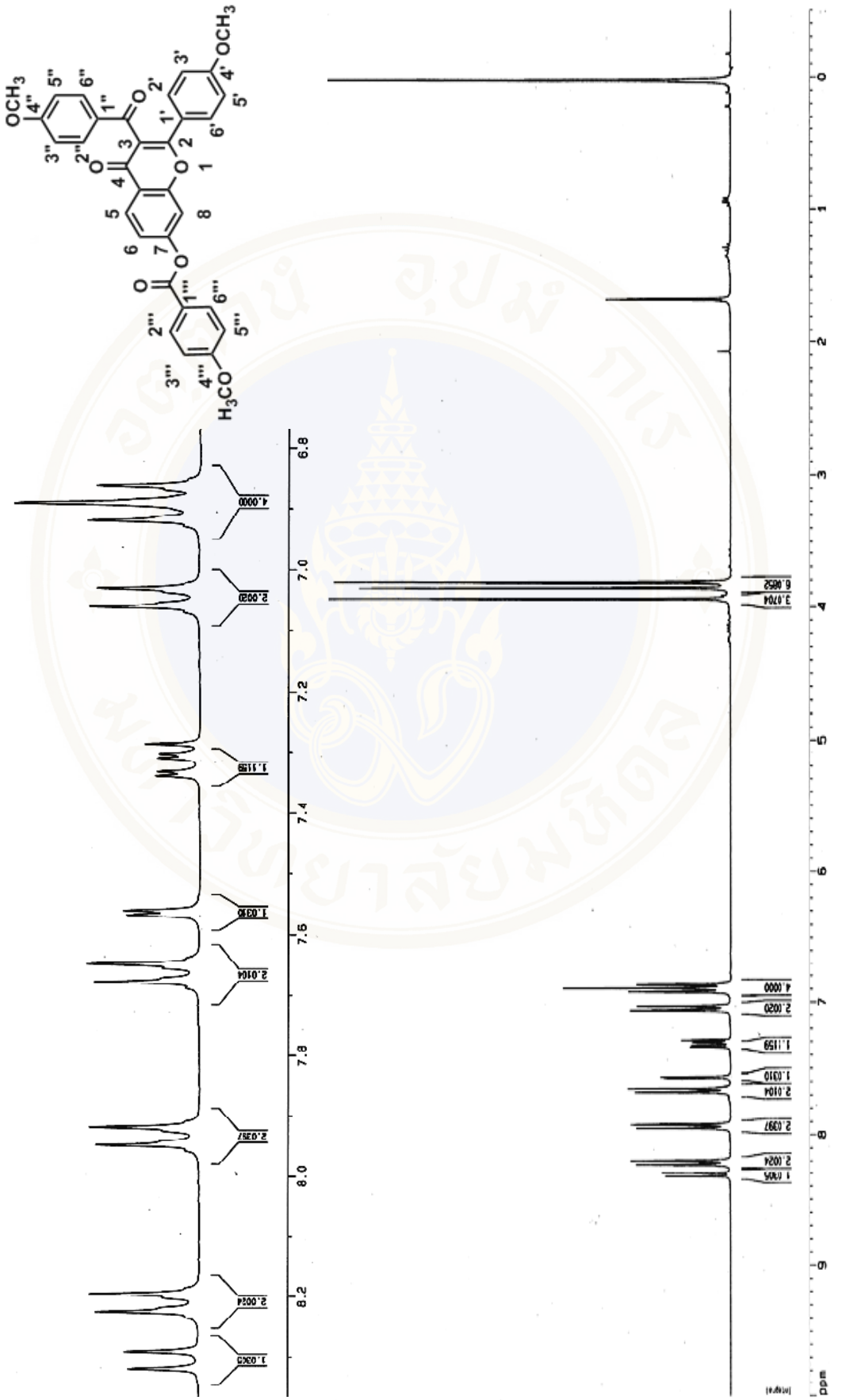

7-(4'''-Methoxy)benzoate-2-(4'-methoxy)phenyl-3-(4''-methoxy)benzoyl chromone **9f**

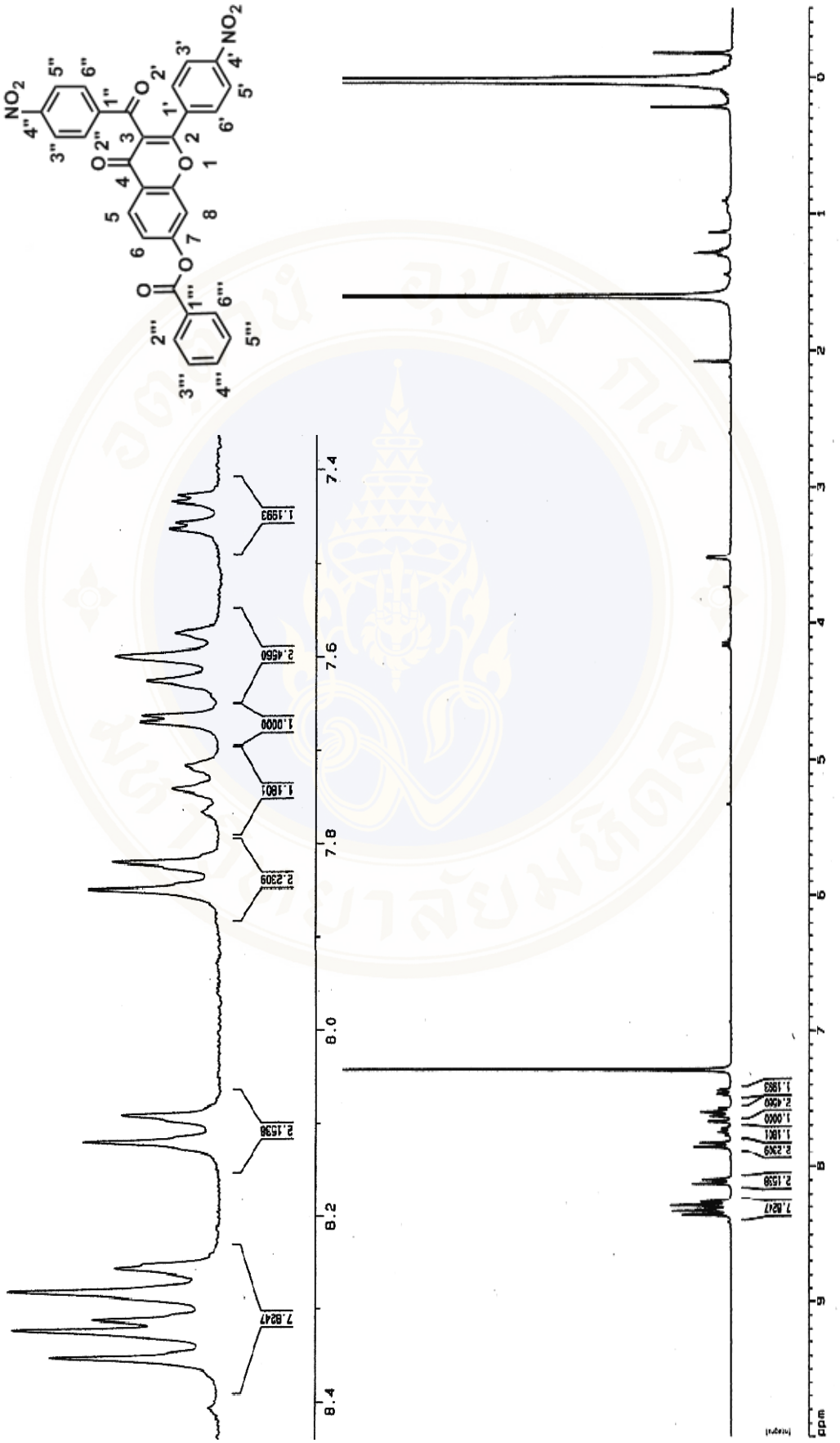

7-Benzoate-2-(4'-nitro)phenyl-3-(4''-nitro)benzoyl chromone **11b**

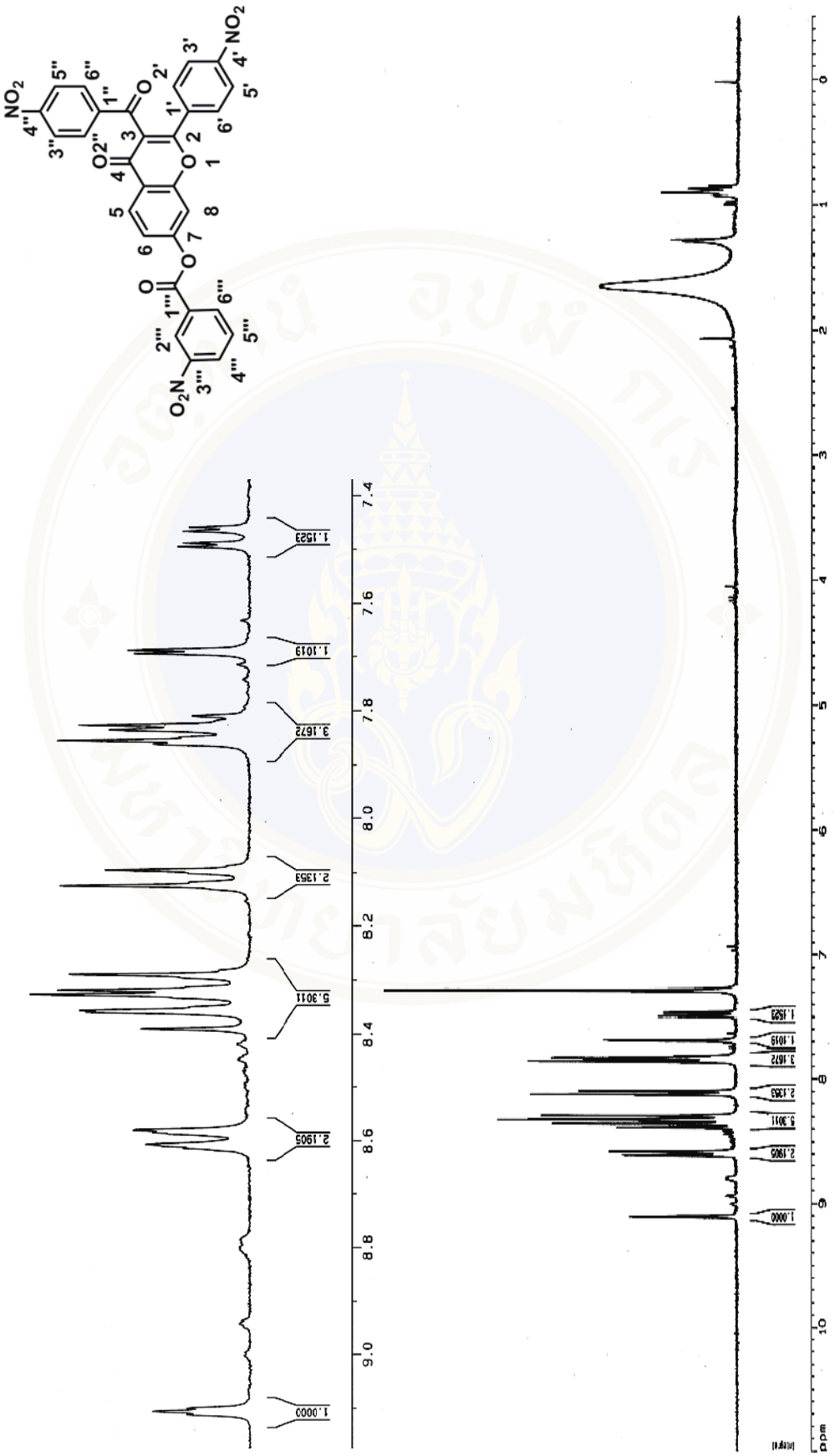

7-(3'''-Nitro)benzoate-2-(4'-nitro)phenyl-3-(4''-nitro)benzoyl chromone **11c**

BIOGRAPHY

NAM E	Miss Chirattikan Maicheen
DATE OF BIRTH	5 June 1984
PLACE OF BIRTH	Saraburi, Thailand
INSTITUTIONS ATTENDED	Rangsit University, 2003-2008 Bachelor of Pharmacy Mahidol University, 2008-2011: Master of Science in Pharmacy (Pharmaceutical chemistry)
RESEARCH GRANTS	-
HOME ADDRESS	22 M.2, Muang-ngam, Saohai, Saraburi
EMPLOYMENT ADDRESS	-
PUBLICATION/PRESENTATION	1. Pure and Applied Chemistry International Conference 2011: Design and synthesis of chromone derivatives as topoisomerase I inhibitors 2. 4th International Symposium on Advances in Synthetic and Medicinal Chemistry: Synthesis, docking study and topoisomerase I inhibitory evaluation of novel chromone derivatives as anticancer agent